Université du Québec

Institut national de la recherche scientifique

Centre Energie Matériaux Télecommunications

DESIGN AND DEVELOPMENT OF NEW DUAL-BAND ANTENNAS DIELECTRIC RESONATOR-BASED FOR MICROWAVE AND MILLIMETER-WAVE APPLICATIONS

Par

Mohamed Sedigh Bizan

Thèse présentée pour l'obtention du grade de
Philosophiae Doctor, Ph.D.
en Télécommunications

Jury d'évaluation

Président du jury et examinateur interne	Tarek Djerafi Institut National de la Recherche Scientifique
Examinateur externe	Halim Boutayeb Université du Quebec en Outaouais
Examinateur externe	Jamal Zaid Huawei Technologies Canada
Directeur de recherche	Denidni Tayeb A Institut National de la Recherche Scientifique

ACKNOWLEDGMENT

First and foremost, I thank Allah for granting me the strength, patience, and perseverance to complete this research journey. Without His guidance and mercy, none of this would have been possible.

I would like to express my deepest gratitude to Professor Tayeb A. Denidni, my thesis supervisor, for his exceptional mentorship, insightful feedback, and continuous support throughout my doctoral studies. His dedication to research excellence and his belief in my potential were pivotal to the success of this work.

I also wish to thank the faculty, researchers, and staff at the Énergie Matériaux Télécommunications Research Centre (INRS) for providing a stimulating academic environment and for their invaluable assistance during my research. Special appreciation goes to my colleagues in the antenna group for their collaboration and helpful discussions.

From the depths of my heart, I thank my beloved wife for her endless patience, strength, and sacrifices. Her unwavering support and love have carried me through this long and demanding journey. She managed our home and children with remarkable dedication, allowing me to focus on my studies when I needed it most.

To my wonderful sons, Mahmud, Ahmed, Siddiq, and Hisham, your energy, laughter, and curiosity are the light of my life. Although, truth be told, without you, I probably would have finished this thesis two years earlier! But I wouldn't trade a moment of it; you've taught me more about love, patience, and purpose than any textbook ever could.

Finally, I extend heartfelt thanks to my extended family and dear friends, whose prayers, encouragement, and moral support have always been with me on this path.

RÉSUMÉ

Avec l'évolution rapide des technologies sans fil, les systèmes de communication modernes exigent des solutions d'antennes capables de fonctionner efficacement sur plusieurs bandes de fréquences. Les antennes double bande sont devenues indispensables dans les réseaux 5G et au-delà, assurant une connectivité fluide en prenant simultanément en charge les fréquences micro-ondes et millimétriques. Cette capacité bimode permet à la fois une couverture étendue et des débits de données ultra-rapides. Les antennes à résonateur diélectrique (DRA), reconnues pour leurs faibles pertes, leur efficacité de rayonnement élevée et leur compacité, constituent une plateforme idéale pour ces systèmes. Leur aptitude à supporter un gain élevé et divers modes résonants les rend particulièrement adaptées aux applications multibandes avancées, où l'isolation et la sélectivité fréquentielle sont des critères essentiels.

Cette thèse présente une étude approfondie sur la conception et le développement d'antennes DRA double bande à haute performance, destinées aux futurs systèmes de communication sans fil 5G et au-delà. La recherche vise le fonctionnement simultané dans les bandes micro-ondes (sous-6 GHz) et millimétriques (mm-wave), en mettant l'accent sur un gain élevé, une large bande passante, la suppression des harmoniques et une excellente isolation entre les bandes.

La première contribution concerne une architecture à double CDRA utilisant deux matériaux diélectriques de permittivités différentes, permettant la suppression des harmoniques et le découplage fréquentiel. Des gains de 6,7 dBi et 15,2 dBi ont été atteints à 2,4 GHz et 28 GHz respectivement, avec une isolation mesurée dépassant 70 dB. Le second article propose une DRA cylindrique hybride intégrant un patch en série et des mécanismes de filtrage avancés, offrant un contrôle fréquentiel indépendant, des gains réalisés de 12,3 dBi et 17,2 dBi à 5,8 GHz et 28 GHz respectivement, et une isolation supérieure à 50 dB. La troisième étude explore un nouveau concept de « filtenna », combinant une antenne patch à 5,2 GHz avec un réseau DRA à 28 GHz, enrichi d'un filtre passe-bas et étendu en un réseau mm-wave de 16 éléments. Cette conception améliore significativement le gain (jusqu'à 19 dBi) et assure une isolation inférieure à 70 dB, tout en maintenant une compacité élevée.

Ces contributions établissent collectivement une base solide pour des systèmes d'antennes double bande dotés de résonances réglables indépendamment, de capacités de filtrage améliorées et de configurations à gain élevé et évolutives. Les résultats obtenus représentent une avancée significative vers des solutions d'antennes intégrées, efficaces et compactes, adaptées aux normes de communication multibande émergentes.

ABSTRACT

With the rapid evolution of wireless technologies, modern communication systems require antenna solutions that can efficiently operate across multiple frequency bands. Dual-band antennas have become essential in 5th Generation Mobile Network (5G) and beyond networks, enabling seamless connectivity by simultaneously supporting microwave and millimeter-wave frequencies. This dual-band capability allows for both broad coverage and ultra-fast data rates. DRAs, known for their low loss, high radiation efficiency, and compact form factor, offer an ideal platform for such systems. Their ability to support high-gain and diverse resonant modes makes them particularly suitable for advanced multi-band applications, where isolation and frequency selectivity are critical.

This thesis presents a comprehensive study on the design and development of high-performance dual-band dielectric resonator antennas aimed at next-generation 5G and beyond wireless communication systems. The research addresses the simultaneous operation in both the microwave (sub-6 GHz) and Millimeter Wave (mm-wave) frequency bands, emphasizing high gain, wide bandwidth, harmonic suppression, and superior inter-band isolation.

The first contribution involves a dual-CDRA architecture using two dielectric materials with different permittivities, enabling harmonic suppression and frequency decoupling. Gains of 6.7 dBi and 15.2 dBi were achieved at 2.4 GHz and 28 GHz, respectively, with measured isolation surpassing 70 dB. The second paper introduces a hybrid cylindrical DRA integrated with a serial-patch and advanced filtering mechanisms, achieving independent frequency control, realized gains of 12.3 dBi and 17.2 dBi at 5.8 GHz and 28 GHz, respectively, and isolation levels exceeding 50 dB. The third study explores a novel “filtenna” concept, merging a 5.2 GHz patch antenna with a 28 GHz DRA array, enhanced with a low-pass filter and expanded into a 16-element mm-wave array. This design significantly improves gain (up to 19 dBi) and isolation of less than 70 dB, while maintaining a compact footprint.

Collectively, these contributions establish a robust framework for dual-band antenna systems with independently tunable resonances, enhanced filtering capabilities, and scalable high-gain configurations. The findings offer a significant advancement toward integrated, efficient, and compact antenna solutions suitable for emerging multi-band communication standards.

SOMMAIRE RÉCAPITULATIF

0.1 Titre de la thèse en français

Conception et développement de nouvelles antennes double bande à base de résonateur diélectrique pour les applications micro-ondes et ondes millimétriques

0.2 Introduction

Avec l'évolution rapide des technologies de communication, la demande pour des systèmes de communication sans fil à haut débit ne cesse de croître. La cinquième génération (5G) des réseaux sans fil est appelée à révolutionner l'industrie des télécommunications en offrant des débits de données plus élevés, une latence réduite et une meilleure couverture. Toutefois, pour atteindre ces objectifs, le développement de technologies d'antennes adaptées aux bandes de fréquences micro-ondes et millimétriques est essentiel.

Les antennes à résonateur diélectrique (DRA) se sont imposées comme une solution prometteuse en raison de leur faible encombrement, de leur gain élevé et de leur grande efficacité de rayonnement. En particulier, les DRAs à double bande suscitent un vif intérêt, car elles permettent un fonctionnement sur une large plage de fréquences.

Cette recherche vise à concevoir et à développer de nouvelles DRAs double bande adaptées aux applications dans les bandes micro-ondes et millimétriques.

0.3 Motivation

L'essor de la 5G et la transition vers les systèmes au-delà de la 5G (B5G) ont accru la demande en antennes compactes et à haute performance, capables de prendre en charge plusieurs services tels que l'eMBB, l'URLLC et le mMTC. Ces services nécessitent un fonctionnement en double bande dans les fréquences sub-6 GHz et millimétriques afin d'atteindre des débits élevés, une large couverture et une faible latence.

Les antennes conventionnelles rencontrent des difficultés à couvrir des bandes aussi éloignées en raison de problèmes liés à la taille, aux interférences et à une mauvaise isolation. Les antennes à résonateur diélectrique (DRA) offrent une solution prometteuse grâce à leurs faibles pertes, leur haute efficacité et leur conception flexible. Cependant, des défis subsistent pour assurer un fonctionnement double bande avec réglage indépendant, suppression des harmoniques et forte isolation. Cette thèse vise à relever ces défis en proposant de nouvelles architectures DRA adaptées aux systèmes sans fil de prochaine génération.

0.4 Problématique

Les futurs systèmes de communication sans fil exigent des antennes capables de fonctionner efficacement à la fois dans les bandes sub-6 GHz et ondes millimétriques. Obtenir cette performance double bande dans un format compact représente un défi majeur en raison du couplage mutuel, de la génération d'harmoniques et du manque de contrôle fréquentiel indépendant.

La plupart des conceptions existantes présentent des limites : absence d'isolation suffisante, incapacité à supprimer les harmoniques, ou impossibilité de régler indépendamment les deux bandes. L'exigence d'un gain élevé et d'une grande efficacité, en particulier aux fréquences millimétriques, complique davantage la conception. Cette thèse propose des antennes DRA double bande compactes, avec contrôle indépendant, forte isolation et filtrage intégré pour combler ces lacunes et répondre aux exigences strictes des réseaux 5G et B5G.

0.5 Objectifs

Cette thèse vise à concevoir, développer et valider expérimentalement des antennes compactes à résonateur diélectrique (DRA) fonctionnant efficacement dans les bandes sub-6 GHz (micro-ondes) et ondes millimétriques, en réponse aux besoins des réseaux 5G et au-delà.

Les objectifs principaux sont :

1. **Gain et efficacité élevés** : Atteindre une performance de rayonnement élevée dans les deux bandes à l'aide de structures compactes et manufacturables.
2. **Forte isolation** : Réduire le couplage mutuel par des techniques de conception telles que l'utilisation de broches de court-circuit et de filtres intégrés.
3. **Réglage indépendant** : Permettre un contrôle séparé de chaque bande grâce au découplage géométrique et électromagnétique des résonateurs.
4. **Suppression des harmoniques** : Intégrer des structures de filtrage compactes pour atténuer les harmoniques indésirables provenant de la bande basse fréquence.
5. **Mise en œuvre pratique** : Utiliser des substrats commerciaux à faibles pertes et valider les performances par des simulations et des mesures expérimentales.

Ces objectifs soutiennent le développement d'antennes double bande pratiques et à haute performance pour les systèmes de communication sans fil de prochaine génération.

0.6 Méthodologie

Cette recherche suit une méthodologie structurée (voir Fig. 1) :

1. **Revue de la littérature** : Analyser les conceptions actuelles d'antennes DRA double bande afin d'identifier les lacunes de la recherche et de définir les objectifs de conception.
2. **Conception et simulation** : Explorer les matériaux diélectriques et les formes des résonateurs ; utiliser des outils de simulation électromagnétique pour optimiser la résonance, la bande passante et l'isolation.

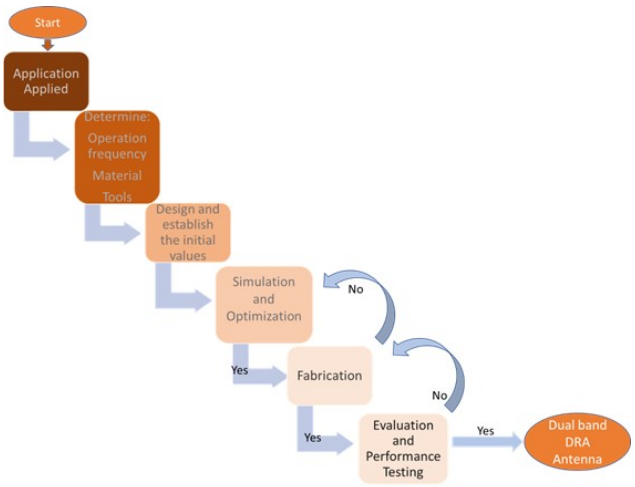

FIGURE 1 : Processus méthodologique.

3. **Prototypage et test** : Fabriquer des prototypes à l'aide de techniques de fraisage de haute précision ; effectuer des mesures en chambre anéchoïque pour évaluer le taux de réflexion, le gain, le diagramme de rayonnement et le rendement.
4. **Optimisation** : Améliorer les conceptions d'antennes sur la base des résultats expérimentaux afin d'accroître leur performance et leur applicabilité pratique.

Cette approche systématique garantit que les conceptions proposées sont à la fois innovantes et en adéquation avec les exigences de performance des systèmes de communication sans fil modernes.

0.7 Contributions de la thèse

Cette thèse présente plusieurs contributions originales à la conception d'antennes double bande à base de résonateur diélectrique pour les applications micro-ondes et ondes millimétriques dans les réseaux 5G et au-delà.

Antennes double bande innovantes : Trois antennes originales ont été conçues et validées par des publications évaluées par des pairs. Ces antennes combinent des DRA avec des éléments patch et des réseaux afin d'atteindre des performances élevées dans les bandes sub-6 GHz et mm-wave, chacune utilisant des structures et techniques d'alimentation distinctes pour minimiser les interférences.

Contrôle fréquentiel indépendant : Les conceptions proposées permettent un réglage indépendant de chaque bande de fréquence grâce à un découplage électromagnétique et géométrique surmontant ainsi le problème d'interdépendance fréquentielle présent dans les conceptions conventionnelles.

Suppression des harmoniques et filtrage : Les antennes intègrent des techniques de filtrage compactes, telles que les CMRC (cavités en anneau résonantes) et les filtres Chebyshev repliés, pour supprimer les harmoniques générées par la bande micro-ondes, améliorer la pureté spectrale et renforcer l'isolation entre les bandes.

Isolation élevée atteinte : Grâce à des stratégies de configuration structurelle et à l'utilisation de broches de court-circuit, les conceptions atteignent une isolation exceptionnelle jusqu'à 73 dB dans la bande micro-ondes et 62 dB dans la bande mm-wave parmi les valeurs les plus élevées rapportées pour des antennes double bande compactes.

Implémentation pratique : Toutes les conceptions utilisent des substrats économiques tels que les Rogers RO3003 et RO3210, compatibles avec les techniques de fabrication standards, les rendant adaptées aux applications mobiles, aux véhicules et aux stations de base.

Ensemble, ces contributions font progresser le développement d'antennes compactes, à gain élevé et à propreté spectrale, répondant aux exigences complexes des systèmes de communication sans fil du futur.

0.8 Antenne double bande : Définition et caractéristiques principales

Une antenne double bande est un type d'antenne capable d'émettre et/ou de recevoir des ondes électromagnétiques sur deux bandes de fréquences distinctes. Cette capacité permet à une seule antenne de fonctionner simultanément dans plusieurs systèmes de communication, tels que le Wi-Fi (2,4/5 GHz), le GSM/LTE, le GPS ou les bandes satellites. La demande croissante en systèmes sans fil compacts, multifonctionnels et à faible coût a rendu les antennes double bande essentielles dans les dispositifs de télécommunication modernes.

Les indicateurs de performance clés pour les antennes double bande incluent :

1. **Double résonance** : Capacité à atteindre deux fréquences de résonance indépendantes ou interdépendantes dans une plage spécifiée.
2. **Haute isolation** : Minimisation des interférences mutuelles entre les deux bandes.
3. **Caractéristiques de rayonnement stables** : Maintien de formes et directions de faisceaux cohérentes sur les deux bandes de fréquence.
4. **Miniaturisation** : Réduction de la taille tout en respectant les exigences en matière de bande passante et d'efficacité.
5. **Facilité d'intégration** : Compatibilité avec des structures planes ou tridimensionnelles pour les applications de type system-on-package ou antenne-sur-puce.

La fonctionnalité double bande peut être obtenue par diverses méthodes de conception physiques et électromagnétiques, notamment l'excitation de plusieurs modes résonants, l'utilisation d'éléments parasites ou couplés, le chargement réactif, les géométries fractales, ainsi que des combinaisons hybrides telles que les structures patch/DRA.

0.8.1 Classification des antennes double bande

La classification des antennes double bande se base généralement sur le principe de conception, la structure rayonnante et la méthode utilisée pour obtenir un fonctionnement double bande. Voici les principales catégories accompagnées d'exemples pratiques issus de la littérature récente.

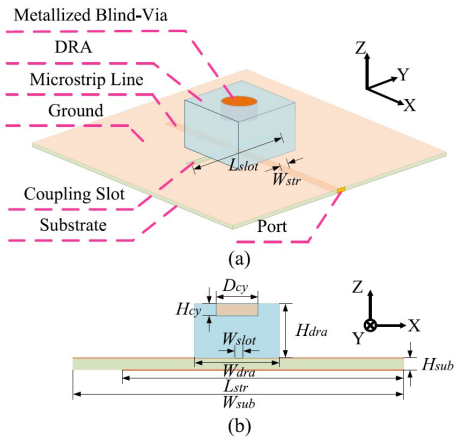

Fig. 1. Configuration of the proposed antenna. (a) Perspective view. (b) Side view. ($H_{sub} = 0.305$, $H_{dra} = 3.8$, $H_{cy} = 0.8$, $L_{slot} = 10.5$, $L_{str} = 19.2$, $W_{str} = 0.69$, $W_{slot} = 0.6$, $W_{dra} = 6$, $W_{sub} = 22.5$, $D_{cy} = 3$, unit: mm).

FIGURE 2 : Configuration de l'antenne proposée dans [1].

0.8.1.1 Antennes multi-modes

Ces antennes utilisent une seule structure rayonnante capable de supporter plusieurs modes résonants. Dans les antennes à résonateur diélectrique (DRA), des modes tels que $TE_{01\delta}$ et $TE_{11\delta}$ sont souvent excités pour générer un fonctionnement double bande. Le contrôle de la géométrie et de la position d'alimentation permet une excitation sélective des modes. Par exemple, les auteurs de [1] ont conçu une antenne DRA excitant les modes TE_{111} et TE_{131}, obtenant ainsi un fonctionnement double bande à 16 GHz et 38 GHz avec un rapport de fréquence de 2,36.

0.8.1.2 Antennes multi-éléments

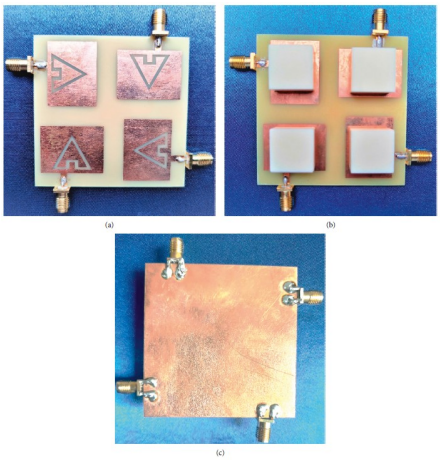

FIGURE 6. Proposed MIMO antenna: (a) top view without DR, (b) top view with DR, and (c) bottom view.

FIGURE 3 : Antenne MIMO proposée dans la référence [2].

Ce type d'antenne utilise deux ou plusieurs éléments résonants distincts, chacun accordé à une fréquence différente. Ces antennes comportent souvent des patchs, des fentes ou des DRAs

co-localisés, arrangés de manière compacte. La référence [2] a intégré des fentes triangulaires dans une configuration MIMO pour permettre un fonctionnement double bande avec une excellente isolation.

0.8.1.3 Antennes à double alimentation

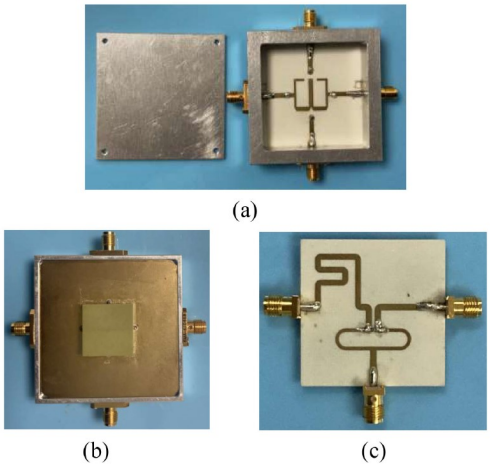

FIGURE 4 : Photographies du prototype fabriqué de l'antenne proposée dans [3].

Ces antennes comportent deux ports d'alimentation distincts, chacun responsable de l'excitation d'une bande de fréquence spécifique. Cette méthode permet un contrôle indépendant, mais augmente la complexité de conception. La référence [3] a implémenté une antenne DRA à alimentation différentielle fonctionnant à la fois comme filtre double bande et radiateur.

0.8.1.4 Conceptions intégrées filtre-antenne

Certaines antennes double bande fonctionnent à la fois comme éléments rayonnants et comme filtres, ce qui réduit la complexité globale du système. La référence [3] a combiné la fonction de filtrage et de rayonnement dans une DRA différentielle.

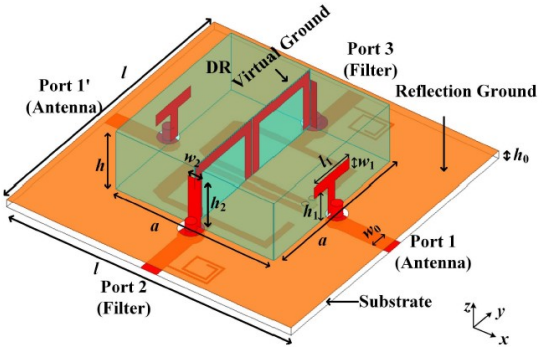

FIGURE 5 : Conception multifonction proposée de DRA différentielle et filtre double bande à contrôle indépendant dans [3].

0.8.1.5 Antennes double bande à gain renforcé

L'amélioration du gain est un objectif clé dans les conceptions double bande à haute fréquence. La référence [4] a augmenté le gain en utilisant un caoutchouc à haute densité.

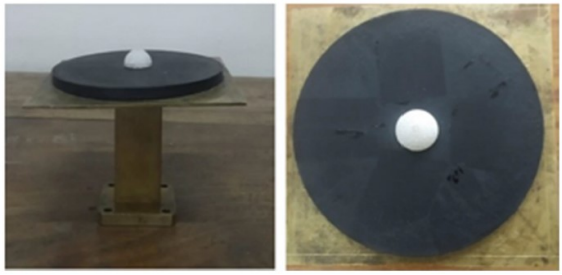

FIGURE 6 : Prototype de l'antenne dans [4].

0.9 Avantages des antennes double bande

Les antennes double bande offrent des avantages essentiels pour les systèmes sans fil modernes. Elles permettent de prendre en charge plusieurs standards (par exemple, LTE, 5G, Wi-Fi, GPS) à l'aide d'une seule structure, ce qui simplifie l'intégration matérielle et réduit le nombre de composants. Cela conduit à des conceptions compactes, idéales pour les dispositifs mobiles, portables et IoT, où l'espace est limité.

Elles rationalisent également l'interface RF en réduisant les réseaux d'alimentation et les interconnexions, ce qui diminue les coûts et la complexité d'assemblage. De plus, lorsqu'elles sont bien conçues, ces antennes peuvent être optimisées pour une haute efficacité dans les deux bandes, améliorant ainsi l'utilisation de l'énergie un avantage crucial dans les systèmes alimentés par batterie.

0.10 Défis et limitations

Malgré ces avantages, les antennes double bande présentent certains défis. Le couplage de fréquence entre les bandes peut altérer les performances et réduire l'isolation. Il est également difficile de maintenir une large bande passante dans les deux bandes, notamment dans des structures compactes.

La fabrication de géométries complexes ou multicouches peut nécessiter une grande précision, augmentant les coûts et réduisant le rendement de production. En outre, le processus de conception implique des optimisations et des simulations complexes, ce qui prolonge les délais de développement. Néanmoins, les conceptions proposées dans cette thèse offrent des stratégies pratiques pour surmonter ces problèmes et améliorer les performances des antennes double bande.

0.11 Antenne résonateur diélectrique double bande avec fonctions de filtrage pour les applications micro-ondes et millimétriques

Cet article présente une nouvelle conception d'antenne résonateur diélectrique cylindrique double (CDRA) capable de fonctionner efficacement aux fréquences micro-ondes et millimétriques pour les applications 5G. L'originalité de cette conception réside dans la capacité de l'antenne à supprimer les harmoniques et les modes d'ordre supérieur, ce qui améliore considérablement ses performances.

Les deux résonateurs sont fabriqués à partir de matériaux diélectriques ayant des permittivités relatives différentes. La procédure de conception comprend l'utilisation d'un grand résonateur diélectrique cylindrique (D_1), alimenté par une ligne micro-ruban verticale fixée à sa surface externe. Un espace d'air est créé à la base de D_1, et un petit CDRA (D_2) y est inséré, couplé via une fente gravée sur le plan de masse. De plus, un filtre passe-bas (LPF) est ajouté à la ligne d'alimentation de D_1 pour supprimer les harmoniques indésirables dans la bande millimétrique.

Le grand CDRA (D_1) avec une permittivité relative de 6 résonne à 2.4 GHz avec un gain réalisé de 6.7 dBi, tandis que le petit CDRA (D_2) avec une permittivité relative de 12 résonne à 28 GHz avec un gain réalisé de 15.2 dBi. Les dimensions de chaque résonateur peuvent être ajustées indépendamment afin de contrôler les deux bandes de fréquence. L'antenne présente une excellente isolation entre ses ports, avec des paramètres de diffusion S_{12} et S_{21} inférieurs à -72 dBi et -46 dBi respectivement, et ne dépassant jamais -35 dBi sur l'ensemble de la bande passante. Les résultats expérimentaux concordent avec les résultats simulés, validant ainsi l'efficacité de la conception. Cette antenne constitue une solution adéquate pour les applications 5G, combinant double bande, suppression d'harmoniques, flexibilité fréquentielle et forte isolation.

0.12 Antenne double bande à gain élevé avec fonctionnement indépendant pour les applications Sub-6 GHz et millimétriques

Ce travail présente une antenne hybride double bande innovante conçue pour offrir un gain élevé et une isolation supérieure, adaptée aux applications micro-ondes et millimétriques. La conception proposée intègre une antenne résonateur diélectrique cylindrique (CDRA) pour la bande micro-ondes, et des résonateurs à anneau patch pour la bande millimétrique, assurant un fonctionnement distinct et optimisé dans chaque bande de fréquence.

La conception suit une approche en plusieurs étapes : la CDRA est d'abord optimisée pour la bande micro-ondes, puis les résonateurs patch sont configurés pour les bandes millimétriques. Ces éléments sont combinés stratégiquement afin de garantir leur compatibilité tout en minimisant l'interférence inter-bande.

Pour améliorer les performances, des filtres sélectifs sont intégrés : un filtre passe-bas (LPF) pour la bande micro-ondes et un filtre passe-bande (BPF) pour la bande millimétrique, permettant de réduire la distorsion harmonique et d'améliorer la pureté spectrale. Des broches de court-circuit sont également utilisées pour renforcer l'isolation entre les bandes.

L'antenne atteint des performances remarquables, avec des bandes passantes de 11.7% à 5.8 GHz et 14.3% à 28 GHz, et des gains réalisés maximaux de 12.3 dBi et 17.2 dBi, respectivement. L'isolation est exceptionnelle, dépassant 54 dB pour la bande micro-ondes et 51 dB pour la bande millimétrique. L'intégration innovante de ces éléments de conception permet un fonctionnement à

fréquences indépendantes, ce qui rend cette antenne particulièrement adaptée aux systèmes de communication double bande de nouvelle génération.

0.13 Intégration d'une filtenna sub-6 GHz avec une antenne à résonateur diélectrique millimétrique en réseau pour les applications 5G

Cet article présente une antenne filtenna à patch fonctionnant à 5.2 GHz, intégrée avec un réseau d'antennes CDRA résonant à 28 GHz, permettant une communication simultanée en bandes micro-ondes et millimétriques.

Une antenne patch elliptique est d'abord conçue pour fonctionner à 5.2 GHz dans la bande sub-6 GHz. Une cavité creuse est introduite au centre du patch pour intégrer le CDRA. Ensuite, un résonateur diélectrique cylindrique (CDR) est conçu pour résonner à 28 GHz. Ces deux résonateurs sont combinés de manière à assurer un fonctionnement harmonieux dans les deux bandes.

Pour supprimer les harmoniques indésirables de la bande inférieure et améliorer l'isolation, un filtre passe-bas est intégré à l'antenne sub-6 GHz. Afin d'augmenter le gain réalisé dans la bande millimétrique, une antenne élémentaire est conçue et ensuite étendue en un réseau 2 × 2, puis à une configuration 4 × 4 (16 éléments) pour renforcer le gain global.

Le système final atteint des bandes passantes de 34.5% et 16.8%, avec des gains maximaux de 9.1 dBi pour la bande sub-6 GHz et 19.0 dBi pour la bande millimétrique. Le design montre également une excellente isolation, dépassant 73 dB à 5.2 GHz et 62 dB à 28 GHz. L'innovation majeure de cette étude réside dans l'intégration d'une filtenna micro-onde avec un réseau millimétrique à gain élevé. Contrairement aux recherches existantes focalisées sur la double bande, cette étude souligne l'importance du filtrage dans la bande inférieure pour améliorer l'isolation et supprimer les harmoniques, tout en assurant un rayonnement à haut gain pour les communications à longue distance. Les autres contributions incluent le contrôle indépendant des bandes, la réduction de la taille globale et la large bande passante.

0.14 Conclusion

Cette thèse a introduit et démontré de nouvelles structures d'antennes à résonateur diélectrique double bande (DRA) conçues pour un fonctionnement efficace aux fréquences micro-ondes et millimétriques, motivées par les exigences croissantes des systèmes sans fil 5G et de nouvelle génération. Trois architectures d'antenne distinctes ont été proposées et développées afin de relever les défis liés à la large séparation des fréquences, au gain élevé, à la compacité et à l'excellente isolation entre bandes.

La première conception utilise deux DRAs cylindriques imbriqués pour obtenir une double résonance à 2,4 GHz et 28 GHz, avec un filtrage passe-bas intégré pour supprimer les harmoniques indésirables. La deuxième architecture présente une structure hybride combinant un DRA cylindrique pour la bande millimétrique avec un réseau d'antennes patch en série, intégrant des filtres passe-bas et passe-bande ainsi que des broches de court-circuit pour assurer une forte isolation et un contrôle indépendant de chaque bande. La troisième et dernière configuration intègre une filtenna elliptique sub-6 GHz avec un réseau DRA millimétrique 4×4, atteignant une augmentation substantielle du gain tout en maintenant compacité et intégrité spectrale.

Dans toutes ces conceptions, plusieurs performances clés ont été atteintes, notamment des gains réalisés élevés allant jusqu'à 19 dBi à 28 GHz, des niveaux d'isolation supérieurs à 70 dB entre les bandes, et une capacité de réglage fréquentiel indépendant. Ces antennes ont été fabriquées avec des substrats commercialement disponibles et validées par des simulations électromagnétiques complètes ainsi que des mesures expérimentales, confirmant la faisabilité et l'efficacité des approches proposées. Collectivement, les contributions de cette thèse fournissent des solutions d'antenne pratiques et évolutives adaptées aux systèmes de communication sans fil à haut débit émergents.

0.15 Travaux futurs

Sur la base des résultats et innovations de cette recherche, plusieurs axes prometteurs peuvent être envisagés pour faire progresser davantage la technologie des antennes double bande. Une extension possible concerne l'intégration des structures d'antennes proposées dans des systèmes à entrées multiples et sorties multiples (MIMO), notamment ceux utilisant les techniques de formation et de pilotage de faisceaux (beamforming et beam-steering). Cette intégration nécessitera une conception soignée des dispositions afin de préserver la forte isolation et le faible couplage mutuel démontrés dans ce travail.

Une autre voie importante est le développement d'architectures d'antennes reconfigurables et réglables utilisant des technologies telles que les diodes varicap, les commutateurs PIN, les diélectriques ajustables ou les cristaux liquides. Ces composants permettraient un contrôle dynamique des fréquences, de la polarisation et des caractéristiques de rayonnement, améliorant ainsi l'adaptabilité des antennes dans des environnements variables.

Par ailleurs, les recherches futures pourraient explorer la conception de réseaux d'antennes compacts et multifonctionnels combinant la double bande avec la diversité de polarisation ou la polarisation circulaire, potentiellement facilitée par des métasurfaces ou des mécanismes d'ondes fuyantes. Des méthodes avancées de fabrication, telles que l'impression 3D ou la fabrication additive utilisant des matériaux diélectriques à gradient, pourraient également être étudiées pour réaliser des géométries complexes avec une grande précision et une répétabilité de performances.

Enfin, l'intégration à l'échelle du système complet incluant antennes, circuits d'adaptation, filtres et composants d'interface RF sur une plateforme compacte unique reste une étape cruciale vers la mise en œuvre commerciale. La poursuite de ces axes étendra l'adaptabilité, l'efficacité et le champ d'application des conceptions d'antennes développées dans cette thèse, contribuant ainsi à l'avancement des technologies de communication sans fil futures.

TABLE OF CONTENTS

LIST OF FIGURES

LIST OF TABLES

LIST OF ABBREVIATIONS

5G 5th Generation Mobile Network

B5G Beyond 5G

6G 6th Generation

DRA Dielectric Resonator Antenna

eMBB enhanced mobile broadband

URLLC ultra-reliable low-latency communications

mMTC massive machine-type communications

WRA Waveguide Resonator Antenna

FPRA Fabry–Perot Resonator Antenna

mm-wave Millimeter Wave

dBi Decibels Relative to an Isotropic Antenna

dB Decibels

GHz Giga Hertz

IoT Internet of Things

CST Computer Simulation Technology

CDR Cylindrical Dielectric Resonator

FEM Finite-Element Method

1 INTRODUCTION

With the advancement of communication technology, there is a growing demand for high-speed wireless communication systems. The fifth generation 5G wireless network is anticipated to revolutionize the telecommunication industry by offering higher data rates, lower latency, and better coverage. However, to achieve these features, the development of suitable antenna technology for the microwave and millimeter-wave frequency bands is critical. Dielectric resonator antennas DRAs have emerged as an attractive solution due to their low profile, high gain, and high radiation efficiency. In particular, dual-band DRAs are highly sought after because they can operate over a wide range of frequencies. This research aims to design and develop new dual-band DRAs for microwave and millimeter-wave applications.

1.1 Motivation

The rapid expansion of wireless communication technologies, especially with the emergence of 5G and the anticipated transition to beyond-5G Beyond 5G (B5G) systems, has significantly increased the demand for high-performance antenna solutions. Modern communication networks are expected to support a wide array of services, including enhanced mobile broadband (eMBB), ultra-reliable low-latency communications (URLLC), and massive machine-type communications (mMTC). These services rely on efficient spectrum utilization across both the sub-6 GHz and mm-wave) frequency bands to meet the diverse performance requirements of high data rates, wide coverage, and low latency.

Traditional antenna systems often face limitations in simultaneously operating across multiple widely separated frequency bands, primarily due to issues related to size, interference, poor isolation, and harmonic distortion. This has prompted the need for dual-band antennas capable of operating in both the microwave and mm-wave regimes while maintaining compact size, high gain, wide bandwidth, and minimal inter-band coupling.

Dielectric Resonator Antennas (DRAs) have emerged as a promising candidate for such applications, thanks to their inherent advantages, including low loss at high frequencies, high radiation efficiency, and flexible geometrical configurations. However, designing dual-band DRAs that offer independent frequency control, harmonic suppression, and strong isolation remains a significant challenge.

Motivated by these challenges and opportunities, this thesis focuses on the development of novel dual-band DRA architectures optimized for microwave and mm-wave frequency bands. Through innovative designs integrating filtering structures, hybrid resonators, and scalable array configura-

tions, this research aims to advance the state-of-the-art in antenna technology, offering robust solutions that can be directly applied to future multi-standard wireless systems.

1.2 Problem Statement

The continuous evolution of wireless communication systems, particularly with the advent of 5G and the research toward 6th Generation (6G), has introduced stringent requirements for antenna performance. Modern antenna systems must be capable of supporting multiple frequency bands simultaneously, especially the sub-6 GHz (microwave) band for wide-area coverage and the millimeter-wave (mm-wave) band for high-speed, short-range communication. This dual-band operation is essential to satisfy the diverse needs of high-throughput data, low latency, and ubiquitous connectivity in emerging applications such as autonomous systems, smart cities, and the Internet of Things (IoT).

Despite the critical need, designing efficient dual-band antennas that operate across these widely separated frequency ranges remains a significant challenge. One of the primary difficulties is achieving high isolation between the two frequency bands. Mutual coupling can degrade antenna performance, reduce efficiency, and introduce unwanted interference, particularly when both bands are excited simultaneously within a compact structure.

Another pressing issue is the generation of harmonic signals from the low-frequency radiator, which may interfere with the operation of the mm-wave band. Suppressing these unwanted harmonics without affecting the antenna's performance requires the integration of precise filtering structures. Moreover, most existing dual-band designs suffer from coupled frequency responses, where tuning one band unintentionally alters the other. This lack of independent control hinders flexibility and complicates the optimization process during design.

In addition to these technical challenges, achieving high gain and high radiation efficiency in both frequency bands, especially at mm-wave frequencies, where path loss is inherently high, is also difficult. These performance targets must be met while maintaining a compact and manufacturable antenna design, ideally using cost-effective materials and commercially available fabrication techniques.

Although numerous studies have explored dual-band antennas, very few have successfully addressed all these challenges in a unified design. Many reported solutions either rely on bulky hybrid structures, lack harmonic suppression mechanisms, or fail to offer independently tunable frequency bands with high isolation and gain. Therefore, there remains a significant research gap in realizing practical dual-band antennas for 5G and beyond.

This thesis aims to address these challenges by proposing new dielectric resonator-based antenna architectures that provide independent dual-band operation, high isolation, and harmonic suppression. The proposed antennas offer compact, efficient, and high-performance solutions for

future wireless communication systems through careful integration of filtering elements, optimized geometries, and advanced excitation techniques.

1.3 Applications of the Proposed Antennas

The proposed dual-band high-gain antenna, operating in both the sub-6 GHz and 28 GHz mm-wave frequency ranges, exhibits several characteristics that render it highly suitable for modern wireless communication systems. The compact form factor ($100 \times 100 \times 20$ mm^3), combined with the realized gain levels ranging from 7.6dBi to 12.5dBi in the sub-6GHz band and from 15dBi to 19dBi at 28GHz, enables its deployment in a diverse array of high-performance applications.

First and foremost, the antenna is well-suited for fifth-generation (5G) wireless infrastructure, including base stations and small cells, by supporting both 5G NR Frequency Range 1 (FR1) and Frequency Range 2 (FR2). The high gain at 28 GHz ensures adequate compensation for the increased free-space path loss at millimeter-wave frequencies, which is critical in dense urban environments.

Additionally, the antenna is highly applicable in fixed wireless access (FWA) systems, where its dual-band operation facilitates reliable high-throughput connectivity over long distances. This makes it ideal for delivering broadband internet services in underserved rural or suburban areas.

The antenna's high-gain performance also aligns with the requirements of point-to-point and point-to-multipoint microwave backhaul links, which are crucial for supporting network densification in next-generation wireless networks. Including tunable and filtering capabilities further enhances its utility in mitigating interference and improving spectral efficiency.

Moreover, the antenna is suitable for passive radar and remote sensing systems where fixed directional high-gain radiation is desirable. While the fixed-beam nature at 28 GHz limits dynamic tracking, it does not impede its use in applications where the target location is known or remains stationary.

Finally, the antenna's characteristics make it a viable candidate for ground-based low Earth orbit (LEO) satellite communication terminals operating in the Ka-band. Its ability to offer high gain at mm-wave frequencies within a compact footprint is advantageous in portable or fixed satcom installations.

These multifaceted applications underscore the adaptability of the proposed antenna design in meeting the diverse requirements of contemporary and emerging wireless technologies.

1.4 Objectives

The primary objective of this thesis is to design, develop, and experimentally validate novel dual-band antenna structures based on dielectric resonators that are capable of efficient operation in both the microwave (sub-6 GHz) and millimeter-wave (mm-wave) frequency bands. These antennas are intended to meet the increasing demands of emerging wireless communication systems, particularly those aligned with 5G and beyond, which require high data rates, low latency, and reliable connectivity across heterogeneous frequency spectra.

Specifically, the thesis aims to address several key technical challenges associated with dual-band antenna design. First, it seeks to achieve high gain and radiation efficiency in both frequency bands while maintaining a compact and manufacturable antenna profile. This includes the development of structures that can support high-frequency operation without incurring excessive losses, particularly at mm-wave frequencies where path attenuation is severe.

Second, the research focuses on ensuring high isolation between the two bands to minimize mutual coupling and inter-band interference. This objective is pursued through innovative structural designs, the use of shorting pins, and the integration of filtering elements.

Third, the work aims to realize truly independent frequency tuning for each band. In many existing designs, changes to one band's parameters unintentionally affect the other. By developing geometrically and electromagnetically decoupled resonator structures, the proposed antennas allow precise control over each band individually.

Another important goal is to suppress unwanted harmonics that arise from the microwave band and interfere with the mm-wave operation. To that end, the thesis explores the use of embedded low-pass and band-pass filters that are compact and compatible with the overall antenna architecture.

Finally, the antenna prototypes are to be designed using commercially available, low-loss substrates, and validated through full-wave simulations and experimental measurements. The objective is to demonstrate the practicality and effectiveness of the proposed solutions in real-world scenarios.

Together, these objectives form the foundation of this thesis, which contributes to the advancement of compact, high-performance dual-band antennas suitable for next-generation communication systems.

1.5 Methodology

The flow diagram in Fig. 1.1 shows the research methodology. The research methodology will consist of several phases, as described below :

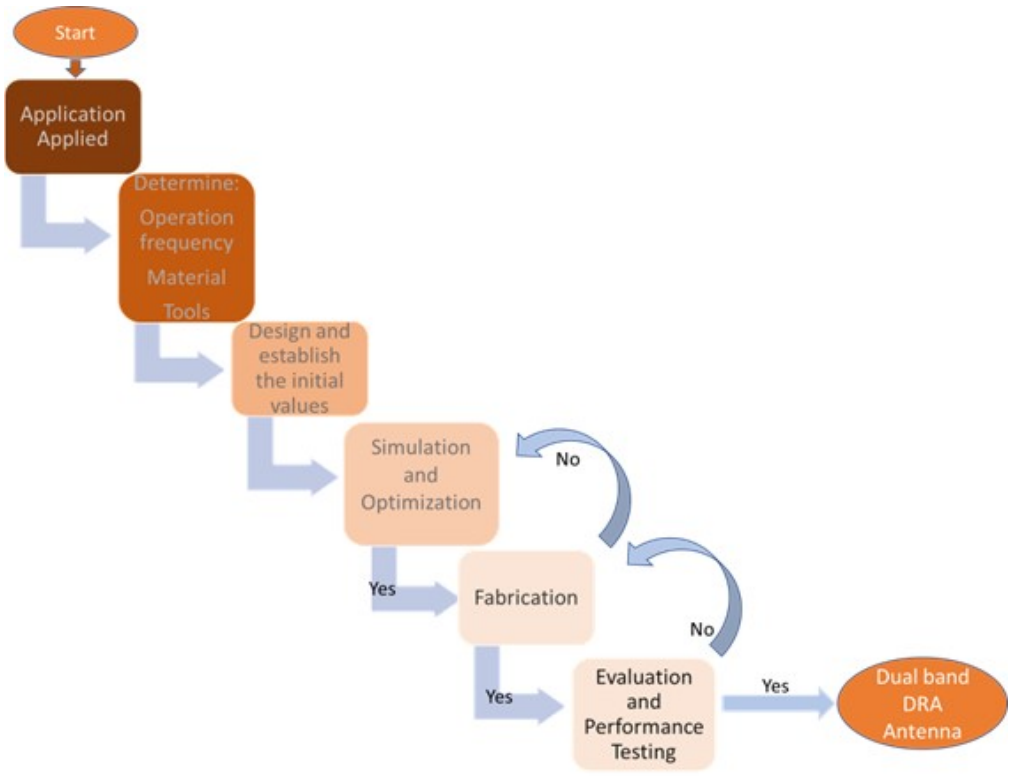

FIGURE 1.1 : Methodology Process.

1. Literature review : A comprehensive literature review will be conducted to understand the current state-of-the-art in dual-band DRAs for microwave and millimeter-wave applications. This will provide the basis for the design and development of new dual-band DRAs.

2. Design and simulation : Different dielectric materials and shapes will be investigated to design new dual-band DRAs. The antennas' performance will be simulated using commercial electromagnetic simulation software to optimize their resonant frequencies and bandwidths.

3. Prototyping and testing : The antennas' prototypes will be fabricated using a high-precision milling machine and tested in an anechoic chamber. The antennas' radiation patterns, gain, efficiency, and return loss will be measured and compared with the simulation results.

4. Optimization : The measured results will be used to optimize the antennas' resonant frequencies, bandwidths, and feed structures.

Overall, the methodology adopted in this thesis aims to ensure a rigorous and systematic approach to conducting a comprehensive and up-to-date literature review on intelligent beam switching antennas based on reconfigurable and to contribute to advancing this promising technology for enhancing the performance of wireless communication systems.

1.6 Thesis Contributions

This thesis presents a series of novel contributions in the field of dual-band antenna design, particularly focusing on dielectric resonator-based solutions for simultaneous operation at microwave and millimeter-wave frequencies. The contributions directly address critical challenges such as high isolation, harmonic suppression, and independent frequency control, all within compact and manufacturable structures suitable for integration into 5G and future wireless systems.

One of the main contributions is the design and implementation of three innovative dual-band antennas, each developed and validated through peer-reviewed journal publications. These antennas introduce hybrid configurations that strategically combine dielectric resonator antennas (DRAs) with patch-based and arrayed elements to ensure optimal performance in both sub-6 GHz and mm-wave bands. Each antenna features unique structural arrangements and feeding mechanisms that support the excitation of distinct frequency modes with minimal interference.

Another significant contribution is the demonstration of independent control over the resonance frequencies of the two bands. Unlike many existing designs where frequency tuning is interdependent, the proposed configurations enable geometric and electromagnetic decoupling, allowing each frequency band to be adjusted separately without compromising the performance of the other. This flexibility is particularly valuable in practical applications where precise frequency allocation is critical.

The thesis also contributes to the advancement of filtering techniques in antenna systems. Embedded low-pass and band-pass filters are employed to suppress unwanted harmonics, especially those generated by the microwave section that could interfere with the mm-wave band. The use of Compact Microstrip Resonant Cells (CMRCs) and folded Chebyshev structures not only improves the spectral purity of the antenna response but also enhances inter-band isolation.

Further, high isolation levels between the two operational bands are achieved through a combination of careful structural layout and the strategic placement of shorting pins. In one of the designs, isolation exceeds 73 dB at the microwave frequency and 62 dB at the mm-wave band—figures that are among the highest reported for compact dual-band antennas.

Lastly, all proposed antennas are realized using low-cost, commercially available substrates such as Rogers RO3003 and RO3210. The use of accessible materials, combined with simplified manufacturing processes, ensures the practicality of the designs for future deployment in mobile, vehicular, and base station platforms. Overall, the thesis provides a set of compact, high-gain, and harmoniously clean antenna solutions that push the boundaries of dual-band performance in modern telecommunication systems.

1.7 Thesis Outline

This thesis is structured as a paper-based dissertation, where each core research contribution is presented as a standalone chapter based on peer-reviewed journal publications. The organization is as follows :

Chapter 1 : Introduction
This chapter presents the motivation and problem statement of this work. It also outlines the applications of the proposed antennas, the research objectives, the methodology, and the main contributions of the thesis.

Chapter 2 : Background and Literature Review
A comprehensive review of related work on dual-band operation and dielectric resonator antennas (DRAs). Existing gaps in the literature are identified, justifying the need for the proposed designs.

Chapter 3 : Dual-Band Dielectric Resonator Antenna with Filtering Features for Microwave and Mm-Wave Applications
This chapter is based on the journal article published in *Micromachines* (MDPI, 2023). It presents a novel dual-band antenna composed of two nested cylindrical dielectric resonators with integrated filtering features to suppress unwanted harmonics and ensure high isolation.

Chapter 4 : High-Gain Dual-Band Antenna with Independent Frequency Operation for Sub-6 GHz and Millimeter-Wave Applications
This chapter corresponds to the article published in *AEÜ - International Journal of Electronics and Communications* (2025). It introduces a hybrid antenna integrating a CDRA with series-fed patch resonators and filtering elements, achieving high gain and independently tunable dual-band operation.

Chapter 5 : Sub-6 GHz Filtenna Integration With Mm-Wave Dielectric Resonator Antenna Array for 5G Applications
This chapter is derived from the paper published in *IEEE Access* (2025). It details the integration of a sub-6 GHz elliptical filtenna with a mm-wave dielectric resonator array, enhancing gain and achieving exceptional isolation through filtering and array configuration.

Chapter 6 : Multi-band Antennas Dielectric Resonator-based For Microwave And Mm-wave Bands
This chapter is based on two conference papers. The first is titled 'Integrating a Fabry–Perot Resonator into a Dielectric Resonator Antenna for Microwave and Millimeter-Wave Operations,' presen-

ted at the 2023 IEEE (USNC-URSI). The second paper is titled 'Triple-Band Dielectric Resonator Antenna for Millimeter-Wave and Sub-6 GHz Applications,' presented at the 2024 (ICTIS) IEEE.

Chapter 7 : Conclusion and Future Work

This chapter synthesizes the accomplishments of this thesis and proposes future work in the research orientation.

1.8 Publications

Journals :

1. **Bizan, Mohamed Sedigh,** and Tayeb A. Denidni. "Sub-6 GHz Filtenna Integration With Mm-wave Dielectric Resonator Antenna Array for 5G Applications." IEEE Access (2025).
(Published).
2. **Bizan, Mohamed Sedigh,** PourMohammadi, Peyman PourMohammadi, Amjad Iqbal, and Tayeb A. Denidni. "High-gain dual-band antenna with independent frequency operation for Sub-6 GHz and millimeter-wave applications." AEU-International Journal of Electronics and Communications (2025) : 155743.
(Published).
3. **Bizan, Mohamed Sedigh,** Hassan Naseri, Peyman Pourmohammadi, Noureddine Melouki, Amjad Iqbal, and Tayeb A. Denidni. "Dual-band dielectric resonator antenna with filtering features for microwave and mm-wave applications." Micromachines 14, no. 6 (2023) : 1236.
(Published).
4. Melouki, Noureddine, Fahad Ahmed, Peyman PourMohammadi, Hassan Naseri, **Bizan, Mohamed Sedigh,** Amjad Iqbal, and Tayeb A. Denidni. "3D-Printed Conformal Meta-Lens with Multiple Beam-Shaping Functionalities for Mm-Wave Sensing Applications." Sensors 24, no. 9 (2024) : 2826.
(Published).
5. PourMohammadi, Peyman, Hassan Naseri, Noureddine Melouki, Fahad Ahmed, **Bizan, Mohamed Sedigh,** Amjad Iqbal, and Tayeb A. Denidni. "A Fabry–Perot antenna using a frequency selective surface layer with wideband and Low RCS for Mm-wave applications." AEU-International Journal of Electronics and Communications 169 (2023) : 154736.
(Published).

Conferences :

6. **Bizan, Mohamed Sedigh,** and Tayeb A. Denidni. "Triple-band Antenna Dielectric Resonator-based for Millimeter-wave and Sub-6 Applications." In 2024 International Conference on Telecommunications and Intelligent Systems (ICTIS), pp. 1-3. IEEE, 2024.
(Published).
7. **Bizan, Mohamed Sedigh,** and Tayeb A. Denidni. "Dual-band Hybrid Dielectric Resonator-patch Antenna for Microwave and Mm-wave Applications." In 2024 International Conference on Computing, Internet of Things and Microwave Systems (ICCIMS), pp. 1-2. IEEE, 2024.
(Published).
8. **Bizan, Mohamed Sedigh,** H. Naseri, P. PourMohammadi, and T. A. Denidni. "Ultra-Wideband Dielectric Resonator Antenna Fed By Printed Ridge Gap Waveguide Technology." In 2024

IEEE International Symposium on Antennas and Propagation and INC/USNC-URSI Radio Science Meeting (AP-S/INC-USNC-URSI), pp. 1933-1934. IEEE, 2024.
(Published).

9. Naseri, Hassan, Peyman Pourmohammadi, **Bizan, Mohamed Sedigh,** and Tayeb A. Denidni. "Butler Matrix-Based Beam Switching with Frequency-Tunable MIMO Array." In 2024 IEEE International Symposium on Antennas and Propagation and INC/USNC-URSI Radio Science Meeting (AP-S/INC-USNC-URSI), pp. 2475-2476. IEEE, 2024.
(Published).
10. **Bizan, Mohamed Sedigh,** Hassan Naseri, Peyman PourMohammadi, and Tayeb A. Denidni. "Integrate Fabry–Perot resonator into dielectric resonator antenna for microwave and mm-wave operations." In 2023 IEEE International Symposium on Antennas and Propagation and USNC-URSI Radio Science Meeting (USNC-URSI), pp. 1161-1162. IEEE, 2023.
(Published).
11. PourMohammadi, Peyman, Hassan Naseri, Noureddine Melouki, Fahad Ahmed, **Bizan, Mohamed Sedigh,** Amjad Iqbal, and Tayeb A. Denidni. "A Wideband Fabry-Perot Antenna with a Bianisotropic FSS Layer." In 2023 IEEE International Symposium on Antennas and Propagation and USNC-URSI Radio Science Meeting (USNC-URSI), pp. 649-650. IEEE, 2023.
(Published).
12. Naseri, Hassan, Peyman Pourmohammadi, **Bizan, Mohamed Sedigh,** Noureddine Melouki, Fahad Ahmed, Amjad Iqbal, and Tayeb A. Denidni. "Reconfigurable dielectric resonator OAM antenna with augmented modes." In 2023 IEEE International Symposium on Antennas and Propagation and USNC-URSI Radio Science Meeting (USNC-URSI), pp. 703-704. IEEE, 2023.
(Published).
13. **Bizan, Mohamed Sedigh,** Mohamed Mamdouh M. Ali, and Tayeb A. Denidni. "Design of sub-6 GHz and millimeter-wave 5g embedded dielectric resonator antenna." In 2022 IEEE International Symposium on Antennas and Propagation and USNC-URSI Radio Science Meeting (AP-S/URSI), pp. 59-60. IEEE, 2022.
(Published).
14. **Bizan, Mohamed Sedigh,** Ghada H. Elzwawi, Muhammad M. Tahseen, and Tayeb A. Denidni. "Bandwidth Enhancement by Position Perturbations in Stacked Dielectric Resonator Antenna." In 2018 IEEE International Symposium on Antennas and Propagation and USNC/URSI National Radio Science Meeting, pp. 2091-2092. IEEE, 2018.
(Published).
15. **Bizan, Mohamed Sedigh,** Peyman Pourmohammadi, Hassan Naseri, Amjad Iqbal, and Tayeb Denidni". "Dielectric Resonator Antenna With Integrated Fabry-Perot Cavity". In 2023 URSI International Symposium on Electromagnetic Theory (EMTS) (URSI EMTS 2023)", Vancouver, Canada, 2,21, may, 2023.
(Published).

16. Hassan Naseri Gheisanab, Peyman Pourmohammadi **Bizan, Mohamed Sedigh,** Noureddine Melouki, Fahad Ahmed, Amjad Iqbal, and Tayeb Denidni."Triple-Mode OAM Generating Dielectric Resonator Antenna". In 2023 URSI International Symposium on Electromagnetic Theory (EMTS) (URSI EMTS 2023)", Vancouver, Canada, 2,21, may, 2023.
(Published).
17. Peyman Pourmohammadi, Hassan Naseri Gheisanab, **Bizan, Mohamed Sedigh,** Noureddine Melouki, Fahad Ahmed, Amjad Iqbal, and Tayeb Denidni."A Wideband Anisotropic Metasurface for Cross-Polarization Applications". In 2023 URSI International Symposium on Electromagnetic Theory (EMTS) (URSI EMTS 2023), Vancouver, Canada, 2,21 May 2023.
(Published).
18. **Bizan, Mohamed Sedigh,** Naseri, Hassan, and Tayeb A. Denidni. "Dual-band Hybrid Patch-Dielectric Resonator Antenna for Mm-wave and Microwave Applications." In 2025 IEEE International Symposium on Antennas and Propagation and USNC/URSI National Radio Science Meeting.
(Published).
19. Naseri, Hassan, Peyman Pourmohammadi,**Bizan, Mohamed Sedigh,** Shuvra Baru, and Tayeb A. Denidni. "Dual-Polarized Reconfigurable Beam-Steering Using the New Feeding Network Topology." In 2025 IEEE International Symposium on Antennas and Propagation and USNC/URSI National Radio Science Meeting.
(Published).

2 BACKGROUND AND LITERATURE REVIEW

This section presents a brief background on the DRA definition, theory of operation, and design formulas.

2.1 Dual-Band Antennas : Background and Fundamentals

2.2 Definition and Key Features

A dual-band antenna is a type of antenna that is capable of transmitting and/or receiving electromagnetic waves at two distinct frequency bands. This feature allows a single antenna to operate in multiple communication systems simultaneously, such as Wi-Fi (2.4/5 GHz), GSM/LTE, GPS, or satellite bands. The increasing demand for compact, multifunctional, and low-cost wireless systems has made dual-band antennas an essential component in modern telecommunication devices.

Key performance metrics for dual-band antennas include :

1. **Dual resonance :** The ability to achieve two independent or interdependent resonant frequencies within a specified range.
2. **High isolation :** Ensuring minimal mutual interference between the bands.
3. **Stable radiation characteristics :** Maintaining consistent beam shapes and directions over both frequency bands.
4. **Miniaturization :** Achieving compact size while meeting bandwidth and efficiency requirements.
5. **Ease of integration :** Compatibility with planar and three-dimensional structures for system-on-package or antenna-on-chip applications.

Dual-band functionality can be achieved through various physical and electromagnetic design methods, including the excitation of multiple resonant modes, use of parasitic or coupled elements, reactive loading, fractal geometries, and hybrid combinations such as patch–DRA structures.

2.3 Dual-Band Antenna Classification and Techniques

2.3.1 Classification of Dual-Band Antennas

The classification of dual-band antennas is generally based on the design principle, radiating structure, and method of achieving dual-band operation. Below are the key categories along with practical examples from recent literature.

2.3.1.1 Multi-Mode Antennas

These antennas utilize a single radiating structure that supports multiple resonant modes. In dielectric resonator antennas (DRAs), modes like $TE_{01\delta}$ and $TE_{11\delta}$ are often excited to generate dual-band performance. Control over geometry and feed positioning enables selective mode excitation. For example, the authors in [1] designed a DRA that excited the TE_{111} and TE_{131} modes, achieving dual-band operation at 16 GHz and 38 GHz with a frequency ratio of 2.36. Similarly, [5] employed TE_{111} and hybrid modes for narrow/wideband dual-band gain enhancement.

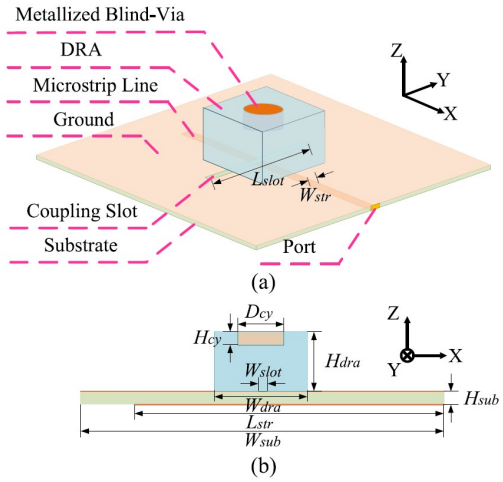

Fig. 1. Configuration of the proposed antenna. (a) Perspective view. (b) Side view. ($H_{sub} = 0.305$, $H_{dra} = 3.8$, $H_{cy} = 0.8$, $L_{slot} = 10.5$, $L_{str} = 19.2$, $W_{str} = 0.69$, $W_{slot} = 0.6$, $W_{dra} = 6$, $W_{sub} = 22.5$, $D_{cy} = 3$, unit: mm).

FIGURE 2.1 : Configuration of the proposed antenna of [1].

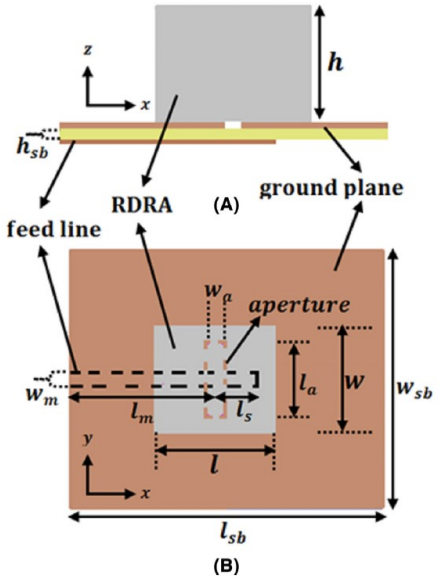

FIGURE 2.2 : Geometry of the dual-band rectangular dielectric resonator antenna (RDRA) in [5].

2.3.1.2 Multi-Element Antennas

This class uses two or more separate resonating elements, each tuned to a different frequency. Such antennas often feature co-located patches, slots, or DRAs arranged compactly. Reference [2] further integrated triangular slots in a MIMO configuration to support dual-band operation with excellent isolation.

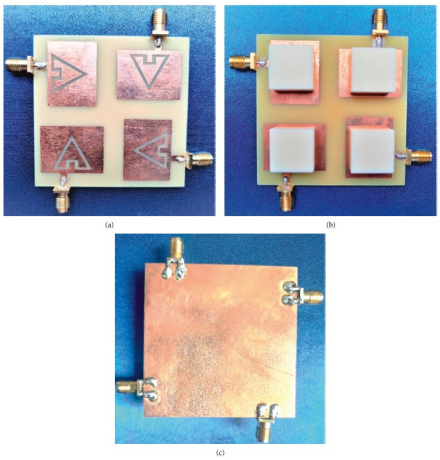

FIGURE 6: Proposed MIMO antenna: (a) top view without DR, (b) top view with DR, and (c) bottom view.

FIGURE 2.3 : Proposed MIMO antenna of reference [2].

2.3.1.3 Dual-Fed Antennas

These antennas incorporate two distinct feed ports, each responsible for exciting a specific frequency band. This method enables independent control but increases design complexity. Reference [3] implemented a differential-fed DRA functioning as both a dual-band filter and radiator.

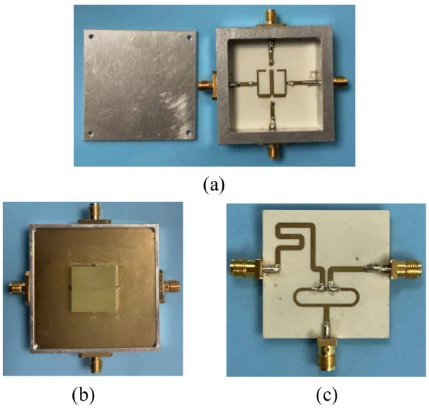

FIGURE 2.4 : Photographs of the fabricated prototype of the proposed antenna in [3].

2.3.1.4 Reconfigurable Antennas

Reconfigurable antennas integrate tunable components, such as PIN diodes, varactors, or MEMS, to dynamically alter resonance and radiation properties. These are especially useful in SDR and cognitive radio systems. For instance, [6] introduced PIN-controlled parasitic elements.

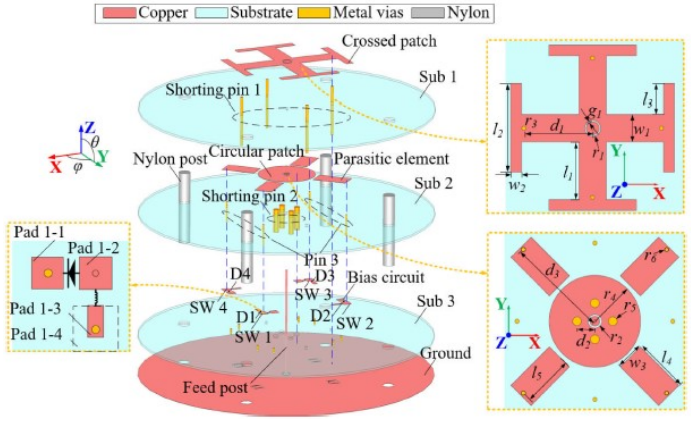

FIGURE 2.5 : Geometry of the proposed antenna in [6].

2.3.1.5 Hybrid Antennas

Hybrid antennas combine different radiating mechanisms, such as microstrip patches, DRAs, and dielectric rods, to enhance impedance bandwidth and radiation characteristics. Reference [7] employed a half-cut cylindrical DRA on a rectangular base to facilitate dual-band operation without complex analytical modelling.

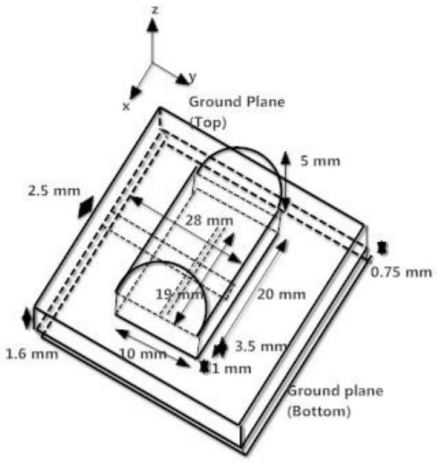

FIGURE 2.6 : Side view of the proposed radiator in reference [7].

2.3.1.6 Circularly Polarized Antennas

Structural perturbation or feed manipulation achieves circular polarization (CP) in dual-band antennas. In [8], orthogonal DRs and I-monopole feed achieved wideband CP at both 3.7–4.4 GHz and 5.8–6.2 GHz.

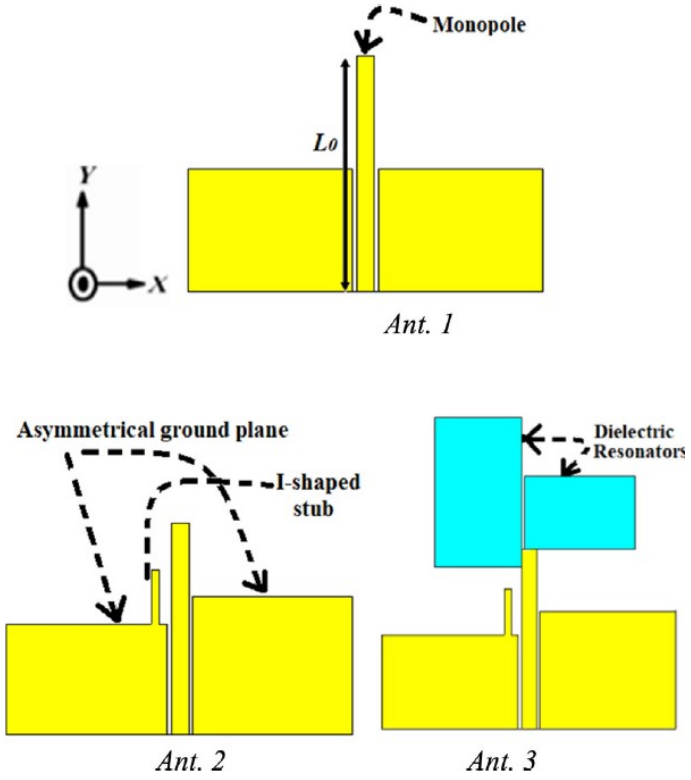

FIGURE 2.7 : Evolution of the proposed antenna from a basic monopole in [8].

2.3.1.7 MIMO-Based Dual-Band Antennas

These designs use multiple elements in MIMO arrangements while maintaining dual-band characteristics. Reference [9] built a 2×2 DBDP array covering 23.5–30.8 GHz and 36.7–47.3 GHz.

2.3.1.8 Filter-Antenna Integrated Designs

Some dual-band antennas function simultaneously as radiators and filters, reducing overall system complexity. Reference [3] combined filtering and radiation in a differential DRA. [10] reused dielectric structures in a shared-aperture configuration, enhancing isolation between dual-band operations.

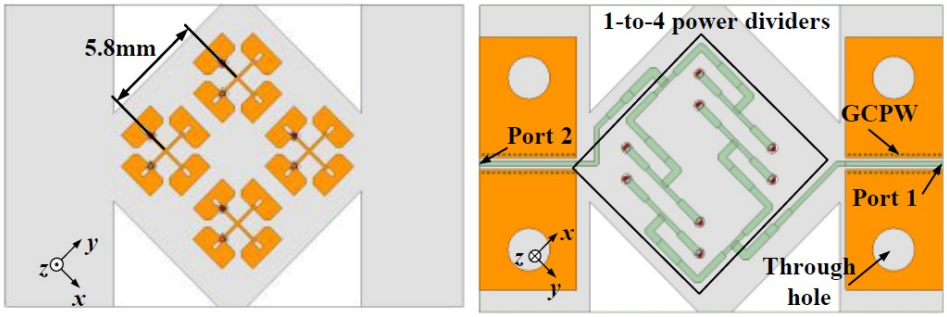

Fig. 8. Configurations of the proposed 2 × 2 array, (a) Top view (b) bottom view.

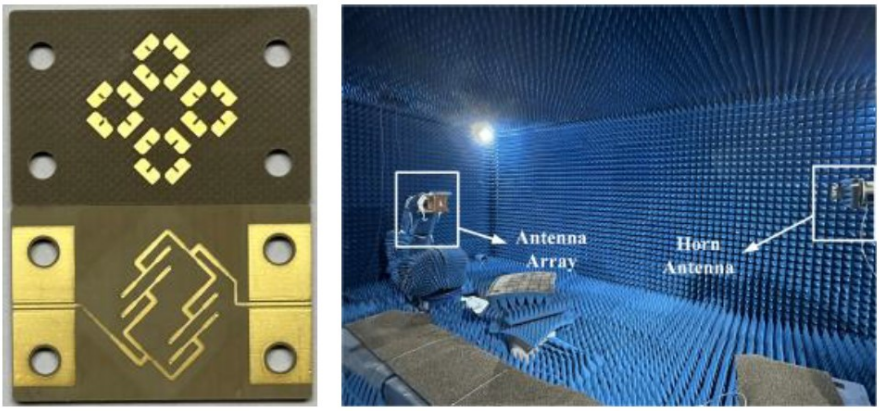

Fig. 9. (a) Top and bottom views of the prototype. (b) Testing environment in the far-field chamber.

FIGURE 2.8 : The proposed 2 × 2 array in reference [9].

2.3.1.9 Gain-Enhanced Dual-Band Antennas

Gain enhancement is a key goal in high-frequency dual-band designs. Reference [4] increased gain using high-density rubber, while [5] employed an FSS superstrate to achieve higher gains across both bands.

2.3.1.10 Application-Specific Antennas

Many dual-band antennas are tailored for specific applications, such as biomedical sensing, GPS, WLAN, and 5G. Reference [11] implemented a dual-band dipole array with rotational feed for multi-service support. Reference [12] provided bidirectional beams using a hybrid reflect/transmitarray for enhanced performance at 12.7 and 29 GHz.

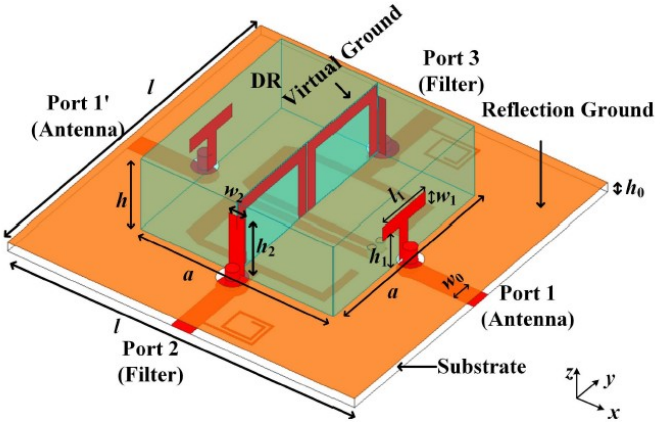

FIGURE 2.9 : Proposed multifunction design of DDRA and independently controllable dual-band filter in [3].

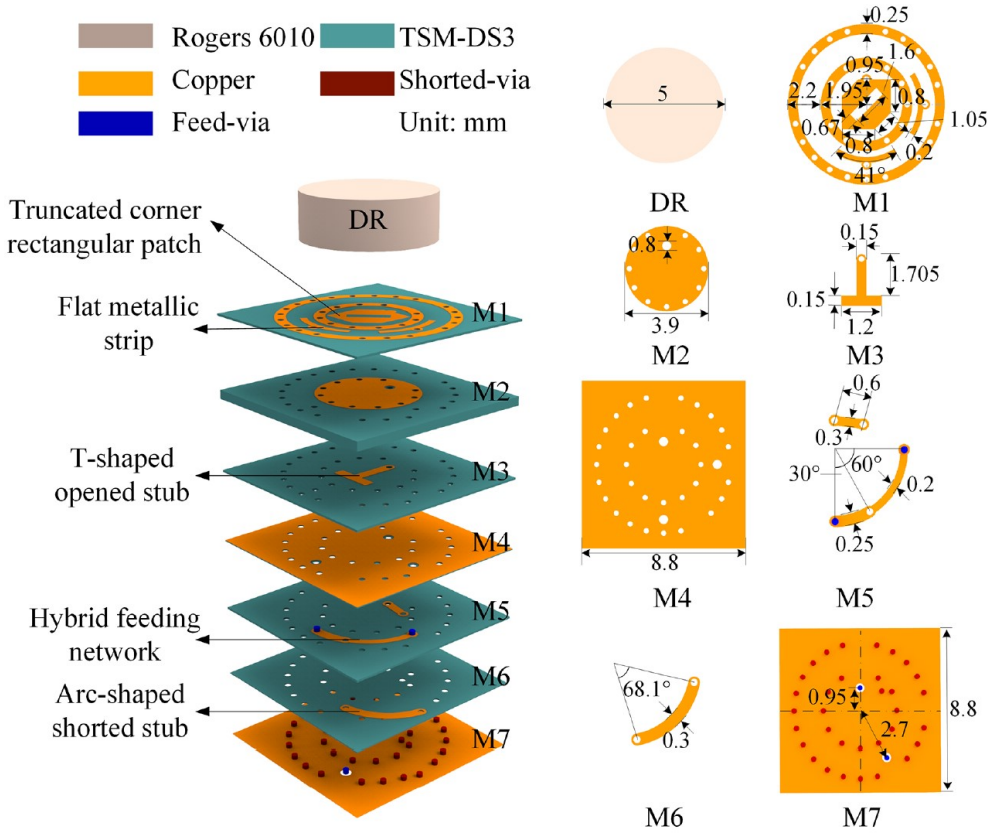

FIGURE 2.10 : Configuration of the proposed antenna in reference [10].

2.3.2 Advantages of Dual-Band Antennas

Dual-band antennas offer several key advantages, making them highly attractive for modern wireless communication systems, particularly in applications where size, cost, and multi-standard support are critical. One of the most important benefits is their ability to support multiple communication standards, such as LTE, 5G, Wi-Fi, and GPS within a single hardware platform. This

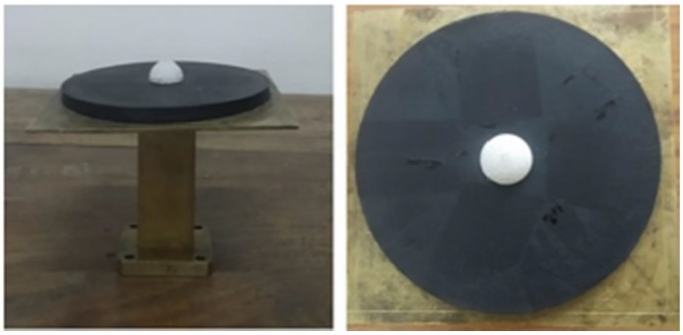

FIGURE 2.11 : Antenna prototype in [4].

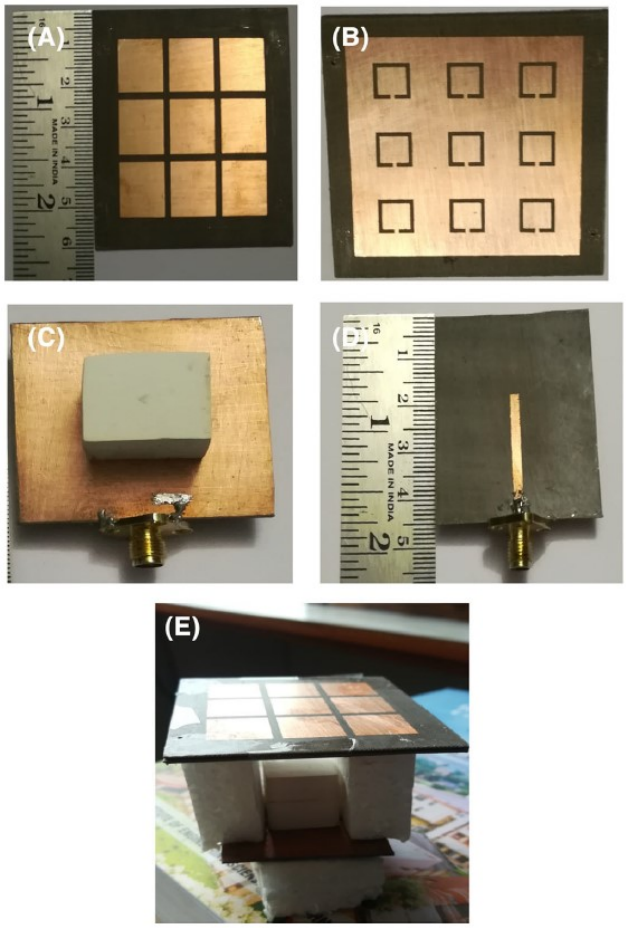

FIGURE 2.12 : Fabricated prototype of the proposed antenna in reference [5].

multi-standard compatibility simplifies device integration and reduces the need for separate antennas.

In addition to functional flexibility, dual-band antennas contribute significantly to space efficiency. By eliminating the requirement for multiple single-band antennas, they enable the design of compact mobile devices, wearable electronics, and Internet of Things (IoT) units, where board

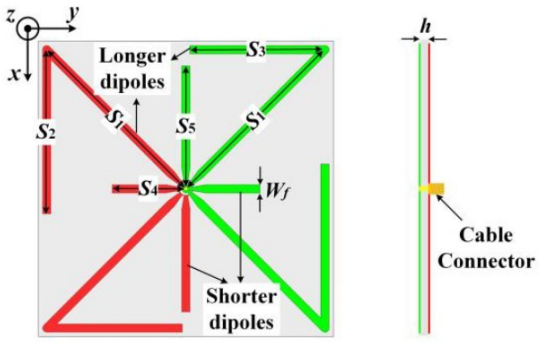

(a) Top view (b) Side view

Fig. 1. Geometry of the proposed CP antenna element. (a) Top view. (b) Side view. S_1=48, S_2=41, S_3=32, S_4=15, S_5=30, W_f=2. Unit: mm.

FIGURE 2.13 : Geometry of the proposed CP antenna element in [11].

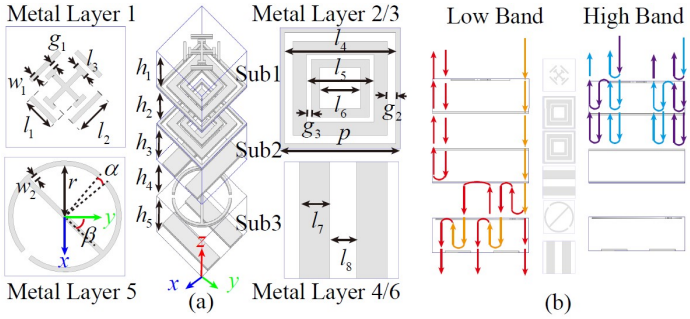

Fig. 2. (a) Structure and dimension of the proposed dual-band full-space unit cell. (b) The operation principle of the proposed dual-band full-space unit cell. (l_1 = 1.44, l_2 = 1.69, l_3 = 0.6, l_4 = 4.6, l_5 = 2.8, l_6 = 1.7, l_7 = 1.33, l_8 = 1.175, w_1 = 0.2, w_2 = 0.2, g_1 = 0.2, g_2 = 0.35, g_3 = 0.2, r = 2.15, p = 5, h_1 = 0.5, h_2 = 3, h_3 = 0.8, h_4 = 1.5, h_5 = 2, Units: mm)

FIGURE 2.14 : Structure of the proposed dual-band full-space unit cell and its operation principle in [12].

space is often limited. This integration also helps streamline the overall system layout and reduces electromagnetic interference between adjacent components.

Another notable advantage is the simplification of the RF front-end. With fewer antennas and associated feeding networks, the complexity of interconnections is greatly reduced. This leads to lower manufacturing costs and easier system assembly. Furthermore, dual-band antennas can be optimized to operate efficiently within each band, thereby minimizing energy loss and enhancing overall system performance. This tailored efficiency is particularly beneficial in battery-powered and energy-sensitive applications.

2.3.3 Challenges and Limitations

Despite their numerous benefits, dual-band antennas also present several technical challenges and limitations that must be carefully addressed during the design and implementation process. One of the primary challenges is the issue of frequency coupling, especially when the two ope-

rating bands are closely spaced. Such coupling can lead to performance degradation, increased intermodulation distortion, and reduced isolation between bands.

Another limitation is the difficulty in maintaining sufficient bandwidth across both frequency bands. In compact structures, achieving wideband performance is often constrained by physical dimensions and the interaction between radiating elements. This limitation can affect data throughput and reliability in high-speed communication scenarios.

Fabrication complexity also becomes a concern in dual-band designs, particularly those involving intricate three-dimensional geometries or multilayer structures. High precision is often required to maintain alignment, impedance matching, and structural integrity, all of which can increase production costs and reduce manufacturing yield.

Lastly, the design and optimization process for dual-band antennas tends to be more time-consuming and computationally intensive. Achieving optimal performance across two distinct frequency bands often requires extensive full-wave simulations, parameter sweeps, and iterative tuning, which can significantly extend the development timeline.

While these challenges are non-trivial, the innovations presented in this thesis offer viable solutions that mitigate many of these issues, pushing the boundaries of what is achievable in compact, high-performance dual-band antenna systems.

2.3.4 Recent Advances and Research Trends

Recent research in dual-band antenna design has seen significant advancements, particularly in response to the evolving requirements of next-generation wireless systems. One notable trend is the integration of filtering functions directly into the antenna structure, leading to the development of filter-antenna systems, commonly known as filtennas. These designs eliminate the need for external filters by embedding bandpass characteristics within the antenna itself, effectively suppressing unwanted harmonics and improving out-of-band signal rejection.

Another important area of innovation is the design of dual-band antennas tailored for Multiple-Input Multiple-Output (MIMO) systems. As modern communication networks demand high data throughput and spatial diversity, compact MIMO antennas that support dual-band operation with high isolation have become essential. These designs are particularly relevant in environments such as base stations, smartphones, and IoT devices.

The extension of dual-band technology into the millimeter-wave domain has also gained momentum. Specifically, antennas that support dual-band operation at frequencies like 28 GHz and 38 GHz are being developed for 5G and beyond applications. These designs must address challenges such as high path loss, precision fabrication, and mutual coupling, which are more pronounced at mm-wave frequencies.

Advancements in fabrication techniques have also contributed to the evolution of dual-band antenna design. Additive manufacturing, particularly 3D printing, has emerged as a viable method for prototyping complex antenna geometries. This approach offers advantages in cost, customization, and design iteration speed, enabling the rapid development of novel antenna structures.

Finally, the use of artificial intelligence (AI) and machine learning has become increasingly prominent in antenna design. Optimization algorithms, including genetic algorithms and deep learning-based models, are now being employed to automate and accelerate the exploration of design parameters. These tools can efficiently identify optimal geometries and material configurations to meet specific dual-band performance goals, reducing design time and improving accuracy.

These recent developments collectively highlight the dynamic nature of dual-band antenna research and its critical role in supporting advanced wireless technologies.

These advancements aim to address the limitations of conventional designs and meet the ever-growing demand for high-performance, compact, and reconfigurable dual-band antennas in next-generation wireless systems.

2.4 Dielectric Resonator Antennas (DRAs) : Theory and Design

This section gives a brief introduction about the DRAs and then it will focus on the cylindrical DRA (cDRA) theory and design.

2.4.1 DRA definition and features

A Dielectric Resonator Antenna (DRA) consists of a dielectric material of a certain shape and dimensions with a dielectric constant of (ϵ_r). The structure is usually fixed on a large ground plane with infinite conductivity [15]. The DRA can be of any shape as depicted in Fig. 2.15 However, basic shapes that are studied extensively in the literature include hemispherical, cylindrical and rectangular shapes [16]. Other shapes were also investigated such as low profile disks, annular and triangular DRAs. Some modifications such as introducing gaps and slits are used to modify the behavior of the DRA such as increasing the bandwidth or obtain circular polarization radiation, etc.

DRAs have many advantages over conventional metallic printed antennas. These advantages include [15] :

(1) DRA Size

The dielectric constant is a function of the electric resonator antenna size, which is expressed in Equation 2.1. The maximum dimension for a DRA is defined by the ratio existing between the wa-

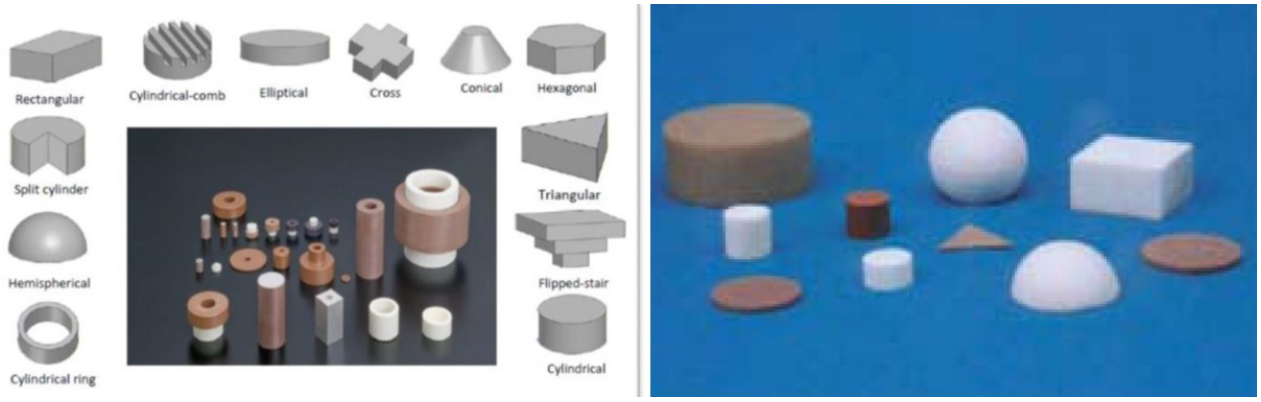

FIGURE 2.15 : Various shapes and types of DRs [13].

velength and the square root of the relative permittivity (ϵ_r). These relationships are both presented in the below equation, where (λ_o) is the free space wavelength (m), (ϵ_r) is the dielectric constant, (f_o) is the resonance frequency (Hz) and (c) the light velocity in free space which is a constant value of ($3 \times 10^8 m/s$).

The relationship is therefore written as :

$$Size_{DRA} = \frac{\lambda_o}{\sqrt{\epsilon_r}}, \lambda_o = \frac{c}{f_o} \tag{2.1}$$

Hence, the designer has the flexibility to control the size by changing/choosing the material from a wide range of dielectric constants, at the expense of its bandwidth. The higher the relative permittivity, the lower the bandwidth (higher Q-factor).

(2) Resonance Frequency and Bandwidth

In addition to (ϵ_r), the resonance frequency and bandwidth are affected by the aspect ratio of the antenna, which, in the case of a cylindrical DRA, is the ratio of the radius of its base to the height of the antenna or (a/h).

(3) High Efficiency

Since the surface waves and metallic losses are not present in dielectric resonators along with low loss tangent values, the total efficiency of the DRAs is very high, as expected from equation 2.2, which gives the total efficiency e_o of the antenna in terms of conductor efficiency e_c, dielectric efficiency e_d and mismatch efficiency e_r [17]. This is very advantageous in mm-wave applications where metallic losses are dominant.

$$e_o = e_c e_d e_r \tag{2.2}$$

(4) Design Flexibility

Since DRAs are 3D structures, they offer additional degrees of freedom that allow the designers to control some design parameters. For example, in cDRAs, the designer can choose between different heights for the same aspect ratio giving him/her flexibility over the bandwidth.

(5) Integration with printed circuit technology

DRAs can be excited by almost all microstrip feeding mechanisms including direct feed, aperture coupling, probe. . .etc. Each mechanism will excite certain modes of the DRA and has its advantages and disadvantages. Design requirement and constrains sometimes forces the designer to choose one mechanism or another.

2.4.2 Dielectric Resonator's shapes

Various shapes of DRA have been put forward for study since it has been reported that shape variation can control the interior field in the DR [18]. Performing controlled modification to the shape also makes it possible to adjust the performance of the antenna by modifying the inner electric field. The shape of the DRA is directly correlated to its performance. The publications of the first papers on the DRA concept has undertaken much work on basic shapes of the DRA. The ability to assume various shapes is among the attractive features that are possessed by DRA. In addition, the operational mode and DRA performance vary when choosing DR with preferred structure. This is to say that numerous shapes have been experimentally tried, with the first experimental study being done on cylindrical disk DRA shape [19]. Various shapes have later been developed to split cylinder, sectored cylinder, cylindrical rings, metalized DRAs, triangular, rectangular, notched rectangular, chamfered DRA, conical, elliptical, spherical, hemispherical, spherical cup, tetrahedral, perforated DRA, stepped DRAs, and hybrid DRAs. A DRAs in the fundamental modes have been said to be radiating like an electric or magnetic dipole, an incidence that relies on the excitation mode and shapes of dielectric material. Conical, stair, stacked triangular etc. are shapes that emanated from dual-band or wideband applications while others like elliptical, hexagonal, cylindricalcomb etc. emanated for circular polarization applications. Fig. 2.15 shows shapes from which we are going to pick three as the basic shapes or the DRA for the purpose of discussion and presentation in this thesis. This is because despite many shapes being introduced, the basic and common ones still remain the cylindrical DRA, hemisphere DRA and rectangular DRA due to the simple nature of their design, fabrication, and analysis.

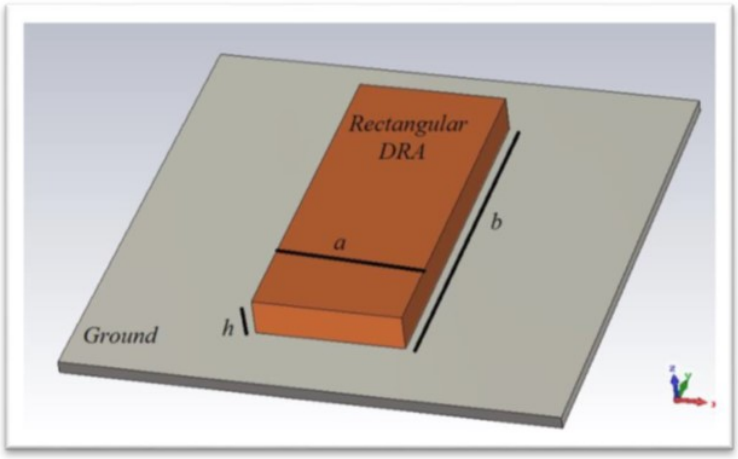

FIGURE 2.16 : Geometry of the rectangular DRA. [14]

2.4.2.1 Rectangular DRA

There are many advantages of rectangular DRA over than cylindrical and hemispherical shapes since it offers a second-degree freedom that is one degree more than the cylindrical shape and two more degrees than the hemispherical shape. This DRA helps the designer have more flexibility in acquiring the desired profile and bandwidth features of a specific resonant frequency and dielectric permittivity. The various modes in an isolated rectangular dielectric guide can be split into TE and TM, even though the DRA mounted on the ground plane can only excite the TE mode. The rectangular DRA maintains TE modes (TEx, TEy, and TEz), which radiate like a short magnetic dipole. The resonant frequency of these modes performs is a function of DRA dimensions. A designer who chooses proper DRA dimensions prevents unnecessary modes from appearing over the frequency band during the operation. By solving the transcendental equation, TE modes will be calculated [15]. The major characteristics of rectangular DRA are length (b), width (a), height (h), beside a dielectric constant. (See Fig. 2.16).

2.4.2.2 Hemisphere DRA

It was stated earlier that a model of the magnetic wall is not efficient for calculating the input impedance of the DRA. (Long) conducted a pioneering analytical theory of the input impedance for the hemispherical DRA, whose shape is illustrated by Fig. 2.17. The major characteristics of hemispherical DRA are radius (r) and relative dielectric constant ϵ_r. The hemispherical DRA is more advantageous over cylindrical and rectangular-shaped DRAs because of the simplicity of the interface between the dielectric and air, thus giving a closed-form expression to perform Green's function. It is assumed that a hemispherical DRA mounted on the ground plane has infinite conductivity alongside infinite excitation. The theoretical picture is important in equating the hemispherical DRA of radius (r) to a dielectric sphere that is isolated, hence the same radius. Transverse electric

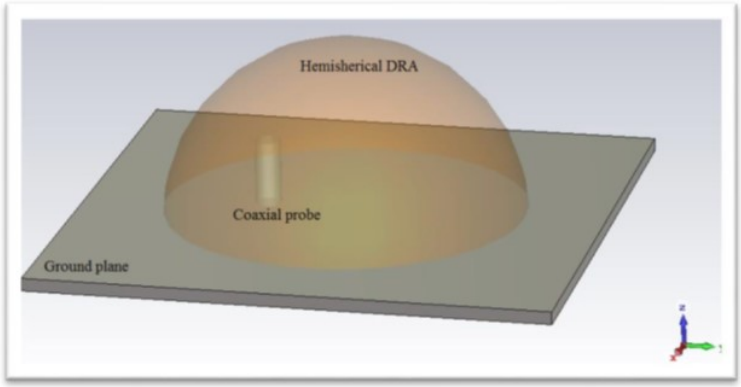

FIGURE 2.17 : Geometry of a probe feeding of hemispherical DRA. [14]

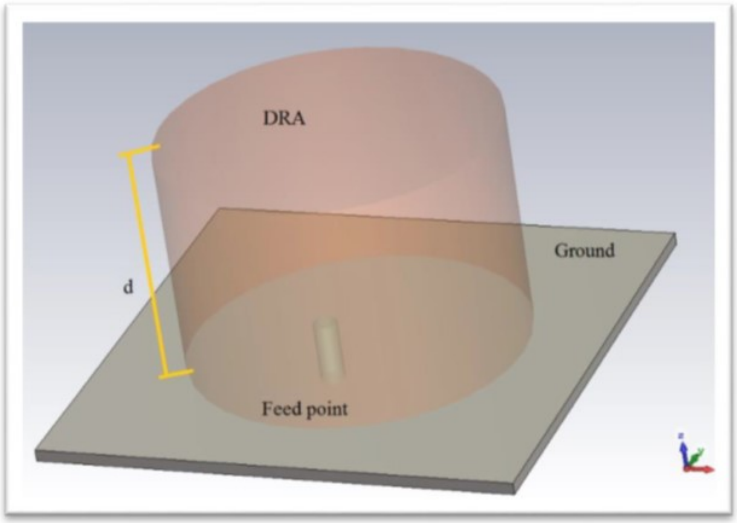

FIGURE 2.18 : The configuration of cylindrical DRA. [14]

(TE) mode is a different mode from a transverse magnetic (TM) in a dielectric sphere with (TE) having radial electric field component whose value is zero, ($Er = 0$), while the Traverse Magnetic mode having zero radial magnetic component field ($Hr = 0$) the two modes of hemispherical DRA that are fundamental are TE_{111}, with the similar radiation pattern to a short electric monopole.

2.4.2.3 Cylindrical DRA

By comparing the three shapes, the cylindrical shape has advantages over all of them because of its ability to offer higher flexibility design with the radius/height are responsible in controlling the resonant frequency and the quality factor denoted as (Q). Various Q factors can be acquired by varying the dimensions of the DRA. A cylindrical DRA has a much easier fabrication with the excitability of the different modes resulting in either round side or omnidirectional radiation patterns. A cylindrical shaped DRA offers more degree freedom than hemispherical by one, with an aspect ratio (a/h) determining Q-factor for a specific dielectric consonant [15]. A cylindrical shaped DRA can

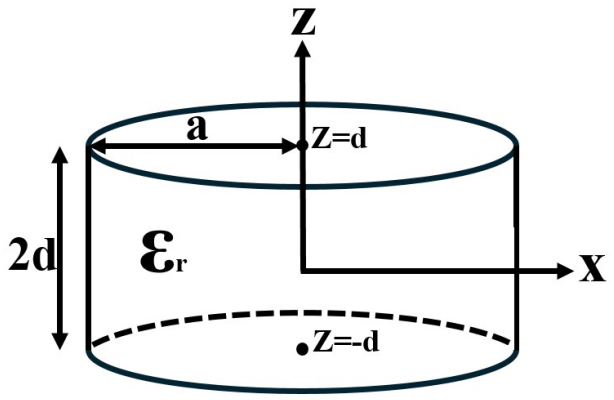

FIGURE 2.19 : Geometry of a cDRA.

provide various subclasses of DRA. These subclasses include cylindrical-ring DRA, split-cylindrical DRA, disk-cylindrical DRA, sectored-ring DRAs, sectored-cylindrical DRAs, elliptical shape DRA, and conical shape DRAs. A ring DRA offers an increase in impedance bandwidth performance. In circuit applications, filters, oscillators and more in microstrip technology employ cylindrical dielectric resonators, with low practicality in resonant waveguide cavities. The geometry of cylindrical DRA, as shown in Fig. 2.18 consists of materials with height h, radius a, and dielectric constant (ϵ_r). The aspect ratio (a/h) determines $k_o a$, and the Q factor for a specific dielectric constant gives this shape a disadvantage over a hemispherical DRA by one degree [15].

Many attempts in the literature took place to set guidelines for designing a cDRA. Two sources [15, 20] provided comprehensive set of equations and curves for the resonance frequency and Q-factor findings based on the material type and shape. These equations do not take into account the effect of the feed and assume that the cDRA is fixed on top of a large ground plane with infinite conductivity.

The center frequency of a cDRA can be calculated using :

$$f(GHz) = \frac{30 k_o a}{2h(\frac{a}{h})} \tag{2.3}$$

where :

k_o – Free-space wave number.

h – the height of the cDRA in cm.

a/h – CDR's aspect ratio.

and $h = 2d$ as shown in Fig. 2.19.

The ($k_o a$) is calculated as one quantity from the design equations listed in Table 2.1; hence, (a) will not cancel out from the numerator and denominator.

TABLE 2.1 : cDRA fundamental modes and design equation summaries

Mode	Equation	Criteria
$TE_{01\delta}$	$K_o a = \frac{2.327}{\sqrt{\epsilon_r+1}}[1+0.2123x-0.00898x^2]$	$0.5 \leq x \leq 5.0$
	$Q = 0.078192\epsilon_r^{1.27}[1+17.31x-21.57x^2+10.86x^3-1.98x^4]$	
$TM_{01\delta}$	$K_o a = \sqrt{\frac{3.83^2+(\frac{x\pi}{2})^2}{\epsilon_r+2}}$	$0.33 \leq x \leq 5.0$
	$Q = 0.00872\epsilon_r^{0.888413}e^{0.039747\epsilon_r}[1-(0.3-0.2x)(\frac{38-\epsilon_r}{28})][9.498186x+2058.33x^{4.322261}e^{-3.50099x}]$	
$HE_{11\delta}$	$K_o a = \frac{6.324}{\sqrt{\epsilon_r+2}}[0.27+0.36(\frac{x}{2})+0.02(\frac{x}{2})^2]$	$0.4 \leq x \leq 5.0$
	$Q = 0.01007\epsilon_r^{1.3}x[1+100e^{-2.05(\frac{x}{2}-\frac{x^2}{80})}]$	
$TE_{011+\delta}$	$K_o a = \sqrt{\frac{2.208}{\epsilon_r+1}}[1.0+0.7013x-0.002713x^2]$	$0.5 \leq x \leq 5.0$
	$Q = 0.03628\epsilon_r^{2.38}[-1.0+7.81x-5.858x^2+1.277x^3]$	
$HE_{12\delta}$	$K_o a = \frac{3.72+0.4464(\frac{x}{2})+0.2232(\frac{x}{2})^2+0.0521(\frac{x}{2})^3-2.65e^{[-1.25(\frac{x}{2})(1+4.7(\frac{x}{2})^2)]}}{\sqrt{\epsilon_r}}$	
	$Q = \epsilon_r^2[0.068-0.0388(\frac{x}{2})+0.0064(\frac{x}{2})^2+0.0007e^{(\frac{x}{2})(37.59-63.8(\frac{x}{2})^2)}]$	

$x = a/h$

The frequency and the bandwidth are affected by the dimensions of the cDRA and its dielectric constant. Table 2.1 shows the first five fundamental modes excited inside the cDRA and their corresponding equations for $k_o a$ and Q-factor. These modes are usually targeted when designing the antennas. Higher modes are more difficult to excite and hence to radiate. The frequency and bandwidth can be calculated from these quantities as shown in equations 2.3 and 2.4.

$$Q = \frac{1}{FBW} = \frac{f_c}{f_2 - f_1} \tag{2.4}$$

The subscripts represent to the variations of the fields in azimuth (Φ), radial (r) and axial (z) directions, respectively. (δ) is a number that varies between 0 and 1 and approaches 1 for high values of (ϵ_r). It must be noted that the design equations in Table 2.1 are approximations based on field equations with many assumptions for the boundary conditions. Also, they do not account for loading effects by the feed or consider the limited size of ground planes [15]. To incorporate all the effects in a practical design, the above equations are used as a starting point, and then the design is optimized and finalized using a full-wave solver.

2.3.2.3.1 cDRA Design Procedure

To design a cDRA, one should have four input design parameters : center frequency, bandwidth, desired resonating mode and the dielectric constant(s) of available material(s).

The procedure for the design follows the following steps :

(1) Start with an estimation for a and h. Take into account the criteria for the aspect ratio for the selected mode.

(2) Calculate the quantities $(k_o a)$ and Q from the table 2.1 based on the mode to be excited.

(3) Calculate the center frequency and the bandwidth from 2.3 and 2.4.

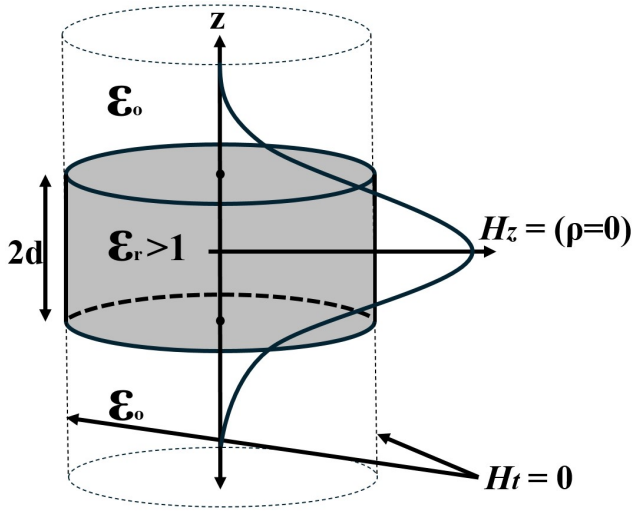

FIGURE 2.20 : Hz **Field inside DRA for** $TE_{01\delta}$

(4) If the obtained frequency is less/more than the target frequency, decrease/increase the aspect ratio and repeat (2) and (3).

(5) If the obtained bandwidth is less/more than the target bandwidth, decrease/increase the aspect ratio and repeat (2) and (3).

2.3.2.3.2 Fields inside the cDRA

Circular waveguide and cavity approach can be used to find the resonant modes and field equations inside the cDRA [21]. The lowest mode that can be realized for a cylindrical dielectric resonator is $TE_{01\delta}$, which corresponds to TE_{011} in a metallic circular cavity. The subscripts refer to the variations of the fields in azimuth (Φ), radial (r) and axial (z) directions, respectively. The symbol (δ) represents a value from 0 to 1 and approaches 1 for high values of ϵ_r. Unlike a metallic cavity, the fields do not vanish at the walls of the cavity, instead –for a dielectric resonator, the fields penetrates the surfaces but fades in the air (evanescent fields) as shown in Fig. 2.20 where it shows $\delta = \frac{L}{\lambda_g}$ where λ_g is the guided wavelength inside the resonator and L is the height of the dielectric resonator where $L = 2d$.

From circular waveguide theory [21], the set of transverse field equations in cylindrical coordinates for a circular waveguide are :

$$E_\rho = \frac{-j}{k_c^2}(\beta\frac{\delta E_z}{\delta_\rho} + \frac{\omega\mu}{\rho}\frac{\delta H_z}{\delta\phi}) \tag{2.5}$$

$$E_\phi = \frac{-j}{k_c^2}(\frac{\beta}{\rho}\frac{\delta E_z}{\delta_\phi} - \omega\mu\frac{\delta H_z}{\delta\rho}) \tag{2.6}$$

$$H_\rho = \frac{j}{k_c^2}(\frac{\omega\epsilon}{\rho}\frac{\delta E_z}{\delta\phi} - \beta\frac{\delta H_z}{\delta\rho}) \tag{2.7}$$

$$H_\phi = \frac{-j}{k_c^2}(\omega\epsilon\frac{\delta E_z}{\delta\rho} - \frac{\beta}{\rho}\frac{\delta H_z}{\delta\phi}) \tag{2.8}$$

where E is the electric field intensity (V/m), H is the magnetic field intensity (A/m), ω is the angular frequency, ϵ and μ are the permittivity and the permeability of the material inside the waveguide respectively, β is the propagation constant and $k_c^2 = k^2 - \beta^2$.

For TE modes, where there is no electrical field component in the direction of the wave propagation $(Ez = 0)$, the wave equation is given by :

$$\nabla^2 H_z + k^2 H_z = 0 \tag{2.9}$$

Where $k = k_o\sqrt{\epsilon_r}$ for $\mid z \mid < \frac{L}{2}$, and $k = k_o$ for $\mid z \mid > \frac{L}{2}$. The solution to the wave equation is given in 2.10 where J_0 is the Bessel function of the first kind.

$$H_z = H_o J_o(k_c\rho)e^{\pm j\beta z} \tag{2.10}$$

Since there is no change in the fields in the azimuth direction for the first mode and a magnetic wall condition (Htangential=0) is applied at $\rho = a$. Equations 2.5-2.8 reduce to :

$$E_\phi = \frac{j\omega\mu}{k_c^2}\frac{\delta H_z}{\delta\rho} \tag{2.11}$$

$$H_\rho = \frac{-j\beta}{k_c^2}\frac{\delta H_z}{\delta\rho} \tag{2.12}$$

Assuming a magnetic wall condition (Htangential=0) at $\rho = a$, we can write the field equations of the first mode TE_{01} for the dielectric waveguide as follows [21] :

$$E_\phi = \frac{j\omega\mu}{k_c^2}H_o J_o'(k_c\rho)e^{\pm j\beta z} \tag{2.13}$$

$$H_\rho = \frac{\pm j\beta}{k_c^2}H_o J_o'(k_c\rho)e^{\pm j\beta z} \tag{2.14}$$

The propagation constant will be real inside the DR (stored) while it will be imaginary in the air (propagating or evanescent). We can write :

$$\alpha = \sqrt{k_c^2 - k_o^2} = \sqrt{(\frac{p_{01}}{a})^2 - k_o^2} \tag{2.15}$$

$$\beta = \sqrt{\epsilon_r k_o^2 - k_c^2} = \sqrt{-(\frac{p_{01}}{a})^2 + \epsilon_r k_o^2} \tag{2.16}$$

Where p_{01} is the first root of the derivative of the first Bessel function. The wave impedance is the ratio of the electric field to the magnetic field. So we can write :

$$Z_d = \frac{E_\phi}{H_\rho} = \frac{\omega\mu}{\beta} \tag{2.17}$$

$$Z_a = \frac{E_\phi}{H_\rho} = \frac{j\omega\mu}{\alpha} \tag{2.18}$$

Where the subscripts (d) and (a) refer to the dielectric and air, respectively. To find the resonance frequency for the first mode, which is even around (z), we can rewrite 2.13-2.14 using 2.15-2.18 as follows :

$$inside.the.DR \begin{cases} E_\phi = AJ'_o(k_c\rho)cos(\beta Z) \\ H_\rho = \frac{-jA}{Z_d} J'_o(k_c\rho)sin(\beta Z) \end{cases} \tag{2.19}$$

$$in.the.air \begin{cases} E_\phi = BJ'_o(k_c\rho)e^{-j\alpha|z|} \\ H_\rho = \frac{\pm jB}{Z_d} J'_o(k_c\rho)e^{-j\alpha|z|} \end{cases} \tag{2.20}$$

Using boundary conditions at $z = L/2$ for the electric and magnetic fields :

$$E_\phi(\frac{L}{2}).inside.the.DR = E_\phi(\frac{L}{2}).in.the.air \tag{2.21}$$

$$B_\rho(\frac{L}{2}).inside.the.DR = B_\rho(\frac{L}{2}).in.the.air \tag{2.22}$$

And since the two materials are dielectric (relative permeability=1), we can reduce equations 2.20 and 2.21 to :

$$-jZ_a sin(\beta\frac{L}{2}) = Z_d cos(\beta\frac{L}{2}) \tag{2.23}$$

which can be reduced using 2.18 and 2.19 to

$$tan(\beta\frac{L}{2}) = j\frac{Z_d}{Z_a} = \frac{\alpha}{\beta} \tag{2.24}$$

As noted from 2.24, the resonance frequency can be found numerically since the equation contains k_o if the dimensions of the cylindrical DR (a and L) and its dielectric constant are known.

3 DUAL-BAND DIELECTRIC RESONATOR ANTENNA WITH FILTERING FEATURES FOR MICROWAVE AND MM-WAVE APPLICATIONS

Bizan, Mohamed Sedigh, Hassan Naseri, Peyman Pourmohammadi, Noureddine Melouki, Amjad Iqbal, and Tayeb A. Denidni.

Micromachines 14, no. 6 (2023) : 1236.

DOI : 10.3390/mi14061236

(Published).

3.1 Abstract

This paper presents a new design for a dual-band double-cylinder dielectric resonator antenna (CDRA) capable of efficient operation in microwave and mm-wave frequencies for 5G applications. The novelty of this design lies in the antenna's capability to suppress harmonics and higher-order modes, resulting in a significant improvement in antenna performance. Additionally, both resonators are made of dielectric materials with different relative permittivities. The design procedure involves the utilization of a larger cylinder-shaped dielectric resonator (D_1), which is fed by a vertically mounted copper microstrip securely attached to its outer surface. An air gap is created at the bottom of (D_1), and a smaller CDRA (D_2) is inserted inside this gap, with its exit facilitated by a coupling aperture slot etched on the ground plane. Furthermore, a low-pass filter (LPF) is added to the feeding line of D1 to eliminate undesirable harmonics in the mm-wave band. The larger CDRA (D_1) with a relative permittivity of 6 resonates at 2.4 GHz, achieving a realized gain of 6.7 dBi. On the other hand, the smaller CDRA (D_2) with a relative permittivity of 12 resonates at a frequency of 28 GHz, reaching a realized gain of 15.2 dBi. The dimensions of each dielectric resonator can be independently manipulated to control the two frequency bands. The antenna exhibits excellent isolation between its ports, with scattering parameters (S_{12}) and (S_{21}) falling below 72/46 dBi at the microwave and mm-wave frequencies, respectively, and not exceeding -35 dBi for the entire frequency band. The experimental results of the proposed antenna's prototype closely align with the simulated results, validating the design's effectiveness. Overall, this antenna design is well-suited for 5G applications, offering the advantages of dual-band operation, harmonic suppression, frequency band versatility, and high isolation between ports.

3.2 Introduction

During the past few decades, researchers have become increasingly interested in DRA antennas due to their distinct benefits. The DRA, or dielectric resonator antenna, offers a range of benefits such as compact size, the ability to operate over a broad range of frequencies, and straightforward excitation [20, 22]. Another advantage is that DRAs are made entirely of dielectric material, meaning their loss can be minimal even at frequencies in the mm-wave band. Combining these characteristics makes the DRA ideal for microwave and mm-wave applications [15,23–25]. In terms of dual-band DRAs, several designs have been suggested. For instance, Xiao-Chuan Wang presented a design that utilizes a cross-slot-coupled dualband (RDRA) [26]. This design realized a right-hand circular polarization. The antenna exhibits an impedance bandwidth of 11.41% and 8.41%, 3-dB axial ratio bandwidths of 2.11% and 2.21%, and antenna gains greater than 5.41 and 4.31 dBi, respectively. Several dual-band or wideband DRA antennas have been proposed in recent studies. In [27], an RDRA was presented with a frequency range of 3.41 to -3.59 GHz and 5.11 to 5.9 GHz. In [28], a hybrid dual-band antenna was proposed with the following two operation frequencies : 2.4 GHz and 5.8 GHz. Another wideband dual-feed DRA was presented in [29], which utilized a slot with an L-shaped and a vertical copper micro-strip to excite the antenna. In [30], a dual-band/wideband quasi-Yagi antenna is proposed, which utilizes the (TE_{11}) and (TE_{13}) modes of the DRA to provide two close-operation frequencies. The experimental impedance bandwidth is 21.71% with a peak realized gain of 8 dBi. Additionally, an array antenna consisting of many elements of CDR antenna resonating at 28 GHz was proposed in [31] by Niayesh and Kouki. The antenna discussed in [31] has a bandwidth of 9.82% at 28.73 GHz, achieving an efficiency of 89% and realized gain of 15.69 dBi. Other works have focused on developing dual-band filtering dielectric resonator antennas, such as the one presented in [32], which was tested at 7.71 and 13.36 GHz with impedance bandwidths of 11.41% and 4.81% and maximum realized gains of 7.66 and 10.51 dBi, respectively. In [33], a hybrid antenna that combines three resonators was proposed to create four operation frequency bands. A compact shared-aperture antenna with a significant frequency ratio is proposed in [34]. The dual-band implementation excites a high-frequency dielectric resonator antenna (DRA) and a low-frequency slot antenna. The operating frequencies of these two antenna parts can be tuned independently. The authors in [35] combine a liquid Dielectric Resonator Antenna (DRA) and a patch configuration to achieve multi-band and multi-mode operation for Wi-Fi applications in the 2.4 GHz and 5 GHz frequency bands. The proposed approach addresses the issue of undesirable higher-order modes in the DRA by suppressing and replacing them with desired modes through a hybrid design. The dielectric resonator (DR) in the antenna design in [36] exhibits the excitation of four resonant modes. This design achieves dual passbands with distinct frequencies and bandwidths in each channel. Additionally, the antenna benefits from two pairs of orthogonal degenerate modes and the chosen excitation principle, ensuring high isolation between the two channels that reach -38 dB. The authors in [37] presented a dual-band antenna design that combines a millimeter-wave substrate-integrated dielectric resonator antenna

(SIDRA) beam-steerable array with a long-term evolution (LTE) folded monopole antenna (FMA). The SIDRA array is integrated within the FMA's clearance area, allowing for a shared substrate and aperture. The LTE FMA operates at 1.78–2.62 GHz (38.2%) with a peak gain of 3.9 dBi, while the MMW array covers 26.4–29.8 GHz (12.2%) with a peak gain of 10 dBi and supports ±45° beam-steering angles. Ref. [38] presents a hybrid antenna design that combines strip, slot, and dielectric resonator antenna (DRA) resonators, generating four resonances within the frequency bands of 28 and 39 GHz. The lower frequency band of 26.41–30.42 GHz is covered using strip and slot modes, while the upper-frequency band of 36.05–40.88 GHz is covered by employing the (TE_{111}) and (TE_{131}) modes of the DRA. In a previous study [39], the authors presented an innovative design that utilizes a dual dielectric resonator antenna (DRA) with opposite orientations. This unique antenna design offers dual-band filtering characteristics and a quasi-isotropic radiation pattern. The upper cylindrical ceramic of the antenna is fed by a conformal strip and a circular patch, while a circular aperture feeds the lower one. This feeding mechanism generates ($HEM_{11\delta}$) and ($HEM_{12\delta}$) modes within the ceramic material at frequencies of 2.8 and 5.4 GHz, respectively, resulting in a dual-band response. However, none of the references mentioned have introduced a dual-band DRA that resonates in both sub-6 GHz and millimeter-wave bands, which is essential for 5G applications where wireless systems need to operate in both microwave and mm-wave bands. Therefore, there is interest in developing this type of DRA.

The authors in [40] propose a two parallel-plate waveguide resonator antenna for microwaves and the Fabry–Perot resonator antenna for millimeter-waves, all combined into one structure. The double-fed dual-band frequency antenna utilizes an air gap in the DRA [41, 42]. In [43], the authors introduce a windowed slow-wave parallel-plate waveguide (WSW-PPW). By incorporating electromagnetic bandgap (EBG) structures into a dual-layer printed PPW, the WSW-PPW enables the transmission and integration of MW antennas while blocking MMW propagation. However, these structures lack filtering capabilities to eliminate unwanted harmonics in the mm-wave band and do not provide independent control of the frequency bands. In addition, they use hybrid resonators, such as the dielectric resonator and Fabry–Perot resonator or patch antenna, to operate in two bands, which limits their ability to control the frequency bands independently. Therefore, there is a need for a dual-band DRA that operates at both microwave and mm-wave frequencies with high isolation levels, independently of frequency bands, and has the ability to suppress harmonics.

This paper introduces a dielectric resonator dual-band antenna for 5G applications operating in microwave and millimeter-wave frequency ranges. The proposed design employs two cylindrical dielectric resonators (CDRs) that are nested together and excited by vertical conducting strips and a coupling aperture slot. The larger CDR resonates at 2.4 GHz with a realized gain of 6.7 dBi, while the smaller CDR resonates at 28 GHz and has a realized gain of 15.2 dBi. Most importantly, LPF suppresses any unwanted harmonics in the mm-wave band from the microwave band. Furthermore, independence of frequency bands is achieved, which helps control each band without any effect on the other. Thus, with all this in mind, it is asserted that the suggested dual-band structure introduces some new features to dual-band DRAs and makes them more suitable for 5G

systems supporting both sub-6 GHz and millimeter-wave bands. Moreover, the antenna provides a high isolation level. (S_{12}) and (S_{21}) fall to ($-72/-46$ dBi) at the desired frequencies and do not reach above (-35 dBi) for all bands.

3.3 Antenna Design

This section describes the steps taken to reach the final design of a new dual-band, double-cylinder DRA antenna. The proposed antenna configuration and its design evolution are shown in Fig. 3.1 and 3.2.

In the first step, as in Fig. 3.2a, a large dielectric resonator is designed for the microwave band to operate at 2.4 GHz. The CDRA comprises Hik500 ($\mathcal{E}$ r = 6 and loss tangent = 0.002). This material has been chosen due to its availability in the customer market for a reasonable price. The radius *(a)* and height *(h)* of a CDRA can be obtained using the following equation [15] :

$$f(GHz) = \frac{30k_{\mathrm{o}}a}{2h(\frac{a}{h})} \tag{3.1}$$

where *(a/h)* is the aspect ratio of the CDR, and (k_o) is the free space wave number. The value (k_oa) can be calculated for the (TE_{011}) mode as follows :

$$k_{\mathrm{o}}a = \frac{1}{\sqrt{r+1}}(1 + 0.7013(\frac{a}{h}) - 0.002713(\frac{a}{h})^2) \tag{3.2}$$

Equations (3.1) and (3.2) provide the initial estimates of the values, but they are not precise because they do not consider how the feed network affects the DRA. This can cause changes in the center frequency and limitations in bandwidth. In addition, an infinite ground plane assumption underlies the equations.

After establishing the large microwave band resonator (D_1), a hollow region is created on the bottom to provide room for the small mm-wave band resonator (D_2). By doing so, the frequency at which resonance occurs increases. To maintain the frequency at 2.4 GHz, optimization is performed on the dimensions of (D_1). Fig. 3.3 illustrates the impact of the hollow on the (S_{11}) of (D_1).

Then, a small dielectric resonator (D_2) is inserted in the air gap for the mm-wave band. The (D_2) is designed to resonate at 28 GHz by following the same steps as (D_1). (D_2) is made of Hik500, with $\mathcal{E}$ r = 12 and loss tangent = 0.002. Finally, to suppress the harmonics that (D_1) causes in the millimeter-wave band, an LPF is added to the feeding transmission line of (D_1) to eliminate unwanted harmonics, especially those occurring at 28 GHz. By comparing Figs. 3.4 and 3.5, we can clearly observe the filter's impact. Adding this filter to the proposed antenna not only raises the level of isolation between the two ports but also improves the reflection coefficient of both the mm-wave band (S_{11}) as well as microwave band (S_{22}). As it is clearly noted that (S_{12}) and (S_{21})

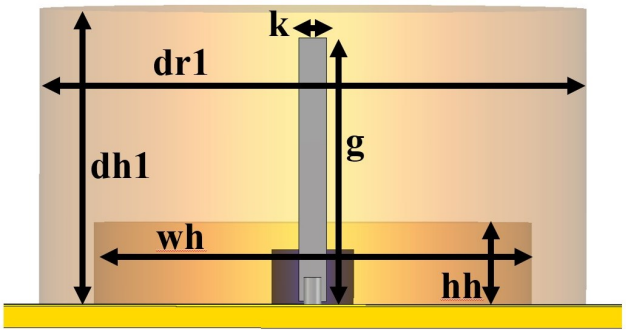

FIGURE 3.1 : (D_1) dimensions.

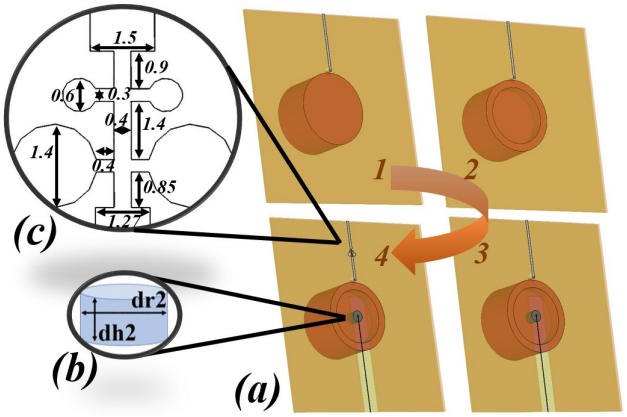

FIGURE 3.2 : The proposed antenna's geometrical structure, (a) the four steps of the proposal antenna, (b) (D_2) dimensions, (c) LPF configuration.

TABLE 3.1 : The Proposed Antenna's Dimensions in Millimeters.

Parameter	W	L	dr_1	dr_2	wh	k	dh_1	dh_2	hh	g
Value	100	100	26	2.0	15	2.0	21.6	3.2	6	19

drop down to ($-72/-46$ dBi) at the desired frequencies and not above (-35 dBi) for the whole bands.

(D_1) and (D_2) are mounted and stacked into two layers of RO3003 material substrate with different thicknesses (1.52 mm for the bottom and 0.13 mm for the top). A cut is made in the middle of the bottom thick substrate, reaching 5 mm beyond its center. A rectangle mutual coupling slot is etched on the ground plane at a 0.7 mm length and 2.8 mm width to excite the fundamental mode of (D_2), while the (TE_{011}) mode is excited in (D_1) by a vertical copper tap glued on it. The only purpose of stacking these two substrate layers is to provide a thin substrate for the mm-wave feeding microstrip line and a thick substrate for the microwave transmission line. Fig, 3.6 illustrates the combined components of the proposed antenna.

The optimized parameters of the proposed antenna, according to Fig. 3.2(a) step 2, are shown in Table 3.1.

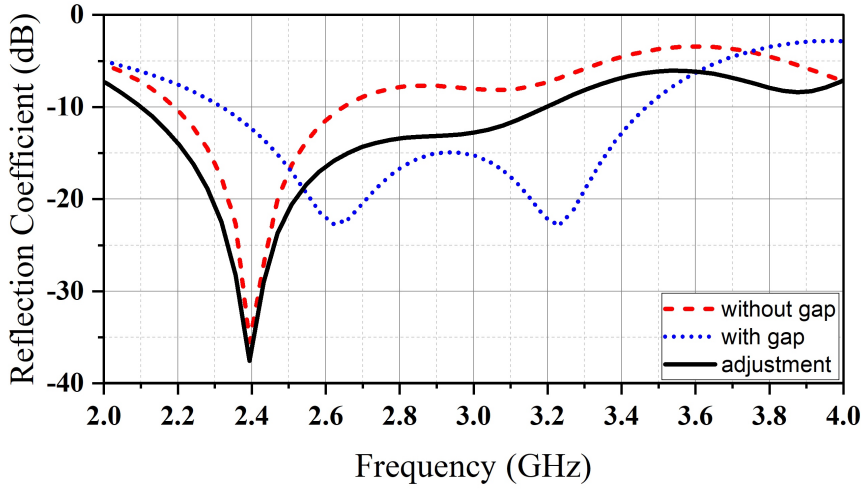

FIGURE 3.3 : The simulated reflection coefficient associated with (D_1).

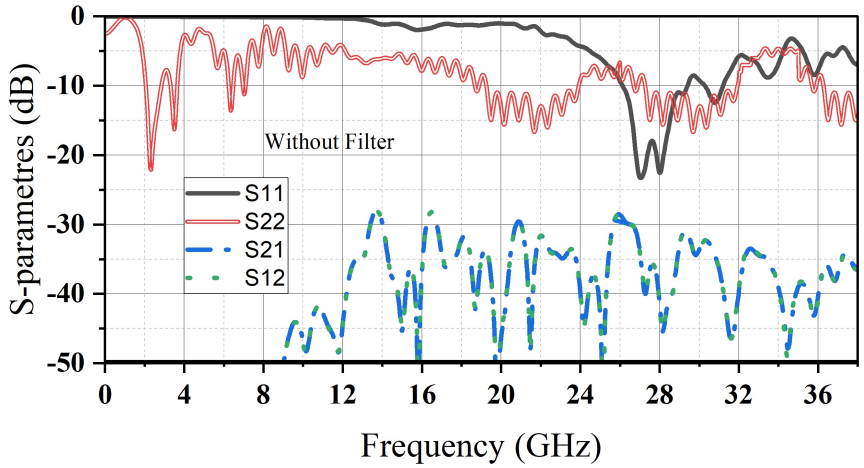

FIGURE 3.4 : S-parameters of the proposed antenna before adding the LPF.

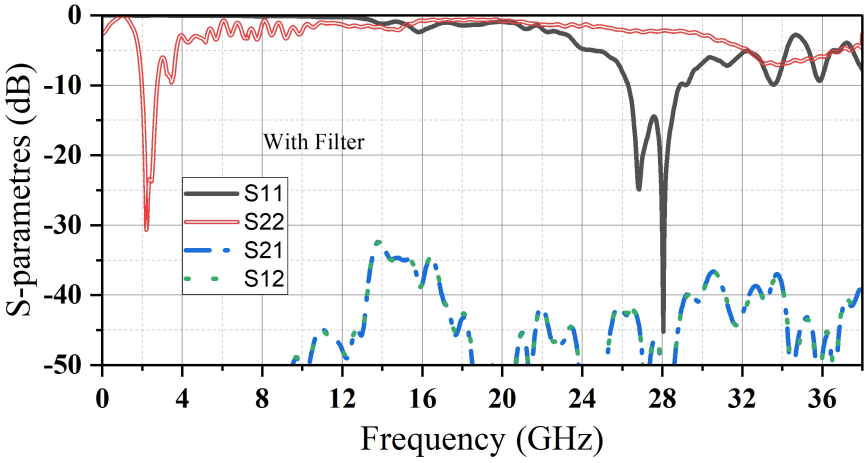

FIGURE 3.5 : S-parameters of the proposed antenna after adding the LPF.

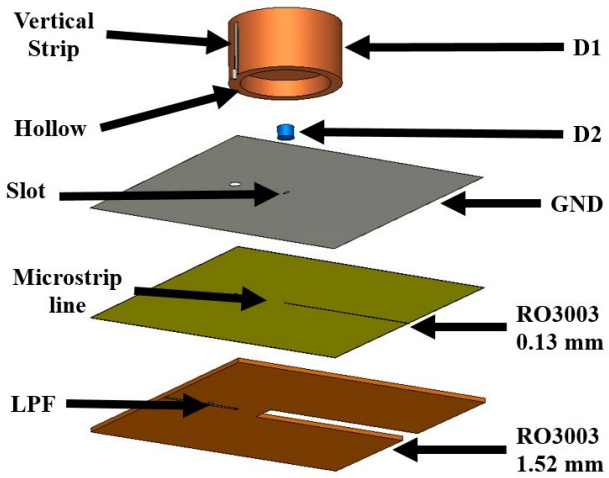

FIGURE 3.6 : The proposed antenna's layers.

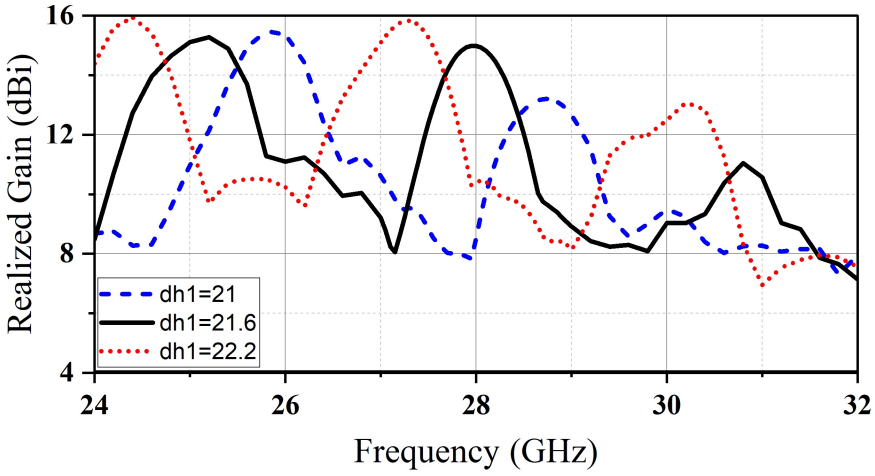

FIGURE 3.7 : The realized gain of the mm-wave band for various values of dh_1.

3.4 Parameteric Study

A parametric study was carried out using Computer Simulation Technology (CST) software to adjust the dimensions of CDR1 and CDR2. To match impedance, the feed line was lengthened by 1mm beyond the center of CDR2. The reflection coefficient and realized gain were examined for various values of dr_1, dr_2, and dh_2. Figure 3.7. shows that we can shift the realized gain of the mm-wave band by adjusting the height of (D_2). Furthermore, the operating frequency of the microwave band (2.4 GHz) can be tuned by monopolizing the radius of the big resonator dr_2; meanwhile, there is no impact on the millimeter-wave band resonance, as illustrated in Fig. 3.8.

In the same way, varying D1's radius dr_1 causes a frequency shift in mm-wave with the stability in microwave resonant frequency of (D_1) (see Fig. 3.9). Figs.3.8 and 3.9. prove the independence of the two bands from each other. In this structure design, the ability to control the resonance frequency of every band separately is realized.

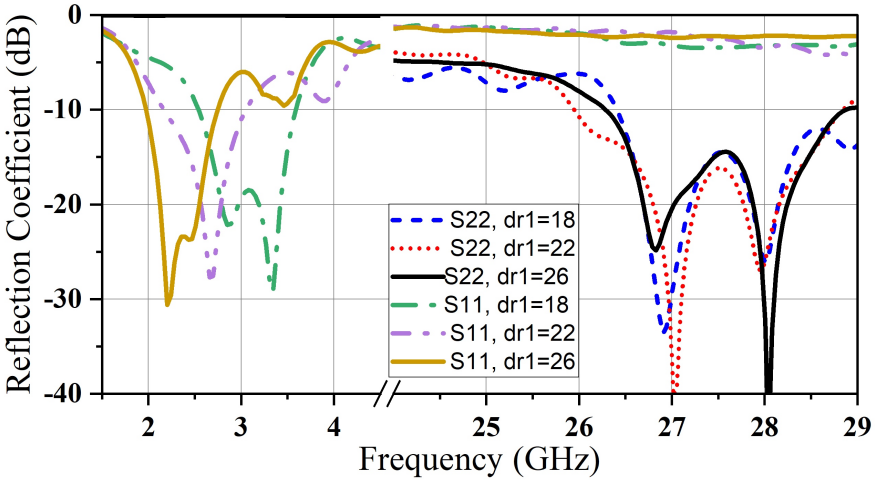

FIGURE 3.8 : Reflection coefficient for various values of dr_1.

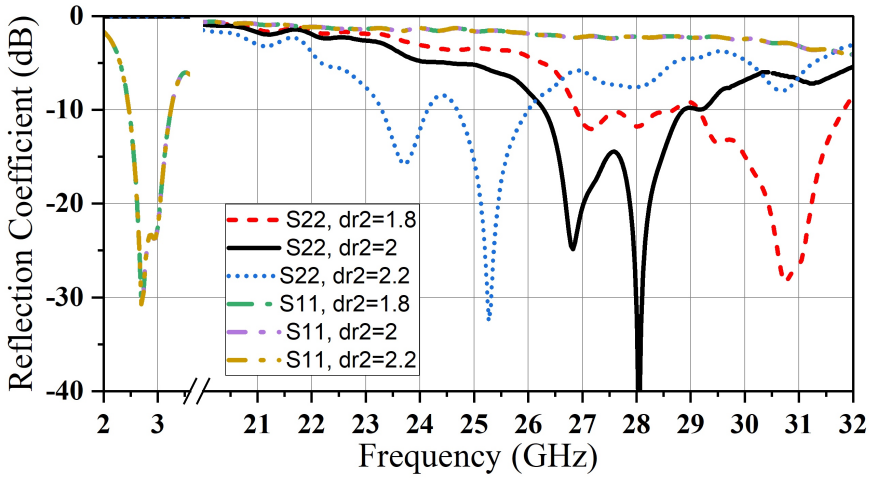

FIGURE 3.9 : Reflection coefficient for various values of dr_2.

3.5 Experimental Results

In order to confirm the accuracy of the optimized simulated results, a model of the proposed antenna was created and physically constructed, as depicted in Fig. 3.10. The Agilent ENA series vector network analyzer was utilized to determine the antenna's reflection coefficient. The prototypes of two embedded cylindrical resonators were made of Hik500 material with different permittivity of 6 and 12, respectively. Both resonators were laid on the two-substrates layer of Roger RO3003 with thicknesses of 0.13 mm and 1.52 mm, respectively. To excite it, a copper microstrip was glued on the big (D_1).

Fig. 3.10 illustrates the experimental and simulated reflection coefficients and the realized gain of both bands (millimeter-wave and microwave bands) with a reasonable agreement. There is a small shift in frequency towards the right side, likely caused by various experimental factors, such as mistakes made during machining and the potential presence of small spaces between the DRAs

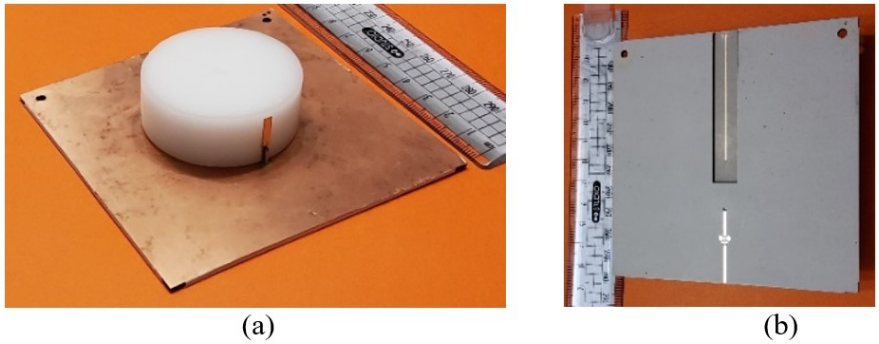

FIGURE 3.10 : The proposed antenna prototype (a) top view and (b) bottom view.

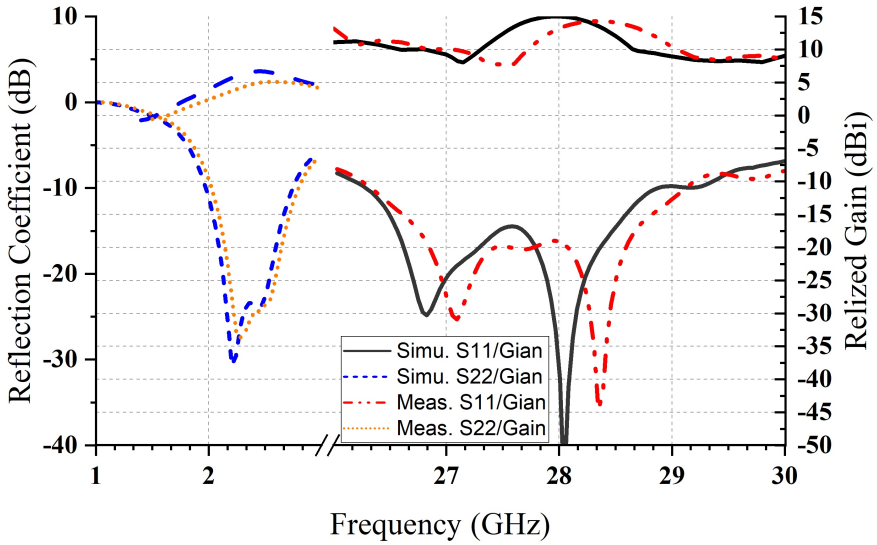

FIGURE 3.11 : Reflection coefficient and realized gain, measured, and simulated.

and the ground plane. The figure illustrates that the antenna gains were measured and simulated at frequencies in the mm-wave bands of 15.2 and 14.6 dBi at 28 and 28.2 GHz, respectively. The measured antenna gain is slightly lower than the simulated gain of 0.7 dB. On the other hand, for the microwave band, the measured reflection coefficient remains almost the same as the simulated one (just a 20 MHz frequency shift to the right side), while the realized gain decreases by 0.5 dBi from 6.7 dBi to 6.2 at 2.4 GHz.

The proposed design's simulated and measured radiation patterns are plotted in Fig. 3.12. A good level of agreement between the simulated and measured results can be observed. The cross-polarization fields are weaker than their co-polar peers by more than 30 dB. Cross-polarization isolation is essential for 5G antenna design. It helps reject interference, maintain signal integrity, enable frequency band versatility, achieve isolation between ports, and enhance system performance and signal quality. By effectively isolating signals of different polarizations, the antenna can operate efficiently and deliver reliable performance in its intended 5G applications.

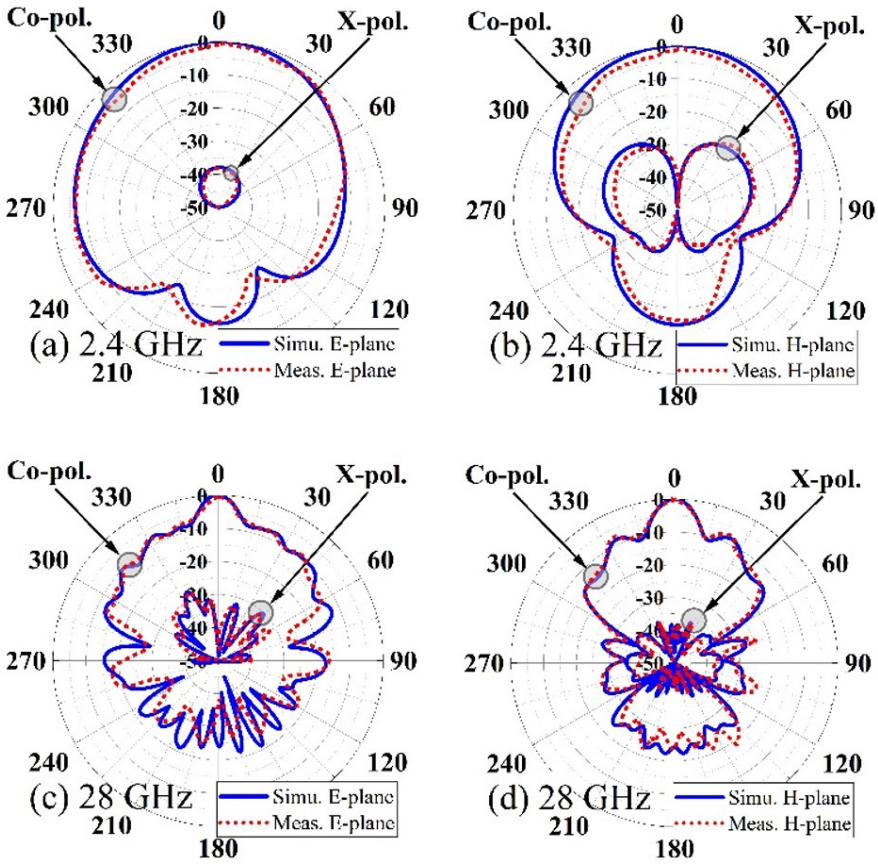

FIGURE 3.12 : Simulated and measured radiation patterns, (a) E-plane at 2.4 GHz, (b) H-plane at 2.4 GHz, (c) E-plane at 28 GHz, (d) H-plane at 28 GHz.

3.6 Discussion

The proposed antenna design is developed, simulated, and experimentally evaluated at 2.4 and 28 GHz for both the mm-wave and microwave bands. This concept has significant advantages, such as the proposed antenna having one dual-band DRA-based structure resonating at both microwave and millimeter-wave bands. Additionally, it has a high isolation level as (S_{12}) and (S_{21}) are less than (35 dBi) for all bands. In addition, the antenna has a harmonics suppression capability provided by the LPF. The antenna is independently tunable. Each band of the dual-band double CRDA antenna is independently controllable. The lower resonant frequency can be controlled by varying the dimensions of CDR1. The higher resonant band can be controlled by modifying the dimensions of the CDR2.

Table 3.2 contains a comparison of the dual-band antennas proposed in the work. In [40–43], the authors designed antennas based on hybrid structures, including a Fabry–Perot, patch antenna and DRA to cover mm-wave 24/28 GHz and microwave 2.4/3.5 GHz bands; however, they fail to eliminate the harmonics that are generated due to the microwave resonator affecting the mm-wave band. Furthermore, they do not mention if their designs have frequency-band independence. Conversely, due to the LPF, the proposed work has the advantages of not including any

TABLE 3.2 : Comparison of this work and other works.

Parameter	[[40]]	[[41]]	[[42]]	[[43]]	This Work
Resonator Type (microwave/mm-wave)	WRA / FPRA	DRA / FPRA	DRA / FPRA	Patch / DRA	**DRA** / **DRA**
Resonance Frequency (GHz) (microwave/mm-wave)	2.4/24	2.4/24	2.4/24	3.5/28	**2.4/28**
Frequency Ratio %	10	10	10	8	**11.7**
Realized Gain (dBi) (microwave/mm-wave)	7.23 / 11.26	6.81 / 18.2	6.71 / 11.93	4.95 / 13.94	**6.7** / **15.2**
Isolation Level (dB) (microwave/mm-wave)	N / A	N / A	N / A	-36 / -40	**72** / **46**
Harmonic Suppression Capability	No	No	No	No	**Yes**
Frequency Response Independently	N / A	N / A	N / A	N / A	**Yes**

unwanted harmonics at the mm-wave band and achieving the total frequency independence of bands. Furthermore, both resonators are dielectric resonators.

3.7 Conclusions

This paper presents the design and fabrication of a cylindrical dielectric resonator antenna that operates on two different frequency bands for 5G applications. The proposed design integrates two cylindrical dielectric resonators (CDRs) with different permittivities of 6 and 12, which are embedded and excited to operate in two frequency bands : sub-6 GHz and millimeter-wave bands. The large CDR resonates at 2.4 GHz and has a 6.7 dBi realized gain, and the fundamental mode is excited using a copper tape glued on its circumference, which is connected to a microstrip line. In contrast, the small CDR (D_2) operates at 28 GHz, reaching a 15.2 dBi realized gain and the fundamental mode is excited using a rectangular coupling slot. To eliminate unwanted harmonics at the mm-wave band, a low-pass filter (LPF) was added to the (D_1) feeding line. This resulted in an improvement in the isolation level and reflection coefficients of both frequency bands. The antenna exhibits independence of frequency bands, making it a unique feature of this design. The simulated and experimental results show good agreement, indicating the effectiveness of the design. In summary, the novel characteristics introduced in the design of the dual-band microwave and mm-wave DRA make this antenna a promising candidate for 5G applications.

4 HIGH-GAIN DUAL-BAND ANTENNA WITH INDEPENDENT FREQUENCY OPERATION FOR SUB-6 GHZ AND MILLIMETER-WAVE APPLICATIONS

Bizan, Mohamed Sedigh, Peyman PourMohammadi, Amjad Iqbal, and Tayeb A. Denidni.

AEU-International Journal of Electronics and Communications (2025) : 155743.

DOI : 10.1016/j.aeue.2025.155743
(Published).

4.1 abstract

This work presents an innovative dual-band hybrid antenna designed to achieve high gain and superior isolation, catering to both microwave and millimeter-wave applications. The proposed design integrates a cylindrical dielectric resonator antenna (CDRA) for the microwave band and patch ring resonators for the mm-wave band, providing distinct and optimized operation in each frequency range. The antenna design incorporates multiple stages : initially, the CDRA is tailored for efficient microwave performance; next, the patch resonators are configured for mm-wave operation. These components are then combined strategically to ensure compatibility and minimal interference between bands. To enhance the antenna's functionality, selective filters are applied—specifically, a Low Pass Filter (LPF) for the microwave band and a Band Pass Filter (BPF) for the mm-wave band—mitigating harmonic distortion and improving spectral purity. Additionally, shorting pins are introduced to boost isolation levels between the bands. The resulting antenna achieves notable performance metrics, including bandwidths of 11.7% at 5.8 GHz and 14.3% at 28 GHz, with maximum realized gains of 12.3 dBi and 17.2 dBi, respectively. It also demonstrates exceptional isolation, surpassing 54 dB and 51 dB for the microwave and mm-wave bands. The innovative integration of these design elements enables independent frequency responses, making the proposed antenna a compelling solution for next-generation dual-band communication systems.

4.2 introduction

The rapid advancement of communication technologies has led to a growing need for antennas capable of delivering high performance while efficiently operating across multiple frequency bands. [44–49]. Among these, dual-band antennas have become essential for modern wireless networks due to their ability to cover different frequency ranges and offer sufficient performance while maintaining a simpler design and better efficiency. As 5G and beyond-5G technologies conti-

nue to emerge, the significance of dual-band antennas in meeting the requirements for faster data rates, wider bandwidths, and enhanced connectivity has become even more pronounced [1, 50]. These antennas are crucial for addressing the challenges of delivering seamless communication performance in advanced networks [38, 51–54].

One effective approach to designing a dual-band antenna and achieving optimal performance across two distinct frequency bands is through hybrid designs, which involve integrating multiple antenna structures. It should be pointed out that selecting the appropriate antennas within this hybrid approach is crucial for obtaining efficient dual-band operation.

On the one hand, Dielectric Resonator Antennas (DRAs) are known for their ability to provide high gain and excellent impedance matching with a low profile [24,55], making them an ideal choice for modern wireless communication applications [56, 57]. On the other hand, series-fed patch antennas provide high gain and wide bandwidth by efficiently distributing current across multiple radiating elements [58–60]. These structures improve performance, particularly in millimeter-wave (mm-wave) frequency bands [61, 62], while easily integrating with other antenna configurations. Moreover, these antennas enhance the effectiveness of hybrid designs for dual-band antenna applications [63, 64]. Incorporating DRAs and series-fed patches to design dual-band antennas improves efficiency and offers new ways to tackle the challenges of communication networks in both microwave and mmwave frequency bands in an era where versatility and adaptability are crucial [65, 66].

Dual-band antennas have been extensively studied in literature. For example, in [1], the authors proposed a dual-band dielectric resonator antenna (DRA) that operates at 16 GHz and 38 GHz, achieving a frequency ratio of 2.36. The TE_{111} and TE_{131} modes have been used. The proposed antenna has been excited by a microstrip-fed slot, showing impedance bandwidths of 13.3–19 GHz and 36.3–40 GHz and gains of 10.6 and 14.2 dBi, respectively.

The Mode Composite Antenna (MCA) has been introduced in [50], which uniquely combines a monopole antenna with a substrate-integrated waveguide (SIW) slot antenna. The MCA achieved high isolation between its low-band and high-band operations by leveraging the strengths of both structures. The shared-surface dual-band antenna proposed by the authors in [51] utilized characteristic mode analysis (CMA) to efficiently integrate metasurfaces and partially reflective surfaces (PRS) for operation in both the S-band and Ka-band. This design achieved the measured impedance bandwidths exceeding 9% and realized gains ranging from 7.27 to 14.6 dBi. Similarly, in [52], Mr. Xiang addressed the coexistence of microwave and millimeter-wave technologies by introducing a novel topology that achieved a frequency ratio greater than 3. Through a signal routing approach, microwave and millimeter-wave signals have been directed to specific elements separately, facilitating flexible dual-band operation with distinct radiation properties. Furthermore, the concept of partial structure has been reused, as given in [53], enabling the development of a compact shared-aperture antenna supporting steerable beams in the millimeter-wave band. The design achieved a dual-band and beam steering capabilities while maintaining a compact form

factor suitable for terminal applications by integrating a 3.5 GHz planar inverted-F antenna (PIFA) with 28 GHz substrate-integrated DRA (SIDRA) arrays. The authors in [54] proposed a magnetoelectric (ME) dipole antenna based on dual-mode operation. This design utilized mirrored U-shaped patches and a substrate-integrated waveguide (SIW) cavity, achieving wide impedance bandwidths of 24–29.3 GHz and 35.5–43.5 GHz, with gains ranging from 4.8 to 8.7 dBi. In [43], a windowed slow-wave parallel-plate waveguide (WSW-PPW) platform has been proposed. This platform integrates electromagnetic bandgap (EBG) structures into a dual-layer printed PPW, allowing for the flexible arrangement of microwave (MW) and millimeter-wave (MMW) antenna elements. By employing this approach, the authors demonstrated a shared-aperture antenna capable of supporting both mm-wave and Microwave bands, with independently steerable beams at each band. Expanding on the concept of dual-band antennas, encapsulated dielectric resonator antennas (E-DRAs) offered a unique solution for efficient radiation across two widely separated frequency bands [67]. Smaller DRAs have been embedded within a larger DRA, enabling simultaneous radiation at both sub-6 GHz and millimeter-wave (MMW) bands. Utilizing a fused filament fabrication (FFF) 3D printing process for manufacturing, the authors achieved impressive performance, including a maximum gain of 18 dBi at 31.5 GHz and over 95% efficiency at sub-6 GHz. Additionally, the bandwidths achieved surpass those of the previous works, positioning E-DRAs as a promising candidate for 5G and beyond. Taking advantage of a shared aperture approach, the authors in [68] have developed a technique to integrate a 26 GHz beam-steering array with a 3.5 GHz bandwidth-enhanced perforated patch antenna. In addition to shared aperture techniques, the concept of a dual-frequency substrate-integrated antenna offered another promising solution [69]. By combining a differentially fed slot antenna and a substrate-integrated dielectric resonator antenna, the authors created a dual-frequency antenna operating at 5.2 GHz and 24 GHz. The measured results exhibit good isolation between the two antenna parts, demonstrating the feasibility of integrating antennas with a large frequency difference. Moreover, the demand for adaptive beam steering in millimeter-wave antennas has been addressed in [70]. The authors have developed an aperture-sharing technique to integrate a 28 GHz array with a 3.5 GHz dipole antenna, enabling stable gain levels and broad impedance bandwidths exceeding 20% in both bands. The compact size of the prototype maked it suitable for terminal applications in future wireless networks. A dual-broadband, dual-polarized magnetoelectric (ME) dipole antenna with a shared aperture has been proposed in [71]. Operating in both the sub-6 GHz and millimeter-wave bands, this antenna provided dual-polarized radiation and achieved a wide impedance bandwidth. Its ability to generate 2-D multiple beams made it highly suitable for 5G base station applications. Additionally, by integrating a millimeter-wave substrate-integrated dielectric resonator antenna (SIDRA) beam-steerable array with a long-term evolution (LTE) folded monopole antenna (FMA), a dual-band antenna has been proposed in [37]. By sharing the same substrate and aperture, the design achieved high space utilization. The antenna demonstrated coverage across both the LTE band and the millimeter-wave frequency band, with beam-steering capabilities.

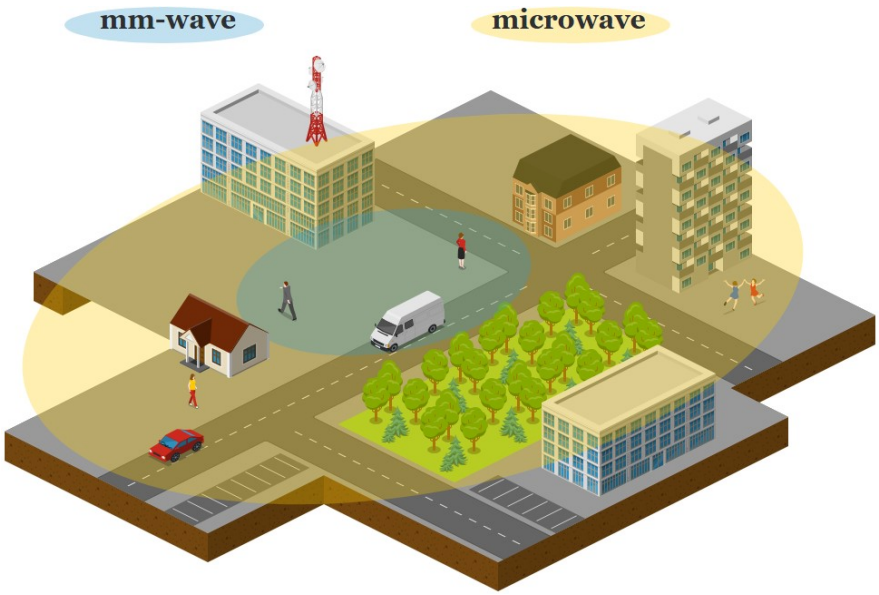

FIGURE 4.1 : Conceptual illustration of a dual-band antenna operating at microwave and mm-wave frequency bands.

Although extensive research has been conducted in the literature, none of the aforementioned structures can simultaneously achieve high gain in both the microwave and mm-wave bands. But here, high gain across both microwave and millimeter-wave is obtained by the proposed configuration. In this paper, a cylindrical dielectric resonator antenna (CDRA) for the microwave band and a series of patch ring resonators for the mm-wave band are employed. After that, a Low Pass Filter (LPF) is incorporated for the microwave band, alongside a Band Pass Filter (BPF) for the mm-wave band, effectively suppressing unwanted harmonics. Finally, the short pins are used to improve the isolation level. The key innovation of the proposed configuration lies in the integration of selective filters that significantly enhance the antenna's gain while ensuring high isolation between the two operational frequency bands by using short pins. The proposed antenna features an independent frequency response, allowing for precise control and optimization in each band, making it a highly effective solution for advanced microwave and millimeter-wave applications.

The lower frequency band is utilized to ensure a stable and reliable user experience, while the higher frequency band is employed for high-speed transmission of large data volumes through fixed millimeter-wave beams, as illustrated in Fig. 4.1.

Note that microwave signals can travel long distances easily, but millimeter wave signals have limited range due to significant atmospheric attenuation and difficulty in passing through obstacles like walls and buildings. Therefore, they are more suitable for short-range and high-speed communication.

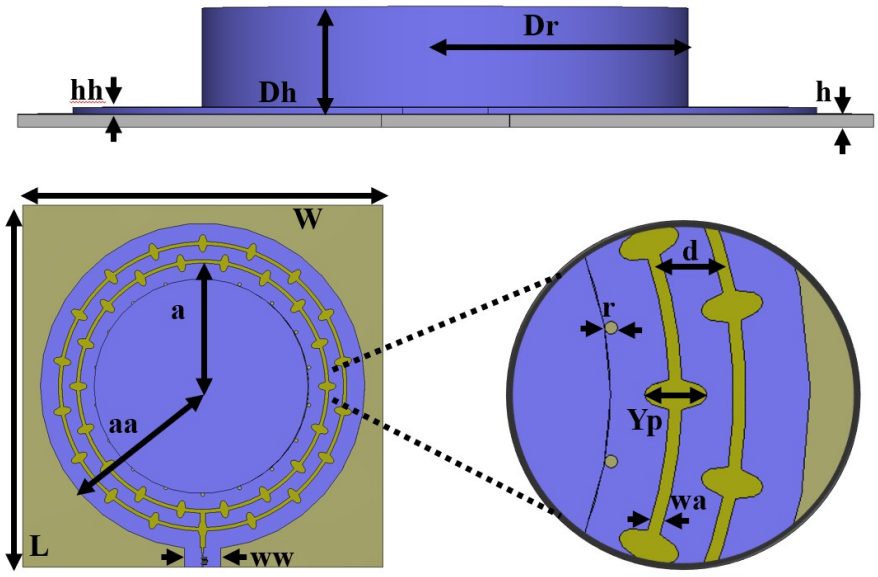

FIGURE 4.2 : The proposed antenna's geometrical structure (all dimensions in millimeter). Dr = 29.5, Dh = 11.4, h = 1.27, hh = 0.64, W = L = 100, a = 36, aa = 40, ww = 10, d = 5.0, r = 1.0, Yp = 4.8, wa = 1.0.

4.3 Antenna configuration

As shown in Fig. 4.2, the proposed dual-band high-gain hybrid antenna mainly consists of two resonators placed on top of the 100 mm × 100 mm Roger RO3003 substrate, which has a relative permittivity of 3 and a thickness of 1.27 mm.

In the first step, a Cylindrical Dielectric Resonator Antenna (CDRA) is designed for the microwave band operating at 5.8 GHz, as illustrated in Fig. 4.3(a). The CDRA has a radius of 29.5 mm and a height of 11.4 mm, made from Roger RO3210 material, characterized by a dielectric constant of 10.8 and a loss tangent of 0.002.

For the $HEM_{12\delta}$ mode, the radius Dr and height Dh of the CDRA is calculated using the following equation [16, 72] :

$$f(GHz) = \frac{30 k_o Dr}{2\pi Dh(\frac{Dr}{Dh})} \tag{4.1}$$

where Dr / Dh is the aspect ratio of the CDR, and k_o is the free space wave number. The value $k_o Dr$ is determined for the $HEM_{12\delta}$ mode as follows :

$$K_o Dr = \frac{3.72 + 0.4464x + 0.2232x^2 + 0.0521x^3}{\sqrt{\epsilon_r}} - \frac{2.65 e^{[-1.25x(1+4.7x^2)]}}{\sqrt{\epsilon_r}} \tag{4.2}$$

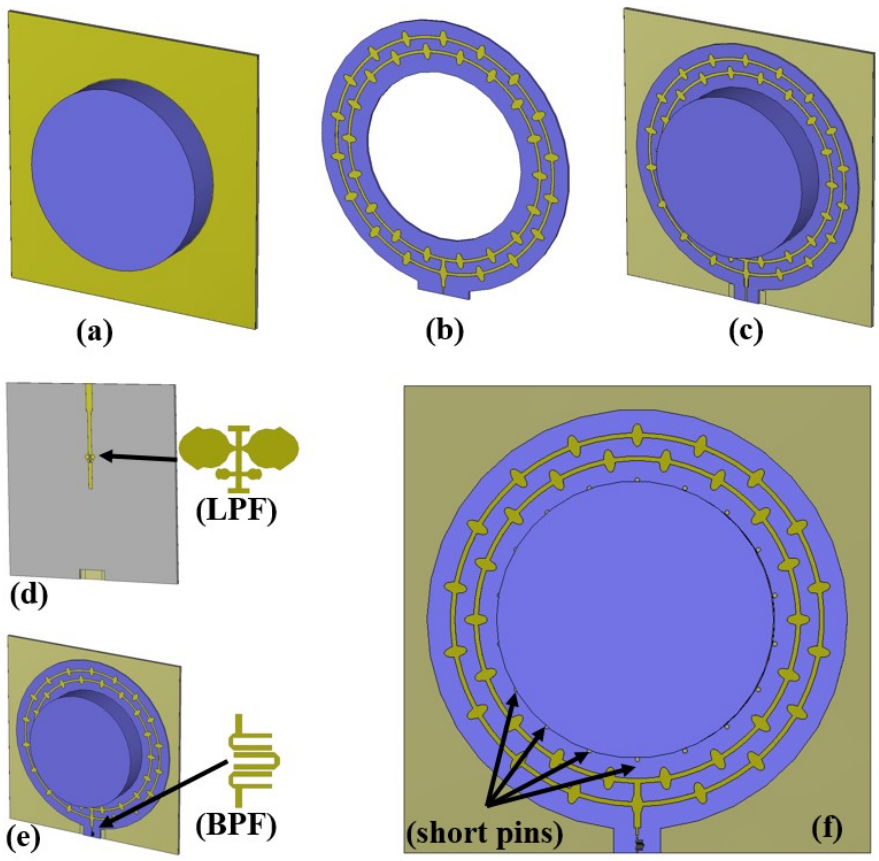

FIGURE 4.3 : The six steps of the proposal antenna (a) only CDRA, (b) only series-fed patch, (c) integrated patch-CDRA, (d) LPF, (e) BPF, (f) short pins.

$$Q = \epsilon_r^2[0.068 - 0.0388x + 0.0064x^2 + 0.0007e^{x(37.59-63.8x^2)}] \tag{4.3}$$

where x = Dr / 2Dh, ϵ_r is the relative permittivity of the CDRA, and Q is the radiation quality factor.

It should be noted that the radiation quality factor equation (4.3) is only valid if the CDRA aspect ratio is between 0.5 and 5.0.

$$0.5 \leq \frac{Dr}{Dh} \leq 5.0 \tag{4.4}$$

Equation (4.1) estimates initial values, which are not accurate because the effect of the DRA's feeding network has not been considered. This oversight can shift the center frequency of the antenna and limit its bandwidth. Additionally, the equations assume that the ground plane is infinitely large, which is not practical and can further affect the results.

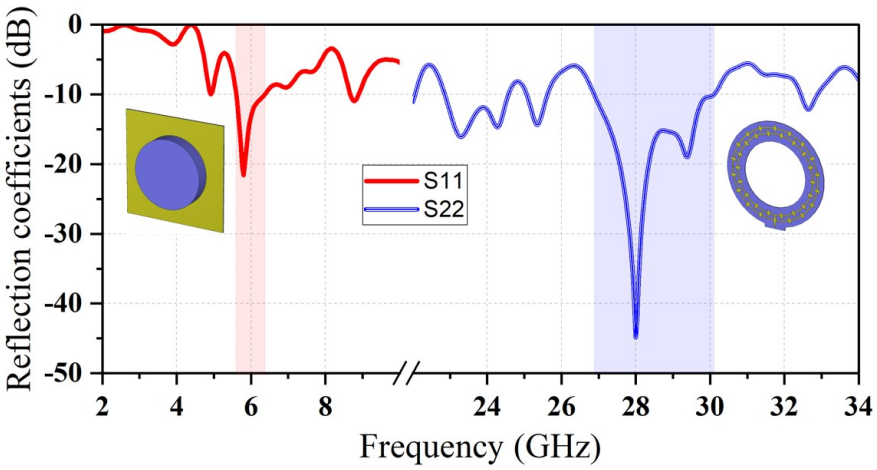

FIGURE 4.4 : Reflection coefficients of the two resonators before merging them.

To excite the $HEM_{12\delta}$ mode of the dielectric resonator, a rectangular aperture with dimensions of 8 mm in length and 2 mm in width is etched onto the ground plane. The reflection coefficient (S_{11}) of the designed DRA in the microwave band at a center frequency of 5.8 GHz, represented by the red line, is shown in Fig. 4.4.

In the second step, the antenna operating in the mm-wave frequency band is designed by exciting the TM_{11} mode in an elliptical patch. The resonant frequency of 28 GHz is calculated using the following equations [17, 73, 74] :

$$a_{eff} = a[1 + \frac{2h}{\pi\epsilon_r a}[ln(\frac{a}{2h}) + [1.41\epsilon_r + 1.77] \frac{a}{h}(0.268\epsilon_r + 1.65)]]^{\frac{1}{2}} \tag{4.5}$$

$$f_{11}^{e,o} = \frac{15}{\pi\epsilon_r a}\sqrt{\frac{q_{11}^{e,o}}{\epsilon_r}} \tag{4.6}$$

$$q_{11}^{e} = 0.0049e + 3.7888e^2 - 0.7278e^3 + 2.314e^4 \tag{4.7}$$

$$q_{11}^{0} = 0.0063e + 3.8316e^2 - 1.1351e^3 + 5.2229e^4 \tag{4.8}$$

where :

a - Semi-major axis

h - Height of dielectric substrate

ϵ_r - Permittivity of the dielectric substrate.

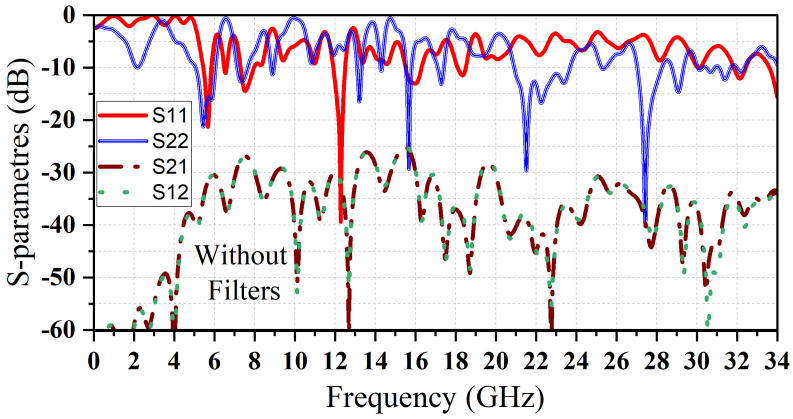

FIGURE 4.5 : S-parameters of the proposed antenna after merging the two resonators and before adding the filters.

a_{eff} - Effective semi-major axis.

e - Eccentricity of an elliptical patch.

$f_{11}^{e,o}$ Dual-Resonance frequency.

$q_{11}^{e,o}$ Approximated Mathieu function of the dominant $TM_{11}^{e,o}$ mode.

After defining the major and minor axes for the elliptical patch, two circular micro-strips are utilized to connect 18 elliptical patches each, resulting in a total of 36 elliptical patches distributed across two circles, 5 mm apart. This configuration is designed on a ring-shaped Roger RO3210 substrate with a relative dielectric constant of 10.8 and a thickness of 0.64 mm, as given in Fig. 4.3(b). The reflection coefficient (S_{22}) of the designed Series-fed patch antenna in the millimeter wave band at a center frequency of 28 GHz, represented by the blue line, is shown in Fig. 4.4.

Following the design of the antennas for the microwave and mm-wave frequency bands, the two antennas are integrated. as shown in Fig. 4.3(c). The results of this configuration are shown in Fig. 4.5. It can be observed that there are a number of harmonics in hybrid configuration which can deteriorate the antenna performance. In the next step, a Low-Pass Filter (LPF) for the lower frequency band and a Band-Pass Filter (BPF) for the higher frequency band are designed. The configurations of the two filters are depicted in Fig. 4.6(a). Fig. 4.6(b) illustrates the configuration of the proposed LPF. A Compact Microstrip Resonant Cell (CMRC) LPF with an innovative structure has been designed, incorporating two pairs of asymmetrically sized, Tulip flower-shaped butterfly open stubs. These flower-shaped elements are symmetrically connected to both sides of a narrow transmission line. The proposed configuration effectively allows frequencies to pass below 10 GHz. Consequently, the filter functions as an open circuit at higher frequencies, significantly reducing current flow and preventing feeding to the series-fed patch antenna. Conversely, at lower frequencies, the filter behaves as a short circuit. The input impedance of the filter is kept at 50 Ω. The overall dimensions of the designed CMRC-based LPF are (8 × 6) mm^2, making it an ideal candidate for integration with small antennas. As shown in Fig. 4.7, the filter exhibits an insertion

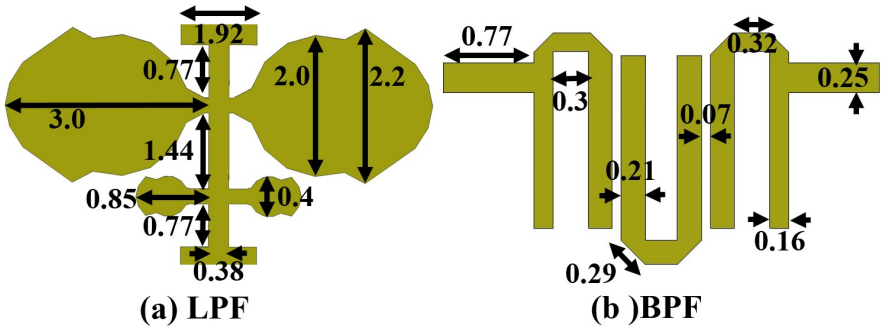

FIGURE 4.6 : Detailed structures of the (a) LPF, (b) BPF (all dimensions in millimeter).

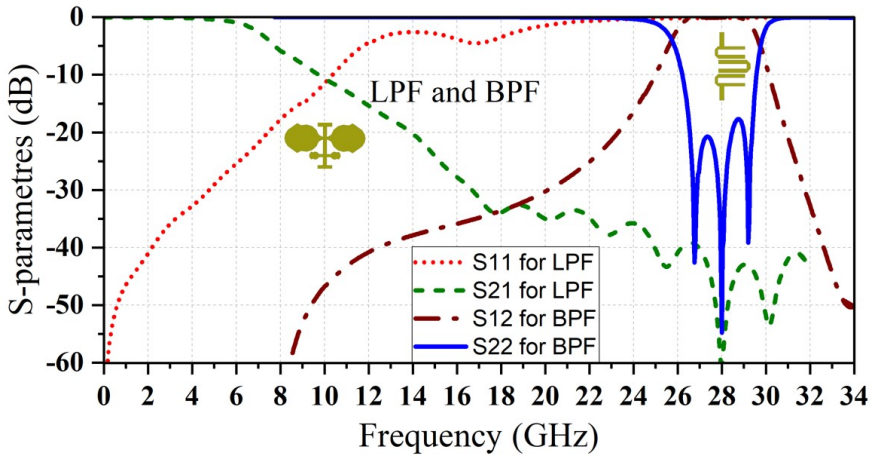

FIGURE 4.7 : Scattering parameters of the LPF and BPF.

loss of less than 0.5 dB within the 1–10 GHz passband, indicated by the green dashed line on the left side of the figure. Additionally, the return loss exceeds 20 dB across the entire passband. The attenuation level in the stop-band (14–34 GHz) is better than -20 dB. This demonstrates that the designed filter offers an ultra-wide stopband at higher frequencies, covering the frequency bands of interest.

Fig. 4.6(b) shows the geometry of the proposed BPF filter. The proposed third-order folded Chebyshev bandpass filter is designed for millimeter-band frequencies ranging from 26 GHz to 30 GHz. As indicated by the blue line on the right side of Fig. 4.7, a bandwidth of 3.5 GHz at the center frequency of 28 GHz ranging from 26.2 GHz to 29.5 GHz is achieved. Besides, it shows an insertion loss of less than 0.5 dB within the 26–30 GHz passband, indicated by the brown dashed line on the right side of the figure. Additionally, the return loss exceeds 20 dB across the entire passband. Also, the attenuation level in the reject bands is better than 20 dB. Then, the two designed filters are added to the proposed antenna to suppress harmonics in both bands. The designed LPF is added to the microstrip line feeding the cylindrical dielectric resonator, while the designed BPF is connected to the two rings of serial patches, as shown in Fig. 4.3(d) and Fig. 4.3(e). The simulated S-parameters of the two filters are shown in Fig. 4.7. It is worth mentioning that both filters were simulated and optimized using the Finite-Element Method (Finite-Element Method (FEM))-based Computer Simulation Technology (CST).

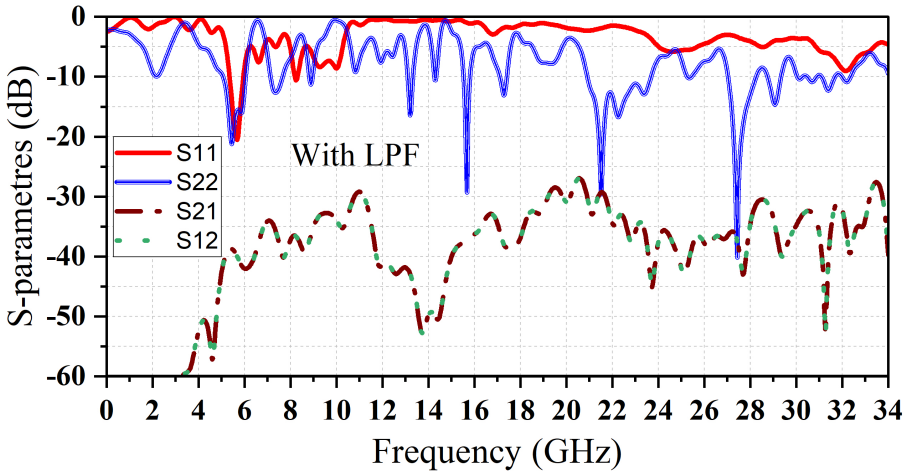

FIGURE 4.8 : S-parameters of the proposed antenna after adding the low pass filter.

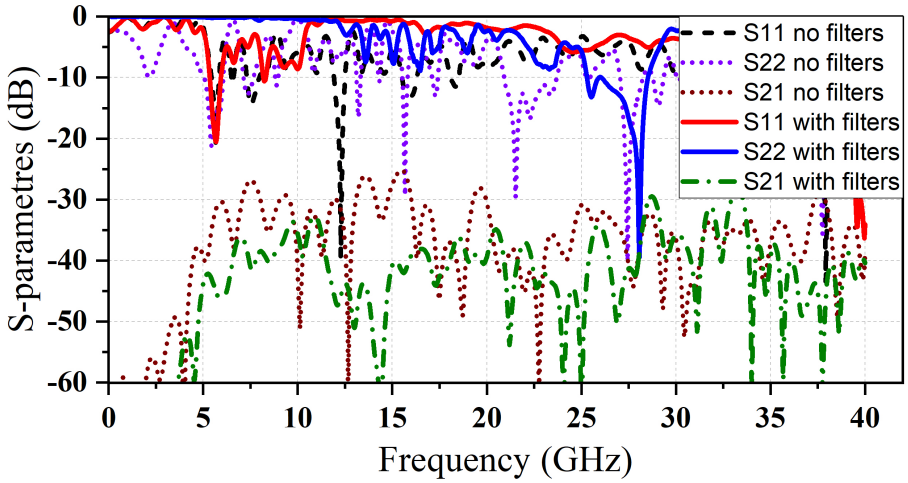

FIGURE 4.9 : Effect of the filters in the proposed structure.

The impact of connecting these two filters is shown in Figs. 4.5, 4.8, and 4.9. Fig. 4.5 presents the proposed antenna's S-parameters before adding the filters, while Figs. 4.8 and 4.9 illustrate the S-parameters afterward.

In the last step, 18 pins are inserted by drilling through the series-fed patch antenna to surround the cylindrical dielectric antenna, as shown in Fig. 4.3(f). The purpose of these pins is to reduce the mutual coupling between the two resonators, thereby enhancing the isolation level (S_{12} and S_{21}). The impact of the pins on the isolation level is shown in Fig. 4.10. In the proposed dual-band antenna, each resonator is designed to operate at its specific frequency bands, creating an electromagnetic field distribution around it. Without any barriers, these fields can extend beyond the resonator and potentially be coupled with the fields of adjacent resonators. Introducing pins, which are connected to the ground plane, between the resonators acts as both a physical and

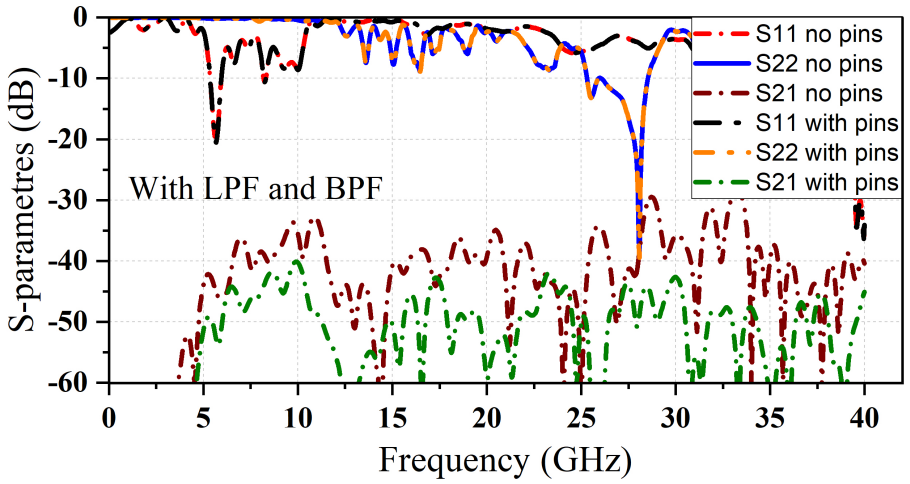

FIGURE 4.10 : Effect of adding the pins on the isolation level.

electromagnetic barrier. These pins disrupt the field lines, preventing them from extending into the space occupied by the adjacent resonators. This reduces coupling between the resonators and decreases interference between the two frequency bands. Furthermore, the pins modify the electromagnetic boundary conditions, altering the distribution of electric and magnetic fields in the space between the resonators. This modification prevents the excitation of certain unwanted resonant modes, ensuring that the resonators operate only at their desired frequencies. Moreover, the addition of shorting pins does not impact the performance of the antenna in terms of its resonant frequency. More specifically, both resonant bands remain the same with and without the shorting pins, as shown in Fig. 4.10.

Fig. 4.9 demonstrates the impact of incorporating filters on the reflection coefficients(S_{11}, S_{22}) and isolation levels (S_{12} and S_{21}). The addition of filters significantly improves the matching conditions, as evidenced by the enhanced (S_{11} and S_{22}) values, while also achieving higher isolation levels, with reduced (S_{12} and S_{21}), ensuring superior performance and minimal interference between the bands.

The following points summarize the steps taken to design the proposed antenna :

a) Designing the First Resonator : Determine the initial dimensions for the dielectric resonator to operate in the microwave band (5.8 GHz) using Equation (4.1) for the fundamental $HEM_{12\delta}$ mode;

b) Designing the second resonator : Design the series-fed patch resonator for the mm-wave band at 28 GHz using Equation (4.6);

c) Integrating the resonators : Combine the two resonators into a single structure;

d) Adding an LPF for the first resonator to the designed antenna for suppressing unwanted harmonics;

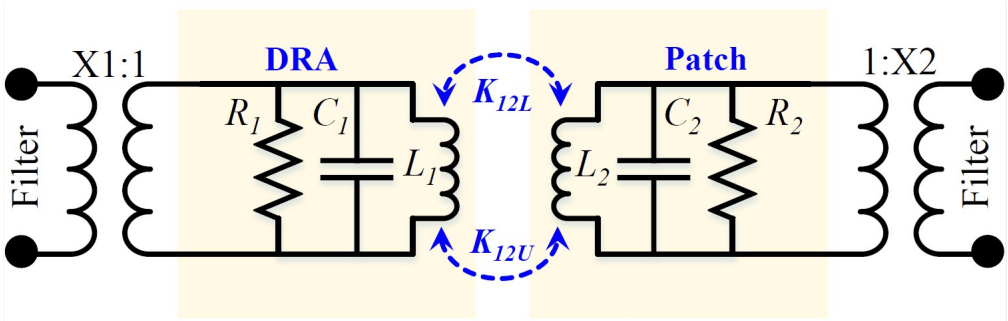

Component	Value	Component	Value	Component	Value
R_1	207 Ω	C_1	1.45 pF	L_1	0.51 nH
R_2	337 Ω	C_2	0.26 pF	L_2	0.19 nH
X1	0.37	X2	0.04	K_{12U}	1.44
K_{12L}	1.43	---	---	---	---

FIGURE 4.11 : Equivalent circuit of the proposed antenna.

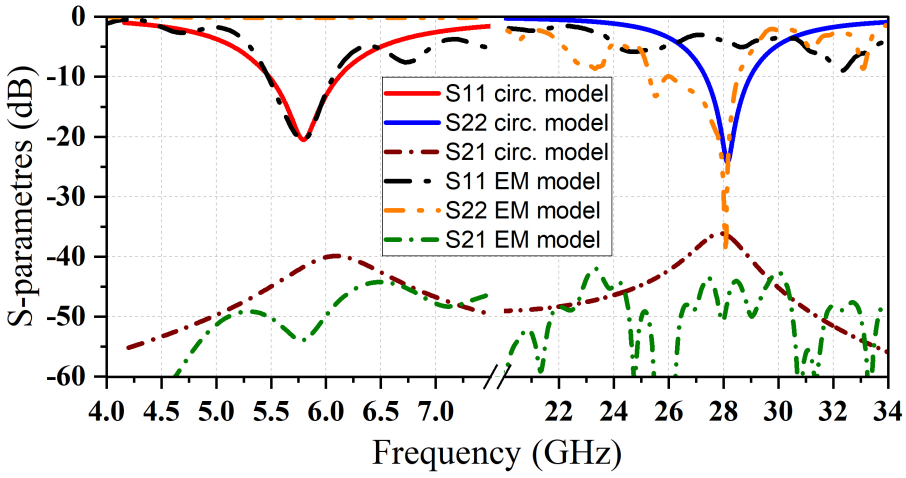

FIGURE 4.12 : S-parameters of the EM model compared with the circuit model of the proposed antenna.

e) Adding a BPF for the second resonator to the designed antenna for suppressing unwanted harmonics;

f) Inserting pins to improve isolation level : Insert pins around the dielectric resonator to enhance the isolation level.

The equivalent circuit model of the proposed design is shown in Fig. 4.11. The proposed design consists of radiating Dielectric Resonator Antenna (DRA) and series-fed patch antennas. In the circuit model, the DRA is modelled as a parallel RLC tank, and the series-fed patch antennas are also modelled as a parallel RLC tank. Both radiating structures are fed through filters. Therefore, the coupling between the filter and the DRA is modelled as X1, while the coupling between the filter

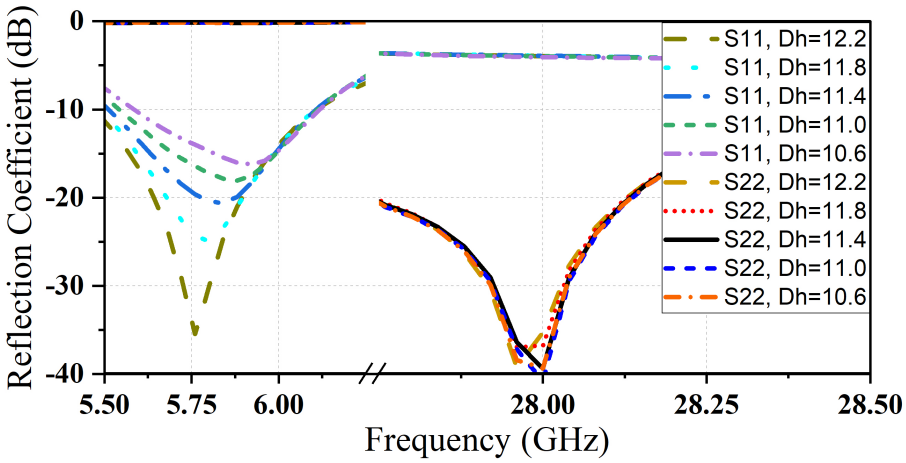

FIGURE 4.13 : Reflections coefficients for different dielectric resonator height values (in millimeter).

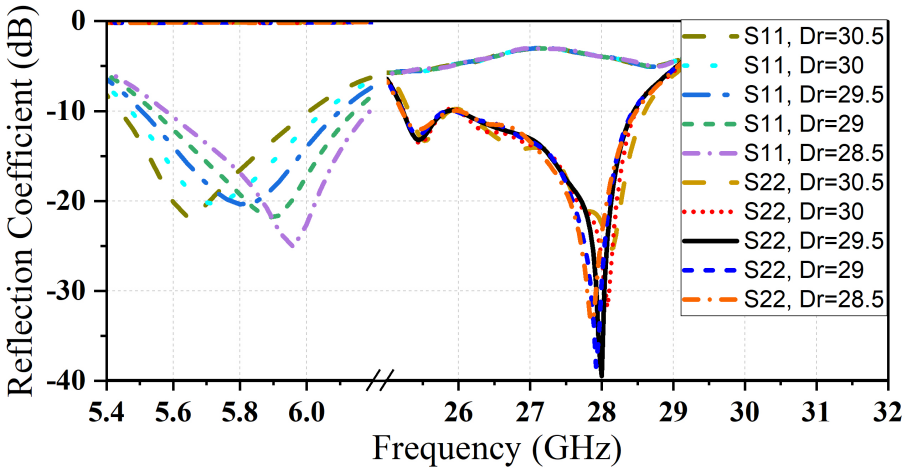

FIGURE 4.14 : Reflections coefficients for different values of dielectric resonator's radius (in millimeter).

TABLE 4.1 : The impact of altering the parameters Dh, Dr, a, and Yp on the key characteristics.

Parameter	S_{11}	S_{22}	Radiation Efficiency	Radiation Pattern (Beamwidth) for Sub-6 GHz Band	Gain for Sub-6 GHz Band	Radiation Pattern (Beamwidth) for mm-Wave Band	Gain for mm-Wave Band	Poynting Vector
Dh	Improved	No Effect	Decrease	Wider	Decrease	No Change	No Change	Reduced
Dr	Shift to the Left	No Effect	Slight Decrease	No Change	No Change	No Change	No Change	Reduced
a	No Effect	Shift to the Left	Increase	No Change	No Change	Narrower	Increase and Shift to the Left	Enhanced
Yp	No Effect	Shift to the Rigth	Decrease	No Change	No Change	Wider	Decrease	Reduced

and the patch antenna is modelled as X2. Moreover, the mutual coupling between both radiating structures is modelled as K_{12U} and K_{12L}, where K_{12U} represents mutual coupling at the upper band, and K_{12L} represents mutual coupling at the lower band. The optimized circuit component values are shown in Fig. 4.11. S-parameters of the EM model compared with the circuit model of the proposed antenna are given in Fig. 4.12.

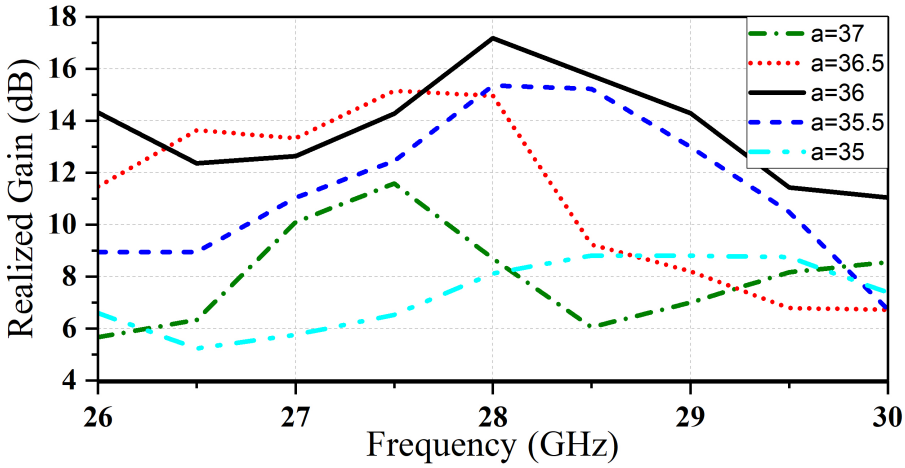

FIGURE 4.15 : The realized gain for different values of the ring radius (in millimeter).

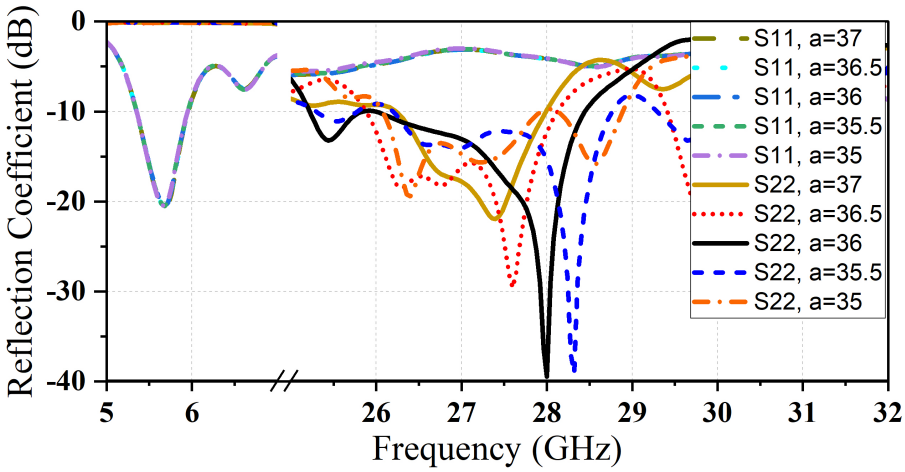

FIGURE 4.16 : Reflections coefficients for different values of the ring radius (in millimeter).

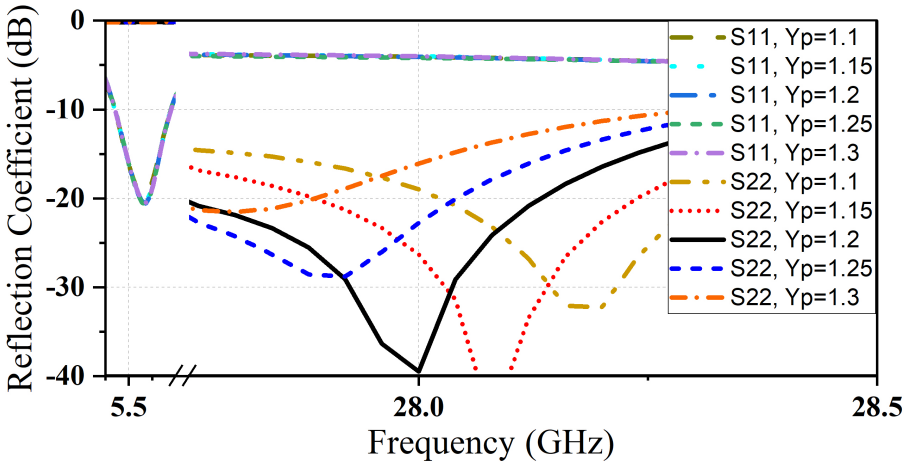

FIGURE 4.17 : Reflections coefficients for different values of patches dimensions (in millimeter).

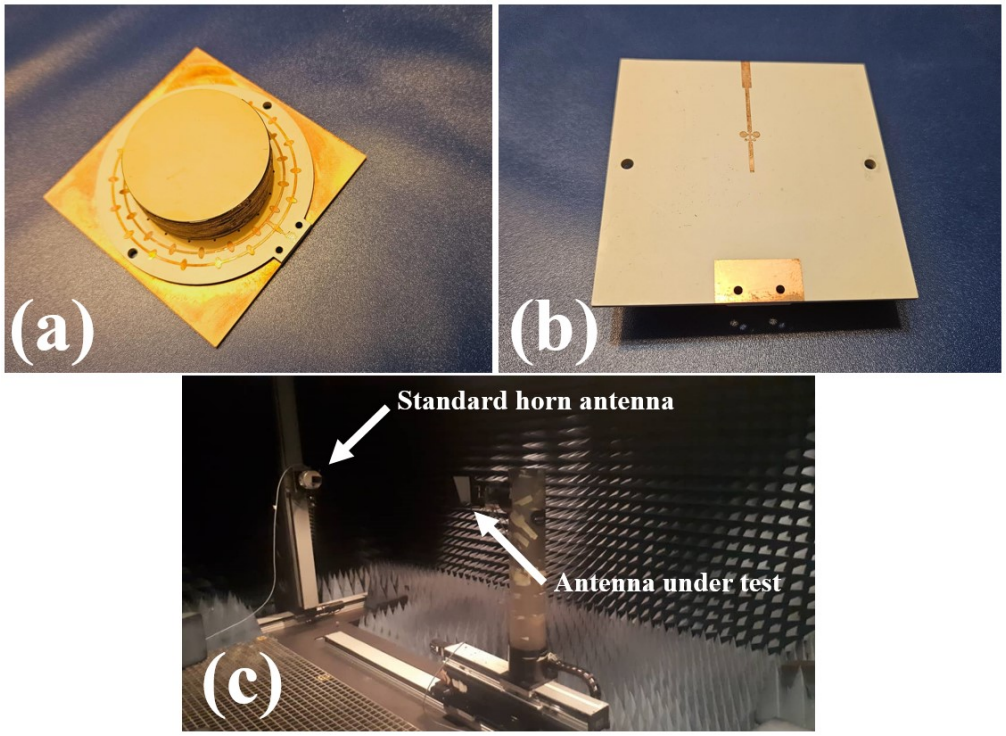

FIGURE 4.18 : The fabricated proposed antenna. (a) top view, (b) back view, (c) in an anechoic chamber to measure the radiation pattern.

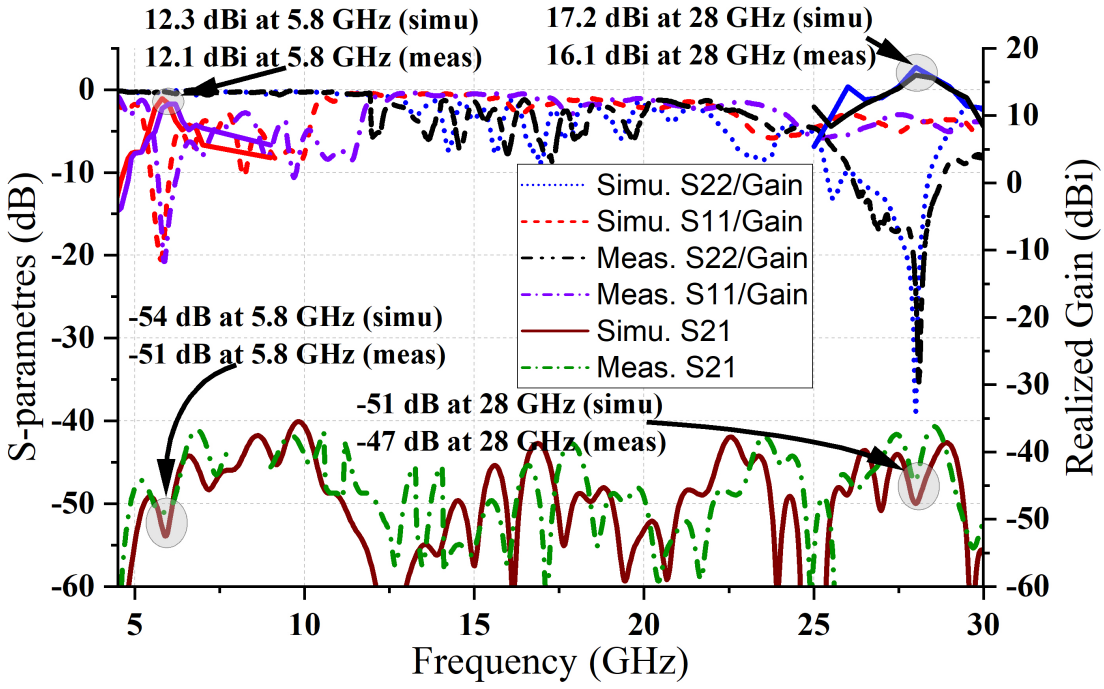

FIGURE 4.19 : The simulated and measured S-parameters and realized gain of the dual-band proposed antenna.

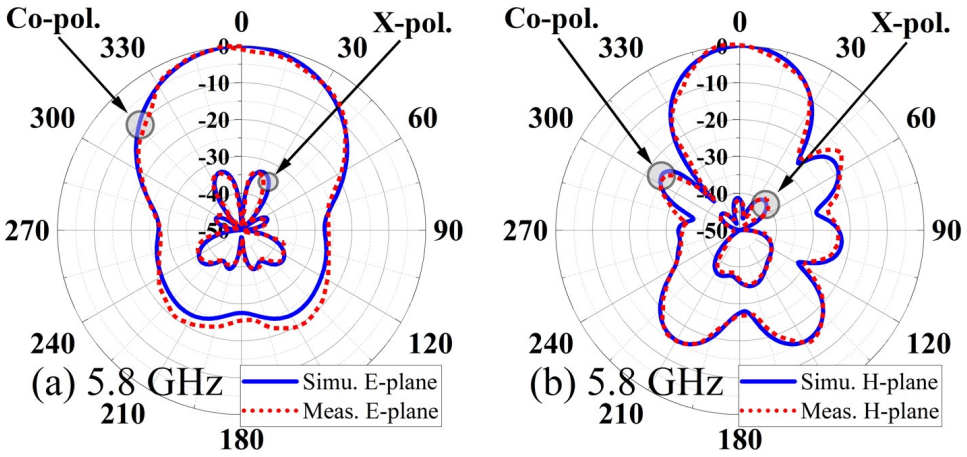

FIGURE 4.20 : Simulated and Measured 2-D radiation patterns, (a) E-plane at 5.8 GHz, (b) H-plane at 5.8 GHz.

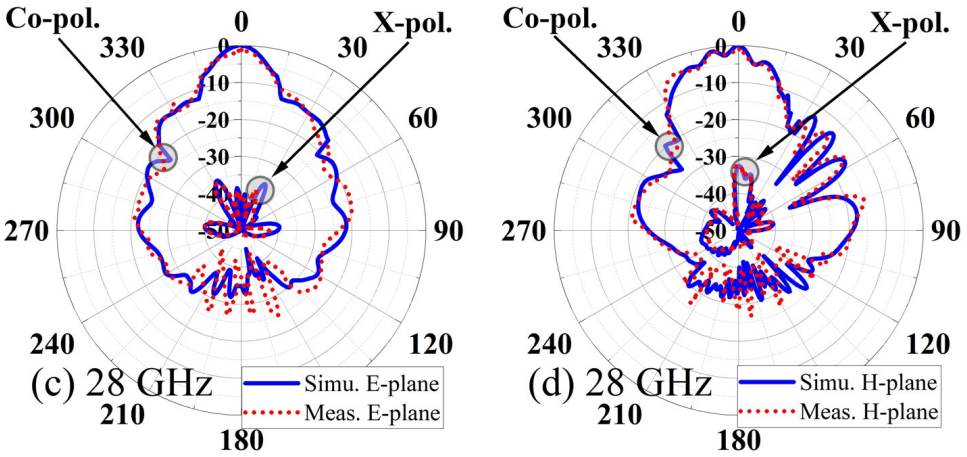

FIGURE 4.21 : Simulated and Measured 2-D radiation patterns, (c) E-plane at 28 GHz, (d) H-plane at 28 GHz.

4.4 parametric study

To optimize the antenna design and understand the impact of structural variations on its performance, a comprehensive parametric analysis was conducted, examining key design parameters such as the height D_h and radius D_r of the cylindrical dielectric resonator (Cylindrical Dielectric Resonator (CDR)), the patch series ring radius a, and the patch size Y_p. These parameters play a critical role in determining the antenna's S-parameters, radiation efficiency, radiation patterns, gain, and Poynting vector. The results have been summarized in Table 4.1, providing insights into these trade-offs. As illustrated in Fig. 4.13, increasing the dielectric resonator height D_h improves the reflection coefficient of the microwave band. However, this improvement comes at the cost of reduced radiation efficiency and gain in the sub-6 GHz band while slightly broadening the radiation pattern. In addition, increasing D_h resulted in a reduced Poynting vector. Notably, Fig. 4.14 demonstrates that increasing the CDR radius D_r also shifts the resonance frequency to a lower frequency but has minimal impact on other performance parameters, apart from a slight reduc-

TABLE 4.2 : Comparison Between The Proposed Antenna And Previous Works.

Parameter	[43]	[67]	[68]	[69]	[70]	[71]	[37]	This work
Operation frequency (GHz) (sub-6/mm)	3.5/28	3.6/30.5	3.5/26	5.2/24	3.5/28	3.5/28	2.2/28	**5.8/28**
Frequency ratio %	8	8.47	7.4	4.6	8	8	12.7	**4.83**
Antenna type (sub-6/mm)	Patch/DRA	DRA/DRA	Patch/ SIDRA	Patch/CDRA	Dipole/ array unit	ME-dipole	FMA/ SIDRAs	**DRA/ Patch**
Realized Gain (sub-6/mm)	4.95/13.94	7.5/18	5/12.9	3.93/6.32	7.07/11.31	10.67/14.85	3.9/11.4	**12.5/17.2**
Isolation level (dB) (sub-6/mm)	36/40	31/25	Not given	35	Not given	55/33	35/20	**54/51**
Filtering Capability (sub-6/mm)	No/No	No/No	No/No	No/No	No/No	No/Yes	No/No	**Yes/Yes**
Frequency response independently	Not given	Yes	Not given	Not given	Not given	Not given	Not given	**Yes**

tion in radiation efficiency. Moreover, the Poynting vector was reduced when D_r was increased. Similarly, as depicted in Fig. 4.15, modifying the patch series ring radius a significantly affects the higher reflection coefficient S_{22}, shifting it to a lower frequency while improving radiation efficiency and increasing gain. However, this adjustment also narrows the mm-wave radiation pattern. Furthermore, by increasing a, the Poynting vector intensified. As shown in Fig. 4.17, increasing the patch size (Y_p) shifts S_{22} to a higher frequency, reduces radiation efficiency, and slightly broadens the mm-wave radiation pattern, leading to a decrease in gain at higher frequencies. Besides, increasing Y_p led to a reduction in the Poynting vector. Importantly, Figs. 4.13 and 4.14 confirm that altering the CDR dimensions primarily affects the microwave band, whereas modifications to the patch size or ring dimensions, as illustrated in Figs. 4.15, 4.16, and 4.17 primarily influence the mm-wave band. This highlights the independent frequency response of the two bands, allowing for tuning of each without undesired coupling effects. Proper selection of these parameters is therefore crucial for optimizing performance, balancing impedance matching, gain, and radiation efficiency to achieve maximum gain, a wider impedance bandwidth, and an improved reflection coefficient.

4.5 Experimental Result and Discussions

The fabricated prototype of the proposed antenna can be seen in Fig. 4.18(a) and Fig. 4.18(b). Note : The fabrication process requires meticulous manufacturing to ensure precision and functionality. The CDRA consists of nine stacked circular pieces made from Roger RO3210 material, characterized by a dielectric constant of 10.8, a loss tangent of 0.002, and a thickness of 1.27 mm. Epoxy Resin adhesive with a minimal layer thickness is used that does not change the overall relative permittivity of the CDRA. The stacking of these pieces achieves the desired resonator height of 11.4 mm. Note that the material selection is based on its cost-effectiveness in the consumer market. The proposed antenna is measured by the Agilent Network Analyzer. Fig. 4.19 demonstrates a good agreement between the simulated and measured S-parameters. Although there are minor deviations in S_{11} and S_{22} towards the right, the antenna maintains a strong reflection coefficient, affirming its reliability.

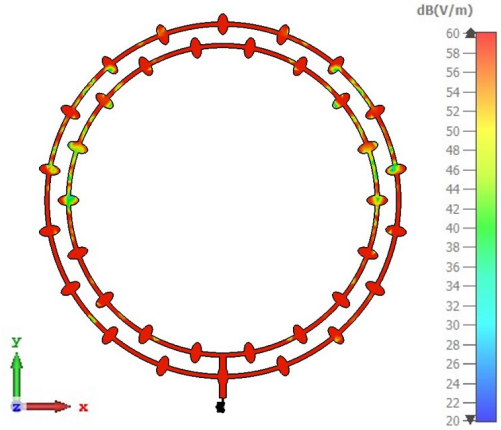

FIGURE 4.22 : Simulated resonant E-field on the surface of the patches ring resonator in xy plane for TM_{11} mood at 28 GHz.

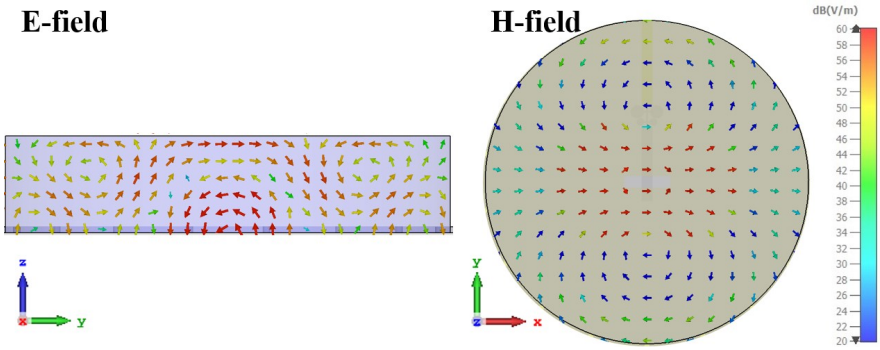

FIGURE 4.23 : Simulated resonant E and H fields inside the CDRA in yz plane for $HEM_{12\delta}$ mood at 5.8 GHz.

As given in Fig. 4.18(c), far-field measurements performed in an anechoic chamber at 5.8 GHz and 28 GHz provided valuable insights into the antenna's radiation characteristics. As depicted in Figs.4.20 and 4.21, the measured co/cross patterns closely matched the simulated patterns, indicating good agreement between simulation and measurement. The realized gains at both frequencies further underscored the antenna's performance, with a high realized gain of 12.3 dBi simulated and 12.1 dBi measured for the microwave band, and 17.2 dBi simulated and 16.1 dBi measured for the mm-wave band, highlighting its suitability for practical applications in wireless communication systems.

It should be pointed out that the series-fed patch resonator in the millimeter-wave band achieves a higher realized gain compared to the CDR in the microwave band. This difference can be understood by examining the field distributions of the two resonators. Fig. 4.22 illustrates the E-field on the surface of the series-fed patch resonator at 28 GHz. A strong E-field is concentrated around the boresight direction (z-axis), resulting in a narrow beam width and high antenna gain. In contrast, Fig. 4.23 depicts a strong E-field spread over a larger area of the CDRA, leading to a wider beam width and, resulting in a lower antenna gain.

Table 4.2 provides a summary of the proposed dual-band antenna performance, comparing it with other dual-band antenna structures operating in the microwave and mm-wave frequency

bands from existing literature. The proposed antenna demonstrates a high realized gain, along with a high level of isolation, despite using microstrip-type feeding and coupling aperture fed. In contrast to previous designs, the proposed antenna exhibits a remarkably high realized gain across both bands and a significantly high level of isolation. Additionally, it demonstrates full frequency response independence for each band, allowing for separate control of the response at different frequencies.

4.6 Conclusion

A new dual-band hybrid antenna that combines a CDRA for the microwave band with a series-fed patch ring resonators for the mm-wave band has been presented in this paper. The four-step design process optimizes impedance matching, realized gain, and isolation level, resulting in excellent performance in both frequency bands. The designed CDRA and series-fed patch ring resonator, operating at 5.8 GHz and 28 GHz, respectively, achieve realized gains of 12.3 dBi and 17.2 dBi. Adding an LPF and a BPF further enhances the antenna's spectral purity. The dual-band hybrid antenna shows outstanding features, including high isolation values above 40 dB across the entire frequency range. The novelty of this design lies in its ability to deliver high gain in both bands, achieved through the innovative use of pins and filters. This approach not only improves gain but also provides high isolation, reducing interference between bands. The design's ability to eliminate unwanted harmonics and its independent frequency response allows for precise and efficient performance across the bands.

5 SUB-6 GHZ FILTENNA INTEGRATION WITH MM-WAVE DIELECTRIC RESONATOR ANTENNA ARRAY FOR 5G APPLICATIONS

Bizan, Mohamed Sedigh, and Tayeb A. Denidni.

IEEE Access.

DOI : 10.1109/ACCESS.2025.3577105

(Published).

5.1 abstract

A patch filtenna operating at 5.2 GHz is integrated with a Cylindrical Dielectric Resonator Antenna Array (CDRA) resonating at 28 GHz to enable simultaneous microwave and milliliter wave communication has been introduced in this paper. First, an elliptical patch antenna is designed to operate at 5.2 GHz for the sub-6 GHz band. A hollow section is introduced at the patch's center to accommodate the CDRA. Subsequently, a cylindrical dielectric resonator (CDR) is engineered to resonate at 28 GHz for the mm-wave band. These two resonators are carefully combined to ensure seamless operation across both frequency bands. To further suppress unwanted harmonics of the lower band and enhance its isolation from the higher band, a low-pass filter was incorporated with the sub-6GHz antenna. To boost the overall realized gain of the mm-wave band, the DRA is translated to design, and the mm-wave resonator single-element antenna is translated to design a 2 × 2 (4-element) antenna array. This array is further utilized to form the proposed 4 × 4 (16-elements) array configuration to boost the overall realized gain of the antenna. The final antenna system design achieved 34.5% and 16.8% bandwidths, with maximum gains of 9.1 dBi and 19.0 dBi for the sub-6 and mm-wave bands, respectively. Additionally, the design demonstrates excellent isolation, with values exceeding 73 dB at 5.2 GHz and 62 dB at 28 GHz. The proposed design's main innovation is the concept of microwave filtenna integration with a high gain mm-wave antenna array. While existing research mainly focuses on dual-band operation design, this study highlights the importance of the lower band filtering effect for enhanced isolation and harmonic suppression, as well as the high-gain mm-wave radiation required for long-distance communication. Other innovative aspects of this work include independent control of each band, a reduced overall size, and a wide bandwidth.

5.2 Introduction

Nowadays, the swift advancement of communication technologies has led to an increasing demand for antennas capable of operating efficiently across multiple frequency bands. Dual-band antennas, in particular, have become indispensable in modern wireless networks due to their ability to support different frequency ranges. As 5G and beyond technologies advance, the importance of dual-band antennas has become even more evident. This helps designers not need separate antennas for each band. Instead, a single antenna element is sufficient. [75,76]. One effective strategy for achieving optimal dual-band performance involves using hybrid antenna designs, which integrate multiple resonators into a single configuration. Carefully selecting components within these hybrid designs is critical to ensuring efficient dual-band operation [25, 64, 77]. For example, DRAs are well-regarded for their high gain, excellent impedance matching, and low-profile form, making them particularly suited for modern wireless applications [24, 56, 78]. Meanwhile, patch antennas offer high gain and wide bandwidth by efficiently distributing current across multiple radiating elements [79–83]. These antennas are especially beneficial at millimeter-wave (mm-wave) frequencies and can be easily incorporated into other antenna architectures to achieve dual-band performance.

By combining DRAs with patch antennas, a hybrid dual-band design achieves superior efficiency and offers an innovative solution for the challenges posed by operating simultaneously with both microwave and mm-wave frequency bands [77]. In an era where versatility and adaptability are essential, these designs pave the way for more effective communication systems capable of supporting the demands of future multi-band wireless networks.

The concept of dual-band antennas is actively explored across various designs to address the demands of 5G and beyond. In [1], a dual-band DRA is introduced for millimeter-wave applications, utilizing the excitation of TE_{111} and TE_{131} modes at 16 and 38 GHz, respectively. One row of four DRAs array was built to enhance the gain to 10.6 dBi and 14.2 dBi across impedance bandwidths of 35.3% and 9.7%. An antenna stricture has been discussed in [84], where five RDRs form a MIMO system operating with ${TE^Y}_{1\delta1}$ and $HEM_{2\delta1}$ modes. The design covers frequencies from 3.3 to 3.8 GHz and 5.725 to 5.925 GHz, achieving gains of 7 dB and 7.2 dB while ensuring low correlation between elements for diverse wireless communication applications. A hybrid structure combining strip, slot, and dielectric resonators is proposed in [38] for mm-wave 5G bands, supporting resonances at 28 and 39 GHz. This design ensures wide steering angles and compactness, with a beam-steering array achieving angles of ±50° and ±40°. Similarly, in [85], a hybrid MIMO consisting of annular rings and CDR operates over two bands (1.75 to 2.4 GHz and 3.5 to 5.5 GHz) with enhanced isolation level S_{12} exceed 20 dB, and optimal diversity parameters, including envelope correlation coefficients and diversity gains. The hemispherical DRA (HDRA) proposed in [4] utilizes a rubber-filled cavity to reach dual-band behavior at 7.65 GHz and 10.04 GHz. The design features high coupling efficiency with gains of 11.72 dBi and 11.5 dBi. Another dual-band DRA

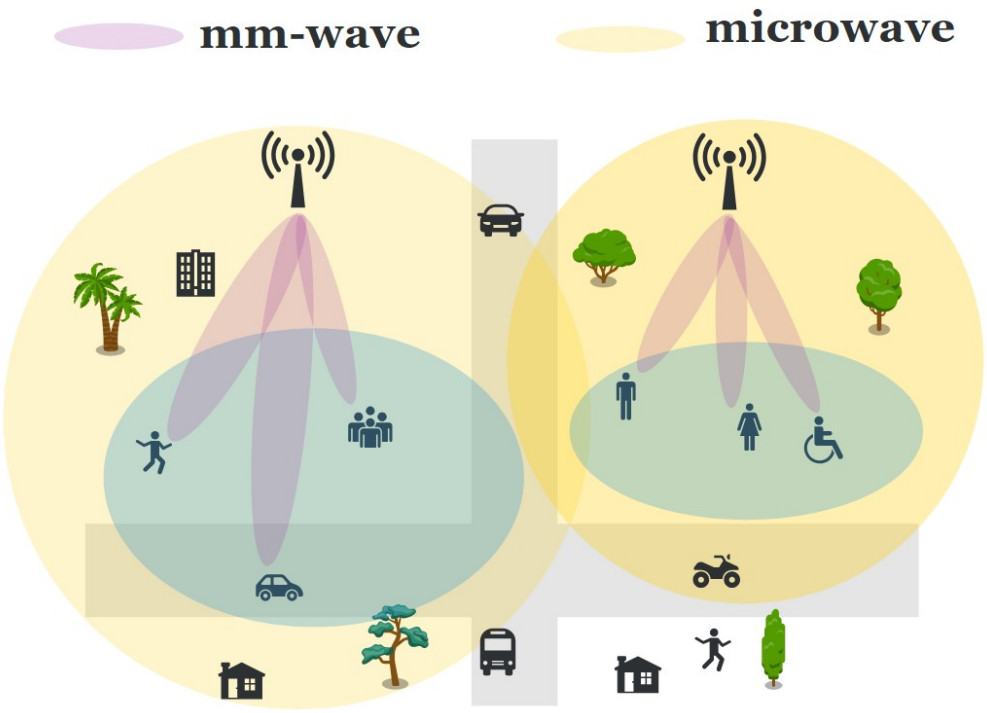

FIGURE 5.1 : Conceptual illustration of a dual-band antenna resonating at mm-wave and sub-6 frequency bands.

configuration employing layered truncated corners has been discussed in [45], achieving circular polarization (CP) at 21.75 GHz, 23.85 GHz, and 28.25 GHz. The design provides 17% and 15.2% impedance bandwidths and maximum gains of 5 and 8 dBic in the respective bands. The compact rectenna design presented in [86] integrates a dual-band DRA and rectifier, achieving broad impedance bandwidths for 5G frequency bands (2.515–2.675 GHz and 3.4–3.6 GHz) with high power conversion efficiency (PCE). This rectenna is tailored for IoT sensor networks. Similarly, a spiroid fractal (SFDRA) in [87] introduces reconfigurable dual-/triple-band circular polarization through quasi-$TM_{11\delta}$, $TM_{21\delta}$, and $TE_{12\delta}$ modes, supporting dynamic switching between bands for enhanced wireless performance. The authors in [88] have introduced a MIMO DRA system with four-port for microwave band, leveraging $TE_{01\delta}$ and $TE_{10\delta}$ modes at 3.3 GHz and 3.9 GHz, respectively. The design achieves isolation levels better than 20 dB and diversity metrics, such as an ECC of 0.01 and TARC of 22.46 dB, ideal for 5G and WiMAX networks.

While the above dual-band antennas operate with a small frequency ratio, making them ideal for closely spaced frequency bands, there are also designs that achieve a significantly larger frequency ratio. This characteristic allows for effective operation across widely separated frequency bands, enhancing their versatility for applications requiring both microwave and millimeter-wave performance. It is worth saying that sub-6 GHz frequencies provide better coverage and penetration, making them ideal for urban areas with many obstacles like buildings and trees. This range ensures stable connectivity over long distances, which is essential for cellular networks (e.g., 4G LTE, 5G low-band). On the other hand, mm-wave frequencies offer higher bandwidth and faster data rates but at the cost of reduced range and limited penetration through walls or other obs-

tructions. These high-frequency waves are ideal for high-capacity networks in dense urban areas or environments requiring ultra-fast communication, such as stadiums, autonomous vehicles, or industrial automation. Thus, The selection between mm-wave and microwave technologies is determined by the specific application requirements : microwave for broader coverage and reliability and mm-wave for speed-intensive, short-range applications. as illustrated in Fig. 5.1. In [72], a dual-band double-CDRA design efficiently operates in mm-wave and microwave bands. It employs two resonators with distinct permittivities, resonating at 2.4 GHz and 28 GHz, with respective gains of 6.7 dBi and 15.2 dBi. A similar focus on the dual-wide band operation has been highlighted in [89] through the mushroom-shaped antenna, which integrates cylindrical dielectric resonators (CDRA) and dielectric lenses (DL). This design has achieved 6.4 dBi at 5.3 GHz and 12.71 dBi at 31.51 GHz, with notable 3-dB gain bandwidths of 21% and 26.21%, respectively. The utilization of 3D printing enhanced control over the dielectric constant, ensuring precision in antenna fabrication. In [42], a rectangular dielectric block antenna with a central groove merges a DRA and Fabry–Perot resonator antenna (FPRA), offering dual-band resonating at 2.4 GHz and 24 GHz. The DRA utilizes multiple modes (TE_{111} and TE_{113}), while an L-probe reduces cross-polarization, contributing to bandwidth enhancement across the microwave and mm-wave frequencies. To further advance dual-frequency designs, [41] integrates a hollow DRA and FPRA, employing separate microwave and mm-wave regions to achieve high gain. This design ensures efficient operation at 2.4 and 24 GHz frequencies, with WR-34 waveguides and strip-based feeding mechanisms. A compact and space-efficient approach has been showcased in [90] using aperture-shared antennas, combining a microwave magneto-electric dipole (MED) antenna with open-ended waveguide arrays. This design supports multiple 5G bands, including n257 and n260, with beam scanning capabilities and gains up to 9.61 dBi, demonstrating the benefits of shared-aperture structures for compact, high-performance antennas. The concept of encapsulated DRAs has been explored in [67], demonstrating embedding smaller DRAs inside larger ones for enhanced dual-band radiation. The larger DRA targets sub-6 GHz frequencies, while the smaller cDRAs cover mm-wave bands. With 3D printing facilitating precise fabrication, the E-DRAs achieved 7.2 dBi and 18 dBi at 3.2 GHz and 31.5 GHz, respectively, with efficiencies exceeding 80% at both frequency bands. In [91], a structure-reused antenna with a quasi-elliptic band-pass feature has employed a frequency-selective surface (FSS) that radiates at 2.5–2.7 GHz while being transparent to K-band radiation (24.2–26.1 GHz). The work in [92] has introduced a composite DRA, integrating annular and cylindrical resonators. The proposed design resonates at 4.44 GHz and 27.92 GHz, with respective gains of 6.8 dBi and 4.3 dBi. The effective permittivity is analyzed to ensure broadside radiation patterns. In [69], a two-port substrate-integrated dual-frequency antenna achieves isolation between its elements, with S-parameters exceeding 35 dB. This design employs a hollow patch-loaded slot antenna for low-frequency operation at 5.2 GHz and a DRA for high-frequency operation at 24 GHz.

Although there have been numerous studies using DRAs for both microwave and mm-wave frequency bands, these designs have several limitations. For example, The unwanted harmonics

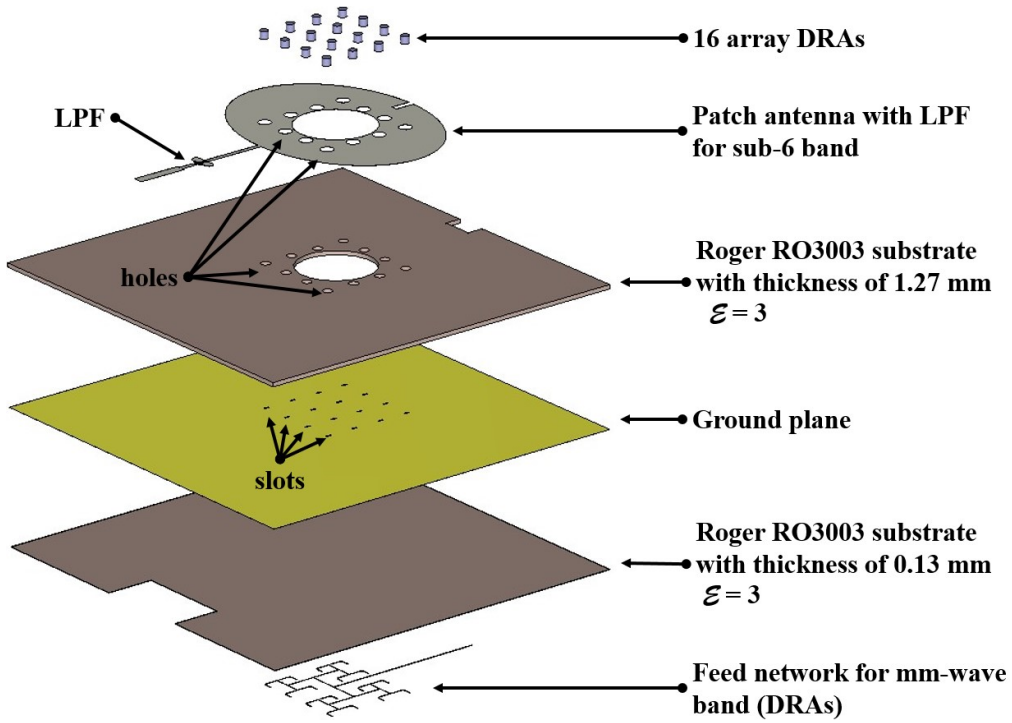

FIGURE 5.2 : Layers of the proposed antenna.

generated by the low-band antenna may introduce interference, leading to performance degradation in the mm-wave antenna. Additionally, to fully leverage the mm-wave band for 5G applications, a high-gain design is essential for long-range communication, but most existing solutions fail to provide the necessary gain. Other challenges include large size and low isolation between frequency bands. Therefore, a new approach addressing these limitations is needed.

In this paper, an elliptical patch filtenna combined with a CDRA is proposed to achieve a highly isolated, high-gain dual-band antenna. This antenna demonstrates maximum gains of 9.1 dBi at 5.2 GHz and 19 dBi at 28 GHz. The isolation between two resonators exceeds 60 dB, thanks to the integration of a low-pass filter with the microwave antenna. These exceptional gain and isolation characteristics make the proposed structure stand out. Additionally, the careful design of the feeding network with the array contributes to a compact form factor. Therefore, With its capability to operate in the mm-wave and microwave bands, the proposed structure emerges as a strong candidate for 5G applications.

5.3 Antenna configuration

The proposed dual-band high-gain hybrid antenna is structured with two resonators placed on a two-layer Roger RO3003 substrate of dimensions $100 \times 100mm^2$ and a relative permittivity of 3, as illustrated in Figs. 5.2, 5.3. To facilitate easier understanding, this section is organized as follows :

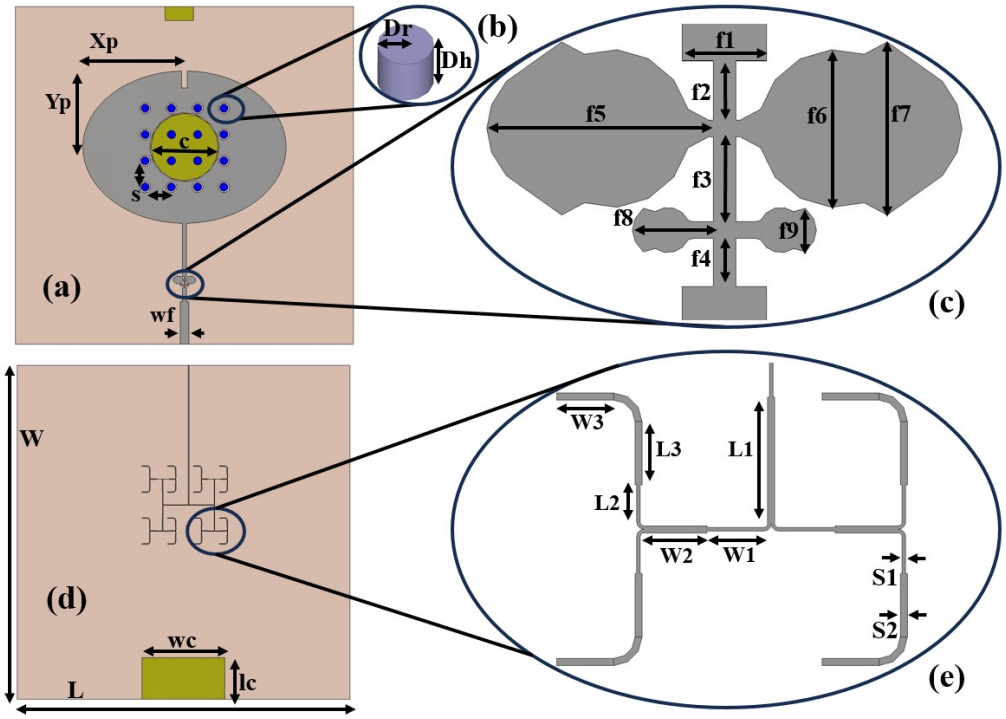

FIGURE 5.3 : Structural configuration of the proposed antenna (a) front view, (b) DRA, (c) LPF, (d) back view, (e) feeding network. W = 100, L = 100, wc = 30, lc = 15, Xp = 36, Yp = 27, c = 24, s = 9, wf = 3.1, Dr = 1.5, Dh = 2.2, L1 = 4.45, L2 = 1.3, L3 = 2.2, W1 = 2.0, W2 = 2.2, W3 = 2.0, S1 = 0.13, S2 = 0.25, f1 = 1.5, f2 = 1.0, f3 = 1.5, f4 = 0.85, f5 = 3.8, f6 = 2.65, f7 = 2.9, f8 = 1.36, f9 = 0.75.(all dimensions in millimeter).

5.3.1 Elliptical patch resonator for sub-6 GHz band :

Initially, as shown in Fig. 5.4(a), the first resonating frequency for the sub-6 band is achieved by exciting the TM_{11} mode in an elliptical patch. The 5.2 GHz resonant frequency is determined using the equations provided in [17, 73, 74].

$$(x_p)_{eff} = x_p[1 + \frac{2h}{\pi\epsilon_r x_p}[ln(\frac{x_p}{2h}) + [1.77 + 1.41\epsilon_r] \frac{x_p}{h}(1.65 + 0.268\epsilon_r)]]^{\frac{1}{2}} \tag{5.1}$$

$$f_{11}^{e,o} = \frac{15}{\pi\epsilon_r x_p}\sqrt{\frac{q_{11}^{e,o}}{\epsilon_r}} \tag{5.2}$$

$$q_{11}^{e} = 0.005e + 3.789e^2 - 0.729e^3 + 2.31e^4 \tag{5.3}$$

$$q_{11}^{0} = 0.00631e + 3.832e^2 - 1.135e^3 + 5.223e^4 \tag{5.4}$$

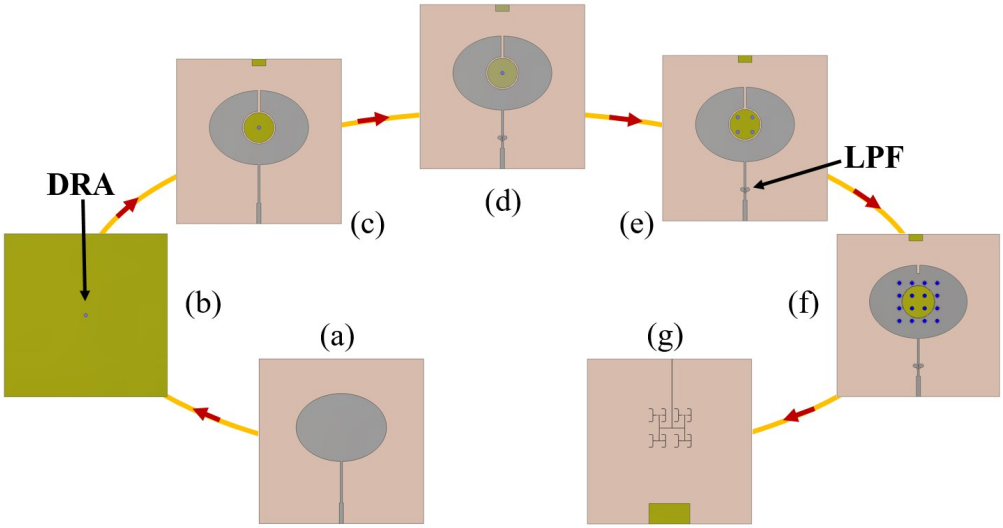

FIGURE 5.4 : The six steps of the design.

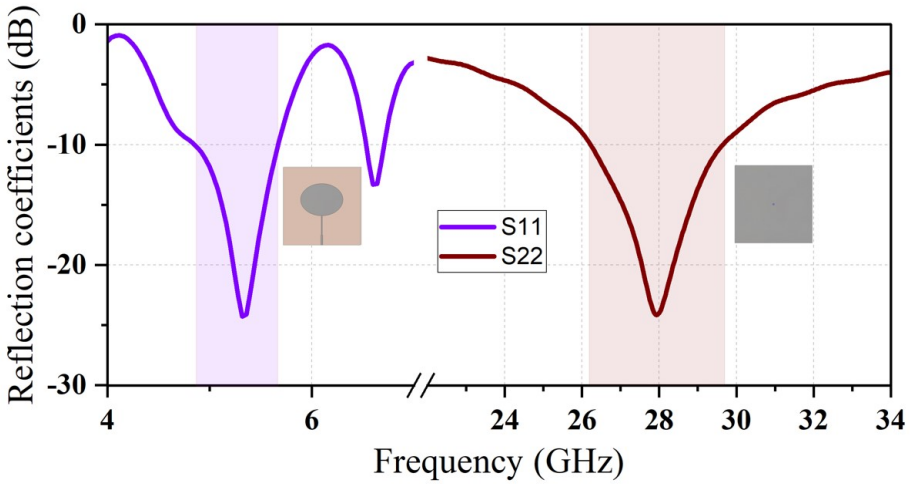

FIGURE 5.5 : (S_{11}) and (S_{22}) of the two bands separately.

where :

— x_p – Length of the semi-major axis of the elliptical patch

— h – Thickness of the dielectric substrate

— ϵ_r – Dielectric constant of the substrate

— $(x_p)eff$ – Effective semi-major axis length

— e – Elliptical patch eccentricity

— $f_{11}^{e,o}$ – Dual-resonance frequency

— $q_{11}^{e,o}$ – Approximate Mathieu function for the dominant $TM_{11}^{e,o}$ mode

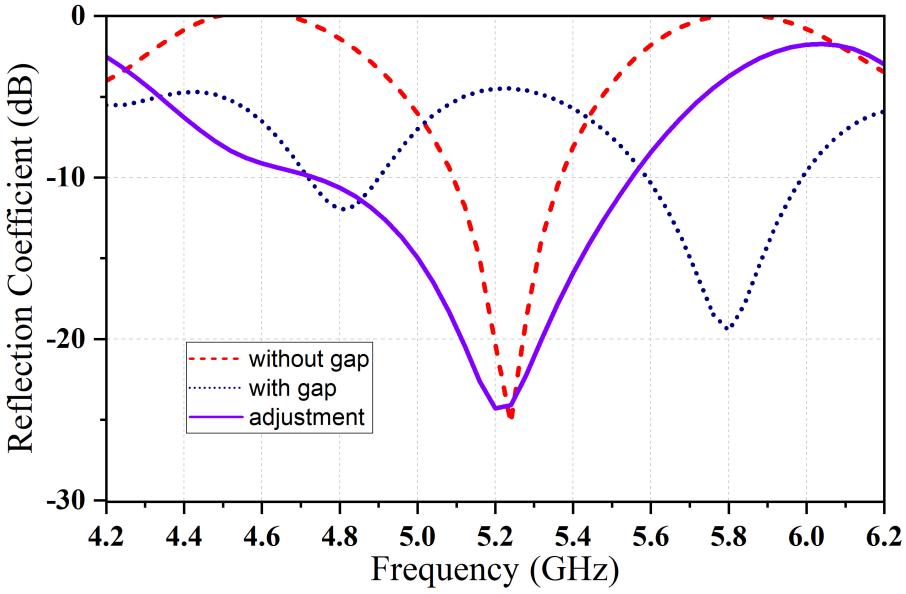

FIGURE 5.6 : The simulated reflection coefficient associated with the elliptical patch.

5.3.2 Cylindrical dielectric resonator for mm-wave band :

As shown in Fig. 5.4(b), the next step involves designing a compact dielectric resonator for 28 GHz operation in the mm-wave band. This design is separate from the elliptical antenna in this step. Mode analysis in CST software has been used to simulate the scattering parameter of this structure. The CDRA is made of Hik500, it has $\mathcal{E}_r = 10$ relative permittivity and 0.002 loss tangent. This material is selected due to its affordability and widespread availability in the commercial market.

The equation provided in [16] is used to calculate the CDRA's height *(Dh)* and radius *(Dr)*.

$$f(GHz) = \frac{30k_oD_r}{2h(\frac{D_r}{D_h})} \tag{5.5}$$

where :

— *(Dr/Dh)* – CDR's aspect ratio

— k_o – Free-space wave number

For the fundamental TE_{011} mode, the value k_oD_r was obtained using the following equation [16] :

$$k_oD_r = \frac{1}{\sqrt{\epsilon_r+1}}(1 - 0.00271(\frac{D_r}{D_h})^2 + 0.701(\frac{D_r}{D_h})) \tag{5.6}$$

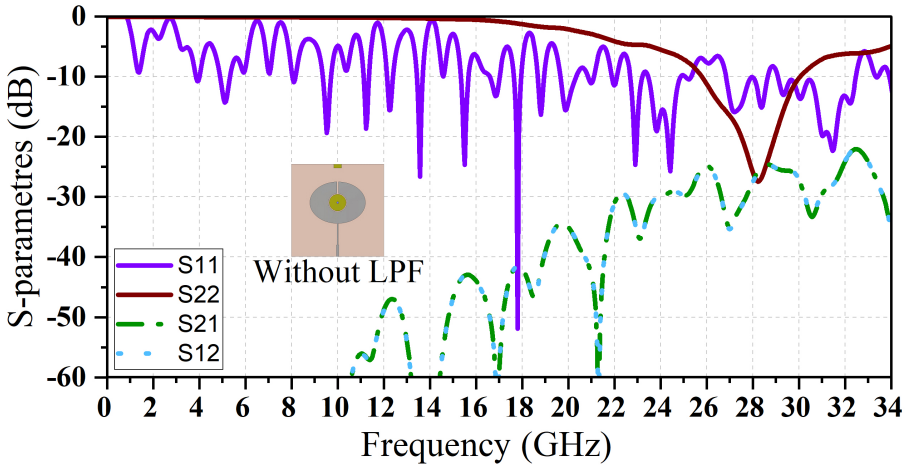

FIGURE 5.7 : S-parameters of the antenna for one element before adding the LPF.

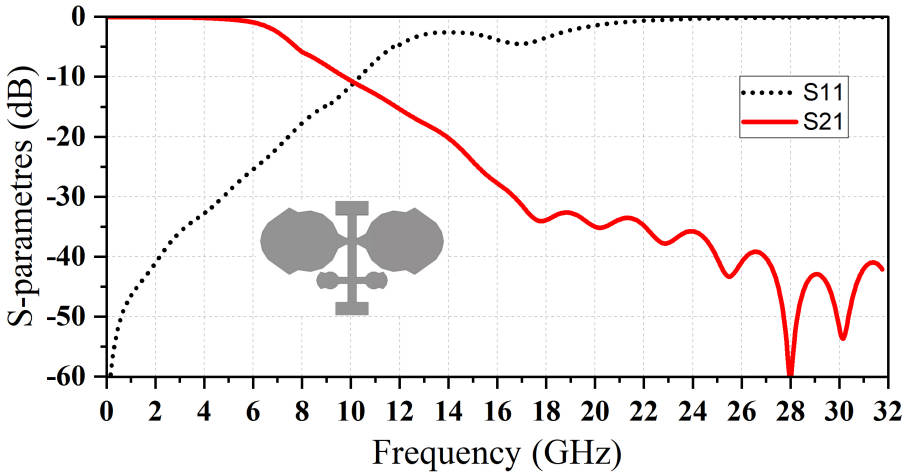

FIGURE 5.8 : LPF's Scattering parameters.

Equations (5.6) and (5.5) offer preliminary estimates for the values; however, they lack precision as they do not account for the influence of the excitation network of the DRA. This oversight may lead to shifts in the center frequency and impose bandwidth constraints. Additionally, the equations are derived under the assumption of an infinite ground plane.

Fig. 5.5 shows the reflection coefficient of both resonators separately before combining them, Fig. 4(a) and (b) separately. The purple line on the left of the figure indicates the reflection coefficient (S_{11}) of the patch for the sub-6 band, while the brown line on the right side indicates the reflection coefficient (S_{22}) of the dielectric resonator for the mm-wave band.

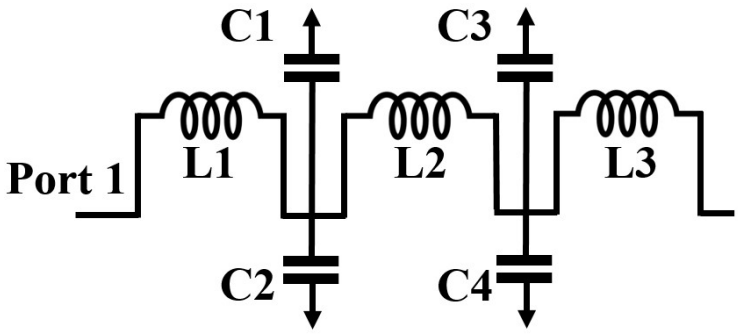

FIGURE 5.9 : Equivalent circuit for the LPF.

5.3.3 Dual-band Patch-Dielectric Resonators :

After separately designing antennas for the mm-wave and microwave frequency bands, they are combined to form an integrated structure, as illustrated in Fig. 5.4(c). A circular hollow is made in the center of the elliptical patch to make room for the second resonator. This hollow causes a shift to the right in the resonant frequency of the patch. Therefore, the next step is to adjust the patch dimensions to bring back the resonant frequency to 5.2 GHz. (See Fig 5.6). To that end, A rectangular slot is introduced on the top surface of the elliptical antenna to enhance the radiating area, resulting in a frequency shift to 5.2 GHz.

The performance outcomes of this setup, after several optimizations for precise resonances at the desired frequencies, are displayed in Fig. 5.7. The hybrid configuration introduces several harmonics that can negatively impact the antenna performance.

5.3.4 Low-pass filter design for harmonic suppression :

To address above mentioned issue regarding the unwanted harmonics, a Low-Pass Filter (LPF) is developed for the lower frequency band. The filter frequency response is presented in Fig. 5.8, and its detailed configuration can be seen in Fig. 5.3(c).

A Compact Microstrip Resonant Cell (CMRC) LPF is devised, featuring a unique design with two pairs of asymmetrical, Tulip flower-shaped butterfly open stubs. These stubs are arranged symmetrically on both sides of a narrow transmission line. This structure ensures that frequencies below 10 GHz pass through seamlessly, while at higher frequencies, the filter acts as an open circuit, blocking current flow and preventing the signal from reaching the patch antenna. At lower frequencies, it functions as a short circuit. The input impedance of the filter is maintained at 50 Ω, and its compact size, measuring (8 × 6) mm^2, makes it well-suited for integration with small antennas. As depicted in Fig. 5.8, the filter achieves an insertion loss of less than 0.5 dB over the 1–10 GHz passband, represented by the solid red curve. Additionally, it has a return loss greater than 20 dB throughout the passband, and the attenuation in the stopband (14–34 GHz) surpasses (-20

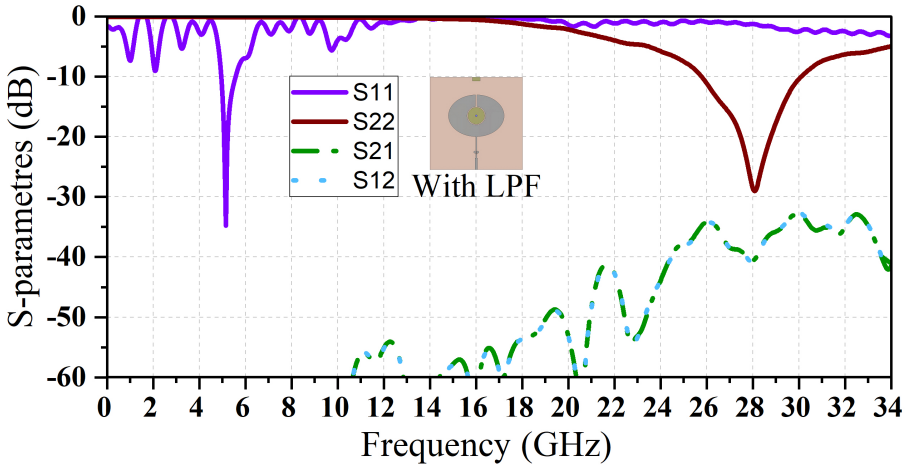

FIGURE 5.10 : Effect of adding the LPF on the S-parameter.

dB), offering an ultra-wide stopband that effectively covers higher frequency ranges of interest. The effect of integrating this filter is demonstrated in Figs. 5.7, and 5.10. Specifically, Fig. 5.7 presents the S-parameters of the proposed antenna before the filters are added, whereas Fig. 5.10 displays the S-parameters following the inclusion of the filters. As we can observe, incorporating the LPF not only suppresses undesirable harmonics in the mm-wave band but also enhances the isolation level.

The equivalent circuit of the low-pass filter (LPF) is depicted in Fig. 5.9, where the filter's key components are modeled using lumped elements to facilitate analysis and design optimization. In this circuit representation, the four capacitors correspond to the four open stub microstrip structures, which act as reactive elements introducing capacitance to suppress high-frequency signals beyond the cutoff frequency. Meanwhile, the three inductors represent the microstrip transmission lines that connect port (1) to the antenna, which play a crucial role in defining the impedance characteristics and ensuring signal continuity. These inductive elements correspond to the structures labeled f_2, f_3, and f_4 in Fig. 5.3(c), indicating their influence on the filter's frequency response. The combination of these capacitive and inductive elements forms a typical low-pass network, effectively attenuating unwanted harmonics while allowing the desired frequency components to pass. This equivalent circuit provides valuable insight into the LPF's behavior and serves as a useful tool for performance optimization and impedance matching within the antenna system.

5.3.5 CDR array design for high gain performance :

In the final stage, to improve "the realized gain of the antenna, the millimeter-wave section of the antenna is upgraded from a single element (Fig. 5.4(b)) to a four elements array (Fig. 5.4(e)) and then to a sixteen elements array (Fig. 5.4(f)). The selection of 16 dielectric resonator antennas (DRAs) in our design is based on a systematic optimization process to achieve a high gain. In-

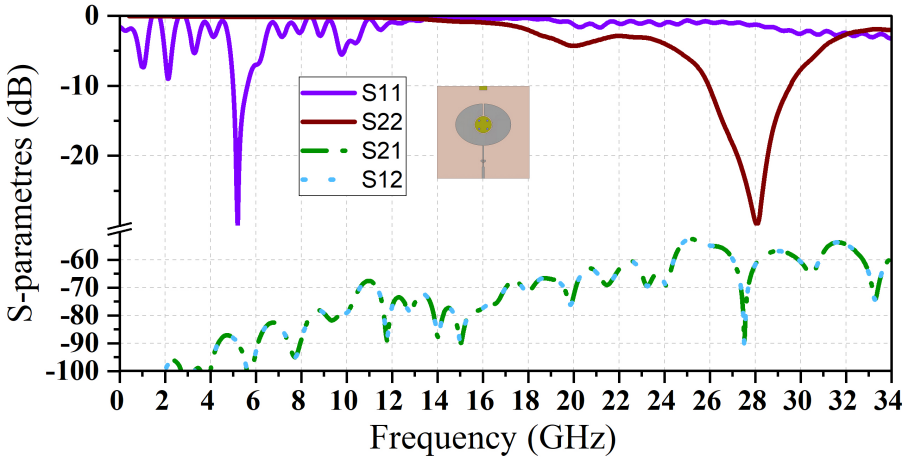

FIGURE 5.11 : S-parameter for 2 × 2 DR array.

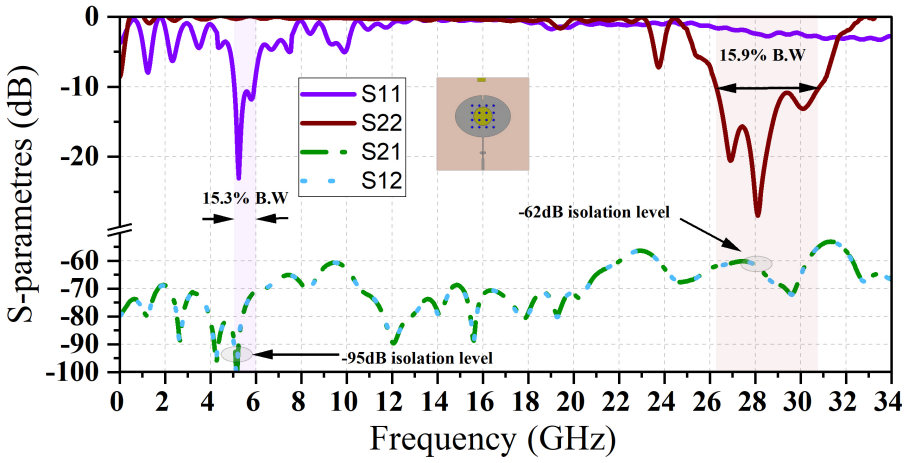

FIGURE 5.12 : S-parameter for 4 × 4 DR array proposed antenna.

creasing or decreasing the number of DRAs significantly impacts key performance metrics such as gain, mutual coupling between elements, and feeding network configuration. Particularly, a higher number of DRAs generally enhances gain due to the increased effective aperture, but it Introduces higher mutual coupling and complexity in feeding networks. Conversely, reducing the number of DRAs degrades the gain. Our configuration ensures an optimal trade-off between these factors, leading to the desired performance.

The scattering parameters of these stages are shown in Figs. 5.10, 5.11 and 5.12. For further clarification, Fig. 5.13 shows the progression of gain improvement with one element, four elements, and sixteen elements.

A passive feed network is developed to meet the design requirements, ensuring equal signal distribution across all branches. A microstrip-based power divider with quarter-wavelength impedance transformers was utilized to maintain a consistent 50 Ω input impedance. To demonstrate,

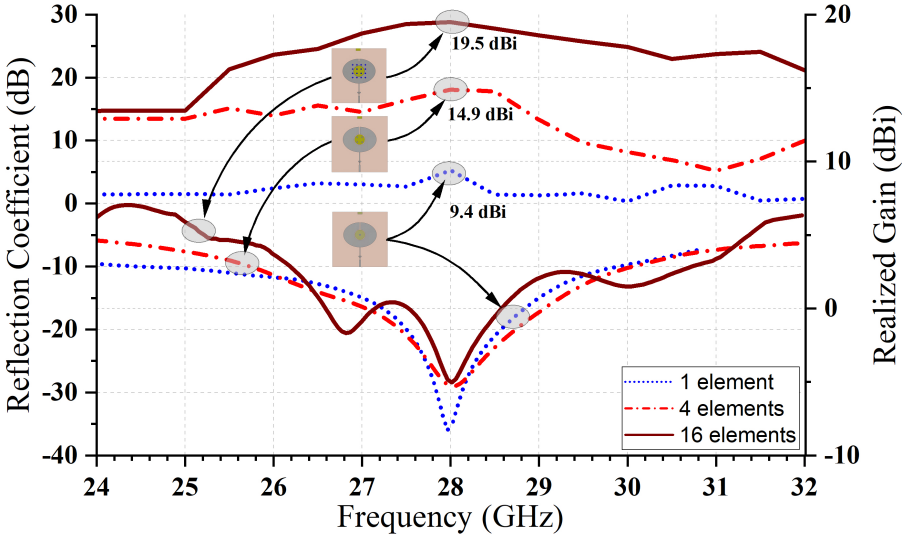

FIGURE 5.13 : Simulated reflection coefficient and gain for one element, 4-elements and 16-elements array.

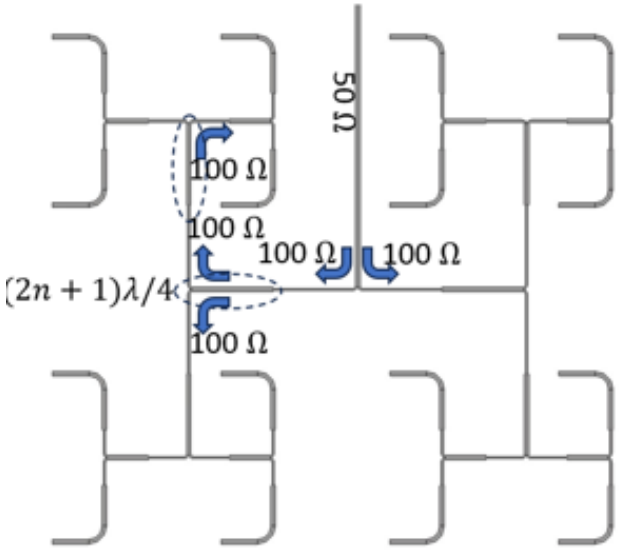

FIGURE 5.14 : Configuration of designed feeding network for CDRA.

according to Fig. 14, at the first T-junction, the equivalence of two parallel 100 Ω branches becomes 50 Ω. To match 100 Ω transmission lines to 50 Ω, the $\frac{(2n+1)\lambda}{4}$ lines are used at 70.7 Ω. This sequence is taken into consideration until we reach the DRAs. 50 Ω transmission line are 0.25 mm and 70.7 Ω own 0.13 mm width. The distance between he antenna elements is kept at 9 mm.

The design process for the proposed antenna can be summarized in the following key steps :

1) Designing the Elliptical Patch Antenna : An elliptical patch antenna is initially designed to operate at 5.2 GHz for the sub-6 GHz microwave band. We used equations (1-4) to design the elliptical patch. More details on this level of design have been provided in section II.A.

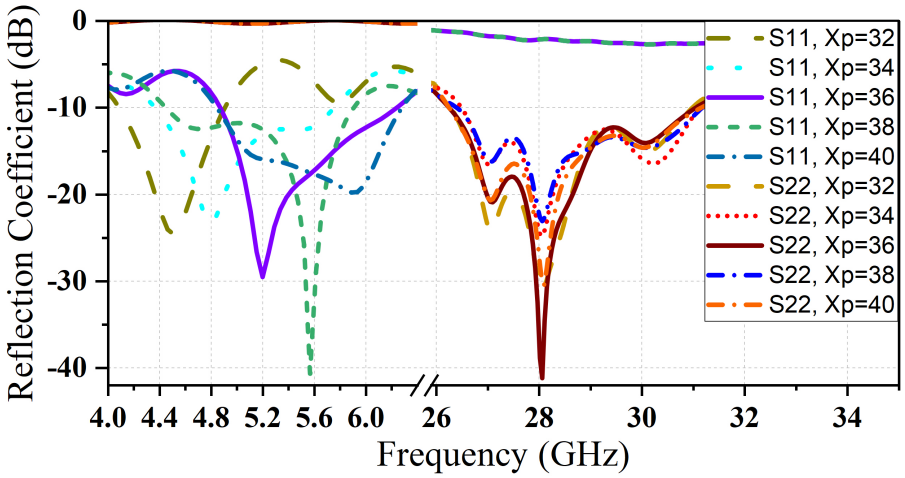

FIGURE 5.15 : The effect of elliptical patch size on the reflection coefficient in both bands (in millimeter).

2) Designing the CDR : A cylindrical dielectric resonator is designed to operate at 28 GHz, targeting the mm-wave band. Equations (5-7) have been considered during the design process. Refer to section II. B.

3) Integration of elliptical patch and CDR : A hollow is introduced at the center of the patch to provide space for integrating the DRAs. The dimensions of the elliptical patch are modified to keep the resonant frequency fixed at 5.2 GHz. More details have been found in section II.C.

4) LPF design to suppress harmonics of low band : An LPF is incorporated into the microwave band to suppress unwanted harmonics and improve isolation between the two bands. Detailed explained in section II.D.

5) CDR array design with proper feeding network : To improve the gain at mm-wave band, a 4×4 array is designed. Furthermore, a 1×16 power divider is designed to feed the array elements. Refer to section II.E for more information.

6) Finalizing the Design : The antenna's performance is optimized, achieving high gain, wide bandwidth, and excellent isolation at both operating frequencies.

5.4 Parametric Study

A comprehensive parametric study is conducted on various design parameters influencing the electrical behavior of the antenna to optimize its performance. In this analysis, each parameter is varied individually while keeping all other parameters fixed, allowing a precise evaluation of its impact on the antenna's characteristics.

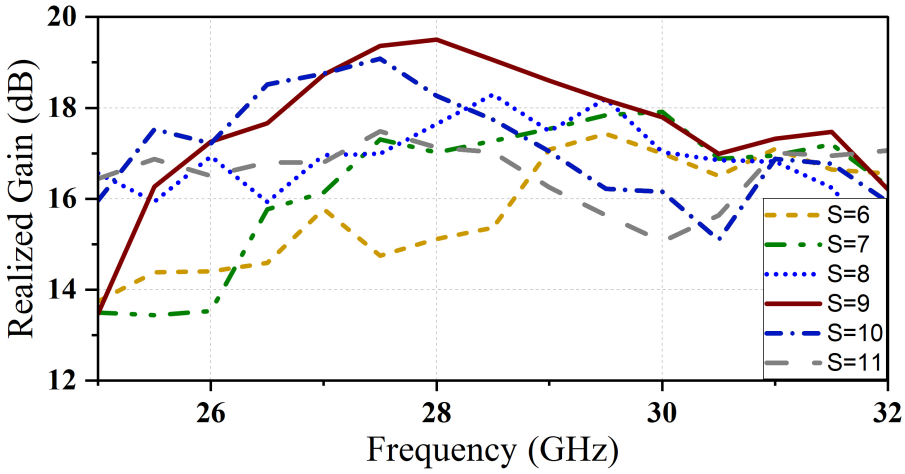

FIGURE 5.16 : Realized gain for various spacing values between DRs array (in millimeter).

5.4.1 patch antenna size (Xp)

The elliptical patch's dimensions are configured such that the major radius (Xp) is set to be half the minor radius (Yp), allowing the patch size to be controlled by modifying a single parameter. As illustrated in Fig. 5.15, increasing the patch size leads to a rise in the resonant frequency within the microwave band. However, it is essential to emphasize that variations in the patch size have no observable effect on the resonant frequency in the mm-wave band.

5.4.2 The spacing between DR array (S)

Several simulations were conducted to optimize the spacing between dielectric resonator (DR) elements. As the separation distance (S) between the DR elements increases from 6 mm to 11 mm, the peak value of the realized gain shifts toward lower frequencies. The maximum realized gain is achieved when the spacing is set to 9 mm (or 0.843λ), as illustrated in Fig. 3(a). This highlights the critical role of element spacing in determining the antenna's performance.

5.4.3 The central hollow radius (r)

The impact of varying the central hollow size on antenna performance is analyzed, focusing on the reflection coefficient and realized gain in both the mm-wave and sub-6 GHz bands. The radius of the hollow was changed from 10 mm to 15 mm in increments of 1 mm. As shown in Fig. 5.17, changes in the hollow's radius do not affect the resonant frequency in either band. However, the realized gain exhibits noticeable variation with changes in the hollow radius (r) for both frequency

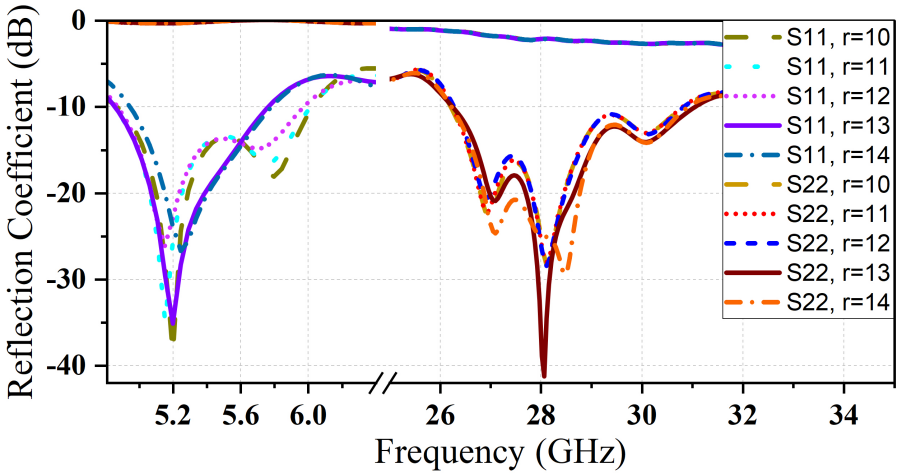

FIGURE 5.17 : Reflection coefficients for different values of patch dimensions (in millimeter).

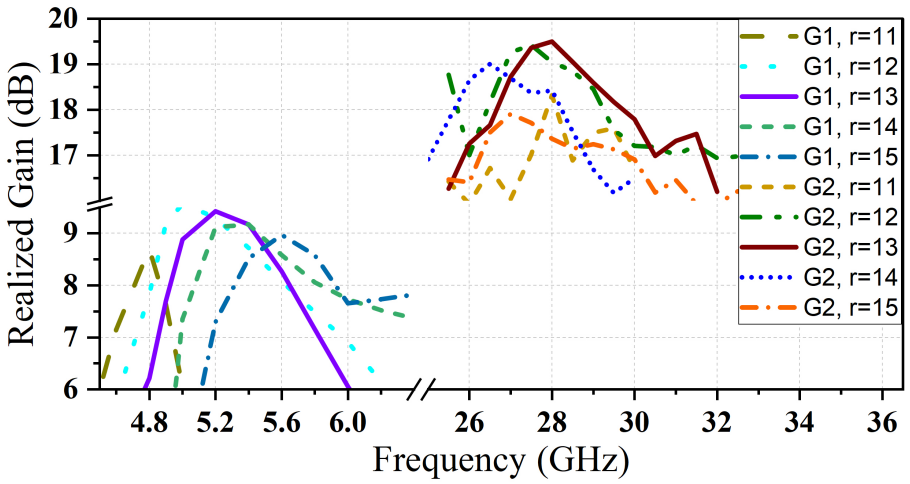

FIGURE 5.18 : The impact of varying the central hollow size on the realized gain (in millimeter).

bands, as also depicted in Fig. 5.18. This indicates that while the central hollow size does not influence the resonance behaviour, it plays a significant role in shaping the gain performance.

5.4.4 The dielectric resonator dimensions (Dr, Dh)

Fig. 5.19 illustrates the effect of varying the dielectric resonator height (Dh) on the resonant frequencies of the mm-wave band. An increase in (Dh) results in a downward shift in the resonant frequencies. This behavior can be explained by the change in the aspect ratio (h/a) of the cylindrical dielectric resonator (CDR), which is inversely proportional to the resonant frequency, as outlined in Equations (5.6) and (5.5).

TABLE 5.1 : Comprehensive comparison of our dual-band DRA with previous similar works.

Parameters	[89]	[42]	[41]	[90]	[67]	[92]	[69]	[93]	Our's
Antenna type sub-6/mm	DRA/DL	RDRA/FPRA	CDRA/FPRA	MED/RWG/RWG	HDRA/CDRA	ADRA/CDRA	Slot/SI-DRA	CDRA/Patch	**Patch/CDRA**
frequency (GHz) (sub-6/mm)	5.15/30.5	2.4/24	2.4/24	5/28/39	3.6/30.5	4.44/27.92	5.2/24	5.8/28	**5.2/28**
frequency ratio	5.92	10	10	7.8	8.47	6.28	4.6	4.83	**5.38**
Antenna Size $(*/\lambda_0^3)$	$0.72 \times 1.28 \times 0.27$	$1.2 \times 1.2 \times 0.304$	$0.8 \times 0.8 \times 0.187$	$0.58 \times 0.58 \times 0.057$	$0.87 \times 0.87 \times 0.35$	0.1	compact, $0.12\lambda_0$ height	$2 \times 2\lambda_o$	$\mathbf{1.25 \times 0.9\lambda_o}$
IBW % (sub-6/mm)	21/26.2	38.24/16.18	32.73/4.67	36.3/11.4/10.1	33/27	19.8/4.1	1.93/6.3	11.7/14.3	**34.5/16.8**
Gain (dBi) (sub-6/mm)	6.4/12.7	6.86/11.93	6.83/18.2	7.67/9.46/9.61	7.2/18	6.8/4.3	3.9/6.3	12.3/17.2	**9.1/19.0**
Array (sub-6/mm)	No/No	No/No	No/No	No/6/6	No/5	No/No	No/No	No/No	**No/16**
ϵ_r of the DR (sub-6/mm)	10/8	10/—	7/—	—/—/—	4/9	8.3/12.94	—/10.2	10/—	**—/10**
Isolation level (dB) (sub-6/mm)	35/37	Not given	Not given	Not given	31/25	Not given	40/35	54/51	**73/62**
Filtering Capability (sub-6/mm)	No/No	No/No	No/No	No/No	No/No	No/No	No/No	Yes/Yes	**Yes/No**
Frequency response independently	Not given	Not given	Not given	Not given	Not given	Not given	Not given	Yes	**Yes**

$*\lambda_0$ is the free space wavelength at the lowest frequency.

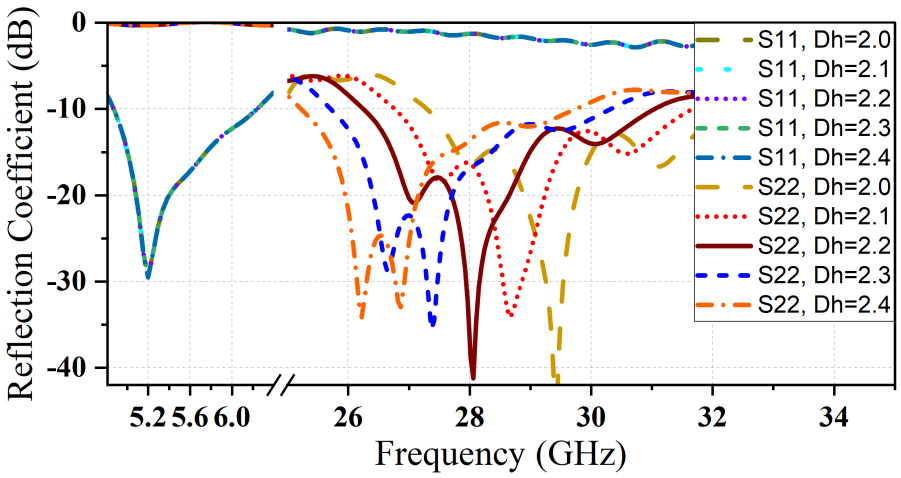

FIGURE 5.19 : Reflection coefficients for different dielectric resonator height values (in millimeter).

Similarly, Fig. 5.20 highlights the influence of the CDR's radius (Dr) on the resonance frequency. Increasing Dr causes a corresponding reduction in the resonance frequency. This relationship demonstrates how the physical dimensions of the CDR significantly impact its resonant characteristics.

Notably, altering the elliptical patch size (Xp) does not affect the resonance frequency of the mm-wave band portion (Fig. 5.15). Similarly, adjusting the dimensions of the CDR does not influence the operating frequency of the sub-6 band (Figs. 5.19 and 5.20). This emphasizes that the two sections of the antenna operate independently in terms of frequency response. These design parameters can be fine-tuned to achieve optimal performance, including the maximum gain, wider impedance bandwidth, and improved reflection coefficient.

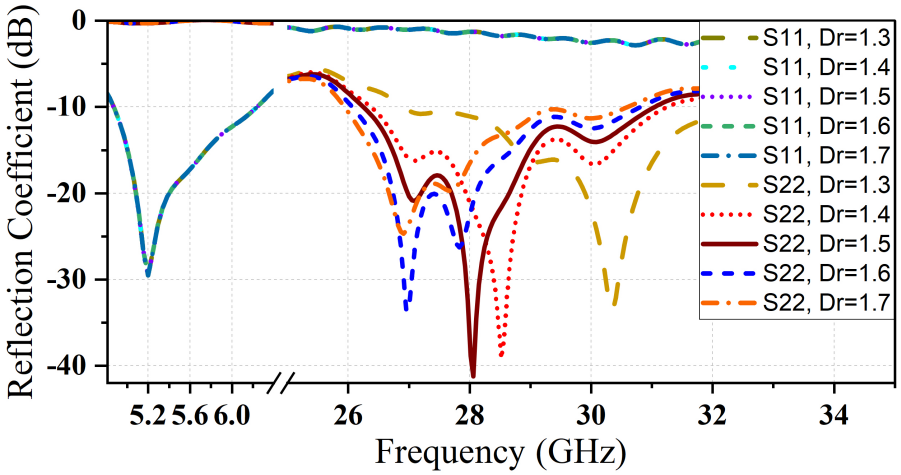

FIGURE 5.20 : Reflection coefficients for different values of dielectric resonator's radius (in millimeter).

5.5 Experimental Validation and Analysis

A prototype was developed and tested to validate the proposed design methodology. The antenna was implemented on a Rogers RO3003 substrate, and its far-field radiation characteristics were evaluated in a microwave anechoic chamber, as illustrated in Fig. 5.21. The experimental results closely align with the simulated ones, confirming the reliability of the design approach.

5.5.1 S-Parameters and Gain

The experimental and simulated gains and reflection coefficients of the dual-band antenna are presented in Fig. 5.22. Both the simulated and measured results exhibit similar trends, with minor deviations attributed primarily to variations in substrate properties during the fabrication process. As shown in Fig. 5.22, the measured impedance bandwidth in the sub-6 GHz band is 18% (4.9–5.85 GHz). Within this range, the antenna reached a stable gain of 8.8–8.7 dBi, with a 9.1 dBi maximum gain at 5.2 GHz.

For the mm-wave band, the measured impedance bandwidth is 15.6% (26.3–30.4 GHz), with 19.0 dBi maximum gain. The 3 dB gain bandwidth is measured at 9.2% (27.0 to 29.6 GHz). Furthermore, the measured and simulated isolation between the mm-wave and sub-6 GHz bands exceeds 73 and 62 dB, respectively, as shown in Fig. 5.22, demonstrating minimal mutual interference between the bands. The minor discrepancies between simulations and measurements may be because of the experimental setup and connector losses.

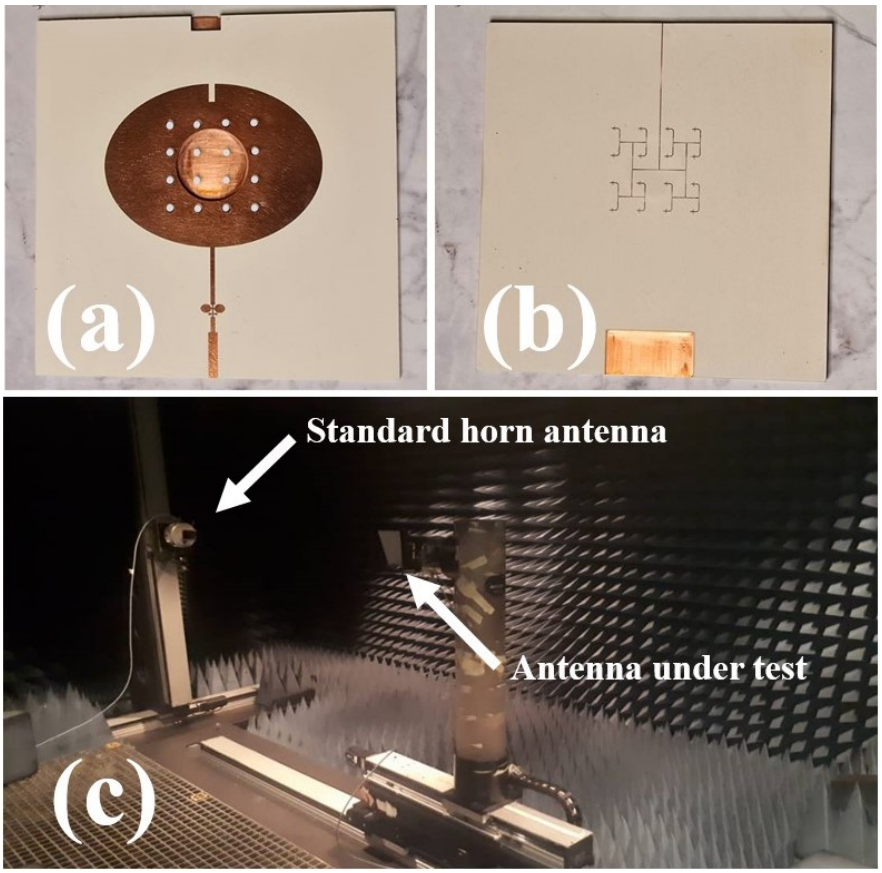

FIGURE 5.21 : A photograph of the Filtenna array prototype. (a) top view, (b) back view, (c) in the anechoic chamber.

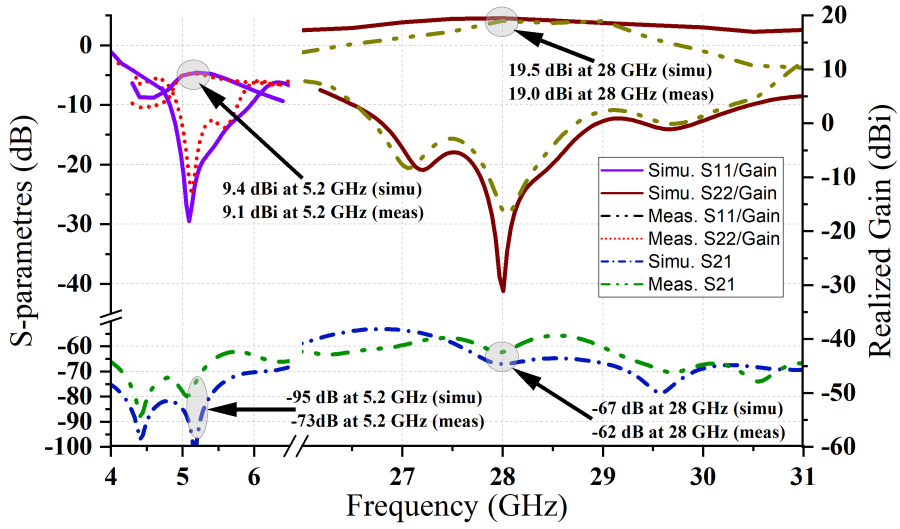

FIGURE 5.22 : The simulated and measured S-parameters and realized gain of the dual-band proposed antenna.

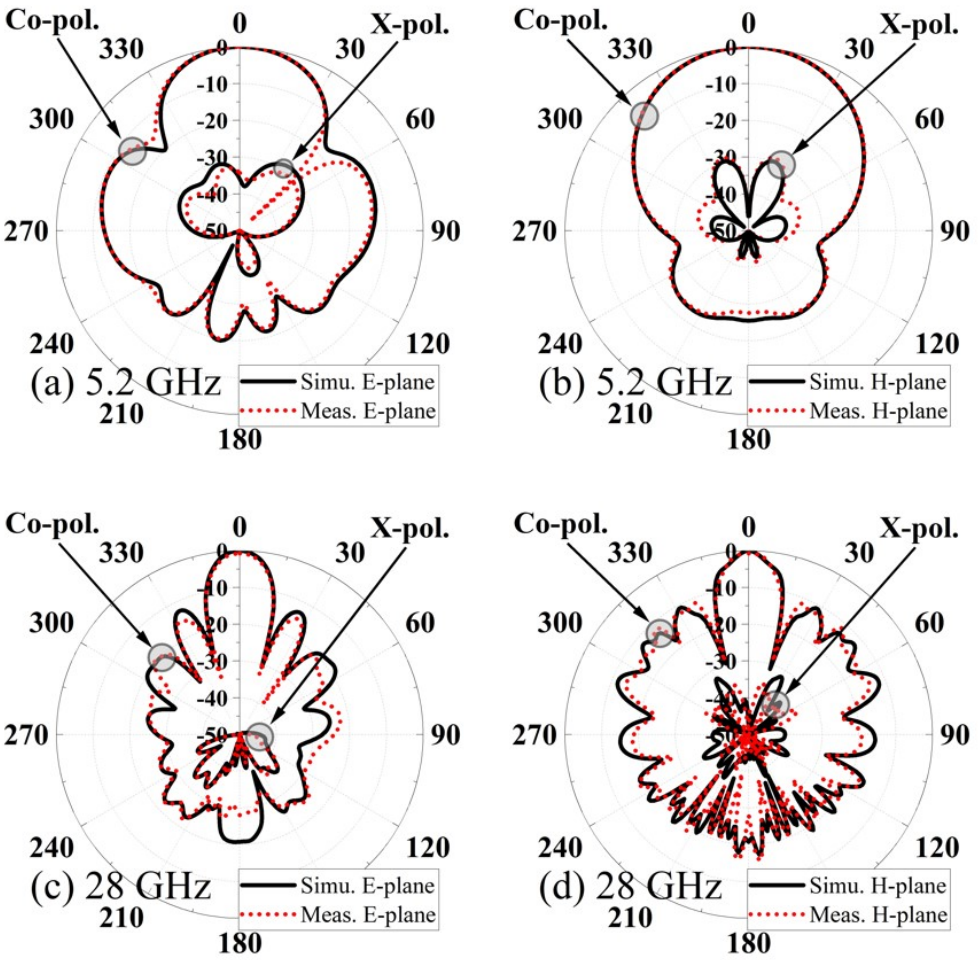

FIGURE 5.23 : Two dimensions simulated and measured radiation patterns at both bands : (a,b) E and H-planes at 5.2 GHz, (c,d) E and H-planes at 28 GHz.

5.5.2 Radiation Patterns

The antenna's radiation patterns, simulated and experimental are illustrated in Fig. 5.23. The results align closely, confirming the accuracy of the proposed design. At 5.2 GHz, the sub-6 GHz band radiation patterns in the E and H-planes (Figs. 5.23(a) and 5.23(b)) demonstrate the absence of side-lobe, with cross-polarization levels exceeding 30 dB.

For the mm-wave band at 28 GHz, the E and H-planes radiation patterns (Figs. 5.23(c) and 5.23(d)) exhibit side-lobe levels below 11.8 dB, with cross-polarization levels better than 34 dB. The minor deviations between simulations and measurements arise primarily from fabrication tolerances and measurement uncertainties.

5.5.3 Discussion

Table 5.1 compares the proposed structure with similar works. In terms of gain, at 28 GHz, the suggested work provides the highest gain in the literature due to the intelligent utilization of arrays integrated with the microwave antenna. The introduced work has a harmonic suppression feature using the LPF, resulting in an excellent isolation level between the bands. The antenna also has independent control of each band and a high impedance bandwidth.

The reported dimensions in Fig.3 ($10cm \times 10cm$) refer to the substrate size, not the effective radiating area. In terms of wavelength, the substrate corresponds to approximately $1.75 \times 1.75\,\lambda_0$. However, we would like to clarify that comparing the substrate size across different designs is not always meaningful, especially when the entire substrate is not actively used for radiation. In many of the referenced works, the radiating elements occupy the full substrate area, whereas in our case, a significant portion of the substrate is non-radiating and was retained primarily for mechanical support and integration convenience. The effective radiating element in our design is the elliptical patch, and its dimensions were used in Table I for a fairer comparison. Our design prioritizes achieving high gain at mm-Wave frequencies for long-range communication, along with strong isolation between bands and effective harmonic suppression. These design objectives were prioritized over minimizing physical size.

As a potential application of the proposed antenna system, it is worth highlighting that the proposed structure is well-suited for use in 5G outdoor antennas for fixed wireless access. Specifically, it can be mounted on the rooftop of a building to deliver high data rate connectivity via the 28 GHz band. The 5.2 GHz band serves as a fallback option; in scenarios where rain or physical obstructions degrade the mmWave link due to high path losses, the 5.2 GHz band can ensure continued operation by maintaining the connection.

5.6 Conclusion

This paper has presented a dual-band hybrid antenna, integrating an elliptical patch filtenna for the sub-6 GHz band and a 16-element CDRA for the mm-wave band. The design follows a seven-step optimization process that fine-tunes impedance matching, realized gain, and isolation, resulting in excellent performance across both frequency ranges. The antenna operates at 5.2 GHz and 28 GHz, achieving realized gains of 9.1 dBi and 19.0 dBi, respectively. A low-pass filter (LPF) has been incorporated to enhance spectral purity, further boosting the antenna's overall performance. With isolation values reaching 62 dB and 73 dB for mm-wave and sub-6 GHz, respectively, across both bands, the hybrid antenna has demonstrated outstanding features. The proposed gain, isolation level between the bands, and harmonic suppression alongside the wide bandwidth make the proposed structure suitable for 5G applications at both mm-wave and sub-6 GHz bands.

6 MULTI-BAND ANTENNAS DIELECTRIC RESONATOR-BASED FOR MICROWAVE AND MM-WAVE BANDS

6.1 Integrate Fabry–Perot Resonator into Dielectric Resonator Antenna

6.1.1 Introduction

In recent decades, the explosive growth of new technology has made the global communication systems get closer and closer to the commercialization of the fifth generation (5G) communication [94]. The existing sub-6 Giga Hertz (GHz) wireless communication technologies are congested and only allow a limited bandwidth, and thus cannot support high-speed data transmission [95]. The next generation of technology, 5G, could be deployed with a new spectrum allocation mechanism that allows a wider bandwidth [96]. Researchers will use two prominent bands for the 5G wireless communication system : the mm-wave band and the microwave band below 6 GHz. This mm-wave technology needs a high gain antenna with a wide impedance bandwidth to compensate the high path loss. To achieve these goals, DRAs can be a good candidate. Indeed, DRAs can provide not only a high gain but also a decent impedance bandwidth [24, 97]. To reduce the antenna size, Feng and Leung have investigated a compact dual-frequency antenna based on a single radiator with two back-to-back folded plates [40]. In this design, the folded plates form a microwave parallel plate waveguide resonator antenna (Waveguide Resonator Antenna (WRA)), while the separation between the folded plates gives a mm-wave Fabry–Perot resonator antenna (Fabry–Perot Resonator Antenna (FPRA)) [98, 99]. Feng and Leung have also investigated a light-weight mm-wave FPRA for a dual frequency. In this structure, the rectangle DRA and FPRA share a single dielectric block with a groove on the top surface. The FPRA has been implemented by sticking adhesive copper tape on the inner surface of the groove [42]. In this paper, a double-feed antenna for microwave and mm-wave applications is proposed. The antenna is composed of an FPRA resonator embedded into a cylindrical DRA structure to resonate at two different frequencies, sub-6 GHz (2.45 GHz) and Millimeter-Wave (28 GHz mm-wave), for 5G applications.

6.1.2 Antenna Structure

As shown in Fig 6.1, the proposed antenna consists of a DRA resonator merged with an FPRA resonator. The dielectric resonator block of Eccostock HIK 500 material with relative permittivity of 10 and tan(δ) = 0.002 is mounted on a square FR4 material substrate, with permittivity of 4.3 and tan(δ) = 0.025 and thickness of 1.584 mm and fed by a vertical strip connected to a 50 Ω-coaxial cable through a hole in the substrate and ground plane. The DR has an elliptical groove with a depth

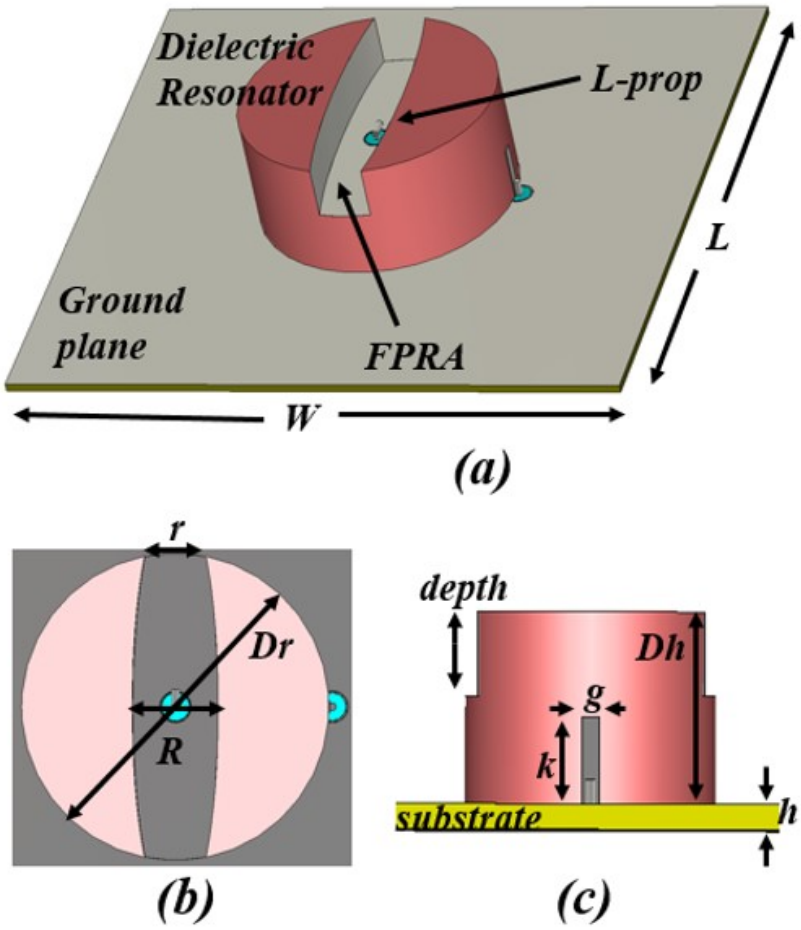

FIGURE 6.1 : The geometrical configuration of the proposed embedded CDR, (a) 3D view, (b) front view, (c) side view.

TABLE 6.1 : The Dimensions of the Proposed Antenna in Millimeteres.

Parameter	W/L	D_r	D_h	R	r	d	h	k	g
Value	100	27.8	23.5	3.3	3.36	10	1.584	10.5	2.0

of (d). To create the FPRA, the adhesive copper tape is stocked on the elliptical groove surfaces. The FPRA is excited by an L-probe. It is connected to a 50 Ω-coaxial cable with a diameter of 1.27 mm. It comprises vertical and horizontal arms of 2.9 mm and 3.44 mm, respectively.

Table 6.1 exhibits the optimal dimensions used in the antenna design.

6.1.3 simulation results and discussion

The performance of the proposed antenna is analyzed in terms of reflection coefficient, realized gain, and radiation pattern in the E- and H- planes. Figs. 6.2 and 6.4 a show the performance of the embedded DRA antenna at the lower frequency of 2.45 GHz (Sub-6 GHz band). It is clear from

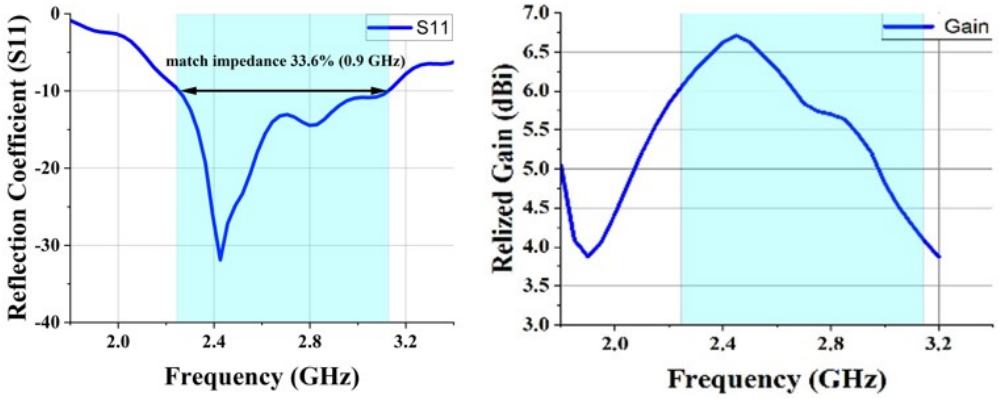

FIGURE 6.2 : Simulated reflection coefficient and realized gain at Sub-6 GHz band.

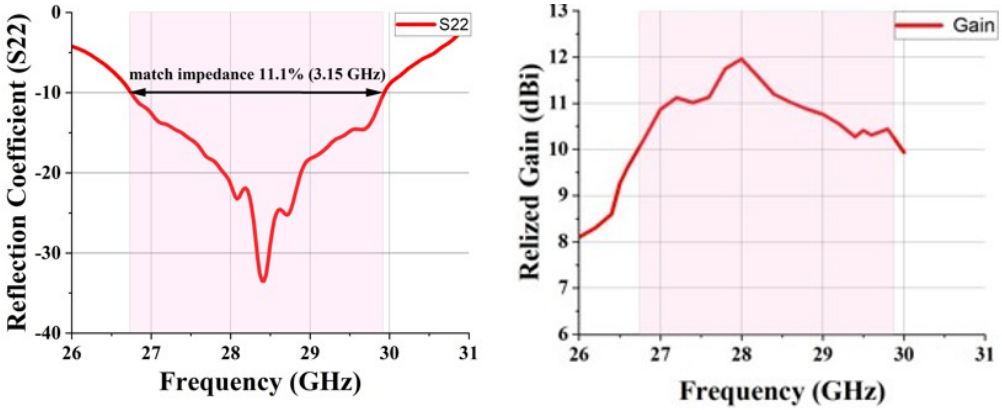

FIGURE 6.3 : Simulated reflection coefficient and realized gain at the mm-wave band.

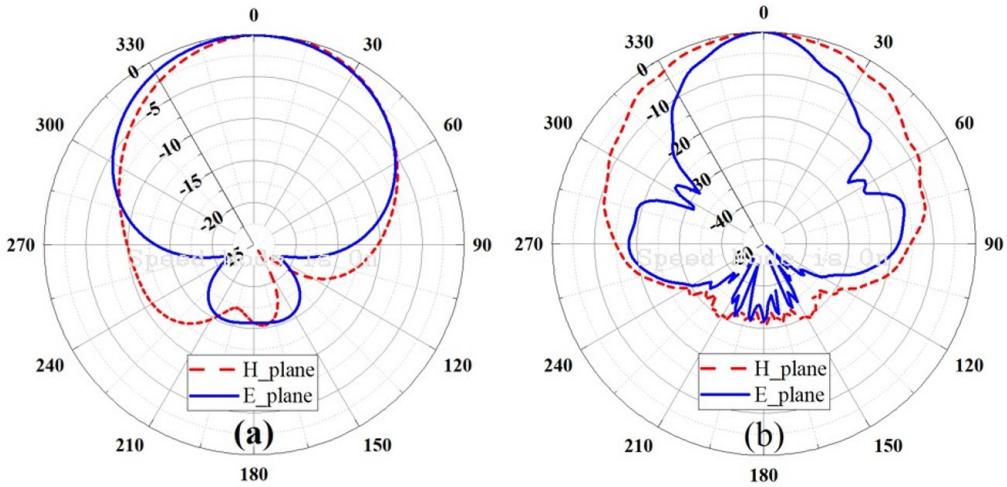

FIGURE 6.4 : Simulated 2-D radiation pattern, (a) Sub-6 GHz band, (b) mm-wave band.

these results that the reflection coefficient shifts down to (-33 dB) with an impedance bandwidth of 3%. At the same time, Fig. 6.2 shows that the realized gain goes up to 6.7 dBi at the desirable frequency (2.45GHz).

Similarly, Figs. 6.3 and 6.4 b show the performance of the proposed antenna in terms of the reflection coefficient, realized gain and radiation pattern at 28 GHz. We can note that the antenna

achieves a realized gain of 11.9 Decibels Relative to an Isotropic Antenna (dBi) with an impedance bandwidth of 11.3% at the mm-wave band (28 GHz). In addition, the reflection coefficient goes down to (-22 Decibels (dB)) at the desirable band.

6.1.4 conclusion

An elliptical Fabry–Perot resonator antenna integrated into a cylinder DRA for sub-6 GHz and mm-wave 5G applications has been presented. The proposed antenna has been designed to exhibit two separate operating resonance frequencies. The DR radiates at 2.45 GHz and has an impedance bandwidth of 33% with a peak gain of 6.7 dBi. On the other hand, the elliptical FP resonates at 28 GHz, achieving a realized gain of 11.9 dBi with an impedance bandwidth of 11.3%. The proposed antenna is a good candidate for the 5G applications based on the achieved promise.

6.2 Triple-band Antenna Dielectric Resonator-based

6.2.1 Introduction

In the ongoing quest to expand wireless communication capabilities, integrating versatile antennas that can operate across multiple frequency bands has become crucial. The advent of 5G and beyond, along with the anticipation of future communication standards, underscores the need for innovative solutions to seamlessly bridge Sub-6 GHz and millimeter-wave (mm-wave) frequencies [100]. Multiband antennas, including dual-band and triple-band configurations, are pivotal in modern communication systems due to their ability to support multiple frequency ranges, optimizing the use of the radio spectrum [77, 78]. Dual-band antennas typically operate in two ranges, such as Sub-6 GHz and mm-wave bands, making them ideal for applications like 5G and Wi-Fi [72][4]. Triple-band antennas further enhance versatility by adding a third band, enabling simultaneous operation across various services like cellular, satellite, and IoT networks [64, 101]. These antennas often employ advanced design techniques, such as dielectric resonators, slot coupling, and filters, to ensure high isolation and minimize inter-band interference [87]. By optimizing gain and impedance bandwidth across each band, multiband antennas provide reliable performance, supporting high data rates and broad coverage areas. Their compact designs, combined with integrated filtering mechanisms, reduce harmonic distortion and improve signal purity, making them essential for future communication technologies [102, 103]. In parallel, dielectric resonator antennas (DRAs) have emerged as a critical component in modern antenna design, offering advantages such as high radiation efficiency, low losses, and compact form factors [24, 56]. The dielectric resonator, usually made of ceramic or composite materials, serves as the radiating element, fostering resonant modes for efficient energy transfer. DRAs are suitable for a wide range of frequency bands, particularly in millimeter-wave communication systems [25]. This paper proposes a novel

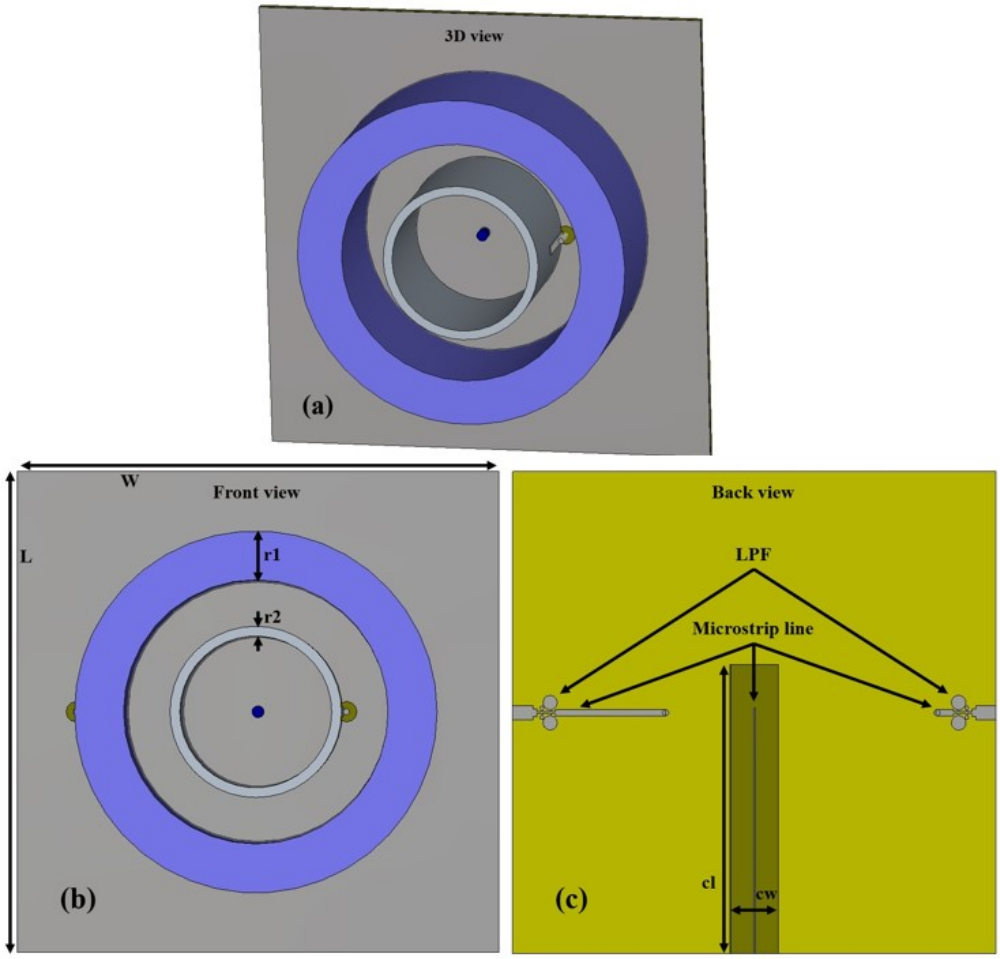

FIGURE 6.5 : The geometrical configuration of the proposed antenna, (a) 3D, (b) front view, and (c) back view.

triple-band dielectric resonator antenna designed for both Sub-6 GHz and millimeter-wave applications. The antenna integrates a cylindrical dielectric resonator with dual ring-shaped dielectric resonators, achieving resonances at 2.4 GHz, 5.2 GHz, and 28 GHz, effectively meeting the demands of 5G and future wireless systems.

6.2.2 Antenna Structure

As shown in Figs. 6.5 and 6.6, the proposed antenna comprises three resonators mounted on dual RO3003 substrates with identical permittivity (ϵ = 3) but different thicknesses, 0.13 mm and 1.52 mm. A rectangular cut has been made in the middle of the bottom substrate to make room for the microstrip line that fed the rectangular mutual coupling slot. The compact cylindrical dielectric resonator (CDR) operates at 28 GHz and is excited by a rectangular coupling slot measuring 1.6 x 0.4 mm^2. The second, larger resonator and the third, medium-sized resonator are tuned to 2.4 GHz and 5.2 GHz, respectively. Both are fed through vertical probes connected to a microstrip line,

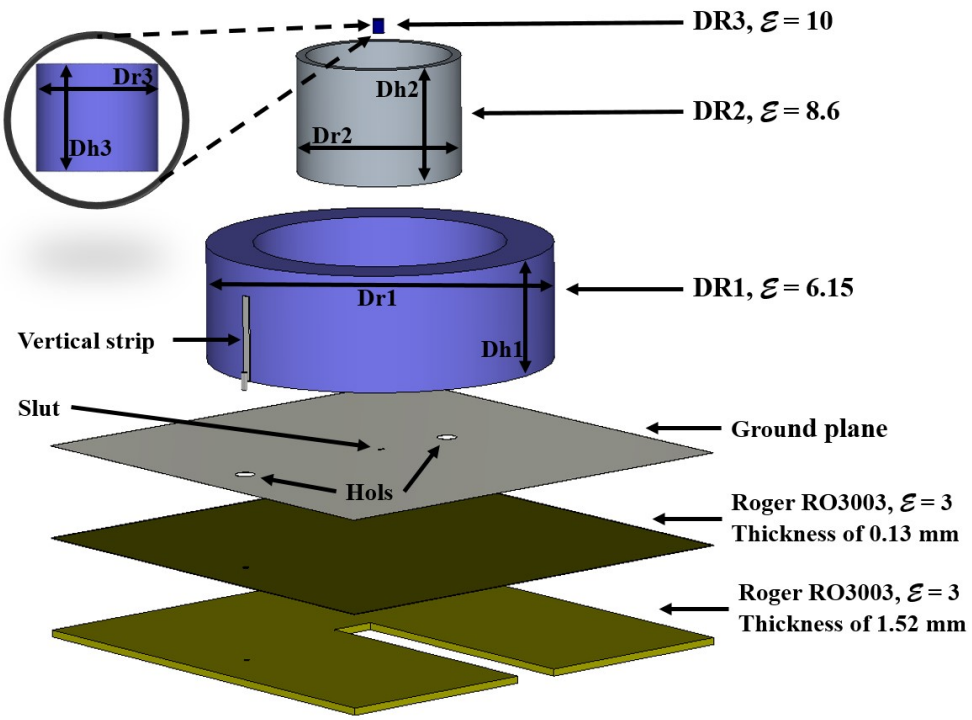

FIGURE 6.6 : The proposed antenna's layers.

TABLE 6.2 : The Proposed Antenna's Dimensions (in Millimeter.)

Parameter	W/L	Dr_1	Dh_1	Dr_2	Dh_2	Dr_3	Dh_3	r_1	r_2	cl	cw
Value	100	74	25	35	25	2.5	2.9	10	2.0	60	10

which includes a low-pass filter (LPF) to suppress unwanted harmonics in the mm-wave band. Fig. 6.5 illustrates the integration of the antenna components.

The optimized parameters of the proposed antenna, as depicted in Fig. 6.5, are listed in Table 6.2.

6.2.3 Simulation Results And Discuss

The antenna's performance is evaluated based on its reflection coefficient, realized gain, and radiation pattern. Fig. 6.7 presents the S-parameters of the proposed antenna, showing three distinct resonant frequencies at 2.4 GHz, 5.2 GHz, and 28 GHz, corresponding to the Sub-6 GHz and millimeter-wave bands. The figure also highlights excellent isolation, with S_{21}, S_{31}, S_{12}, S_{32}, S_{13}, and S_{23}. levels remaining better than 30 dB in the worst case. In the Sub-6 GHz band, the antenna achieves realized gains of 7.5 dBi at 2.4 GHz and 5.3 dBi at 5.2 GHz, with respective impedance bandwidths of 26.9% and 17.2%. At 28 GHz, the antenna demonstrates a realized gain of 17.8 dBi and an impedance bandwidth of 17.3%, as illustrated in Fig. 6.8. Fig. 6.9. presents the two-dimensional radiation patterns in the E- and H-planes, co-polarized and cross-polarized at 2.4 GHz, 5.2 GHz, and 28 GHz. The illustration reveals a symmetric-shaped radiation pattern in

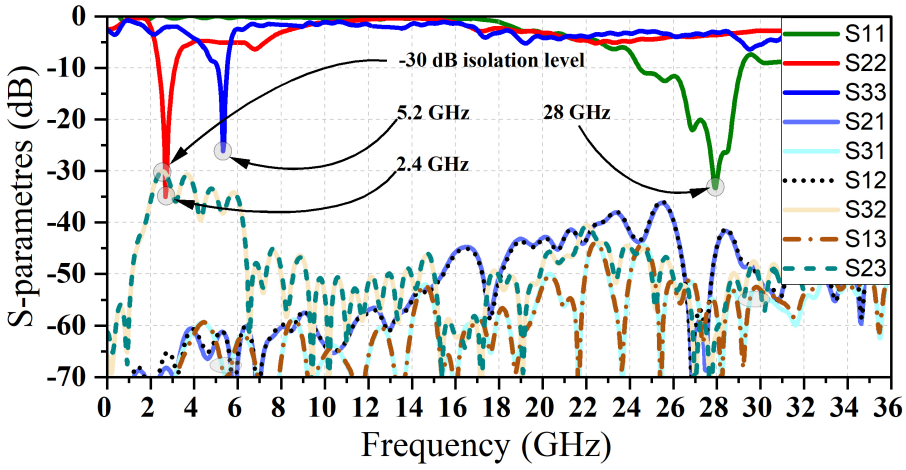

FIGURE 6.7 : S-parameters of The Proposed Antenna.

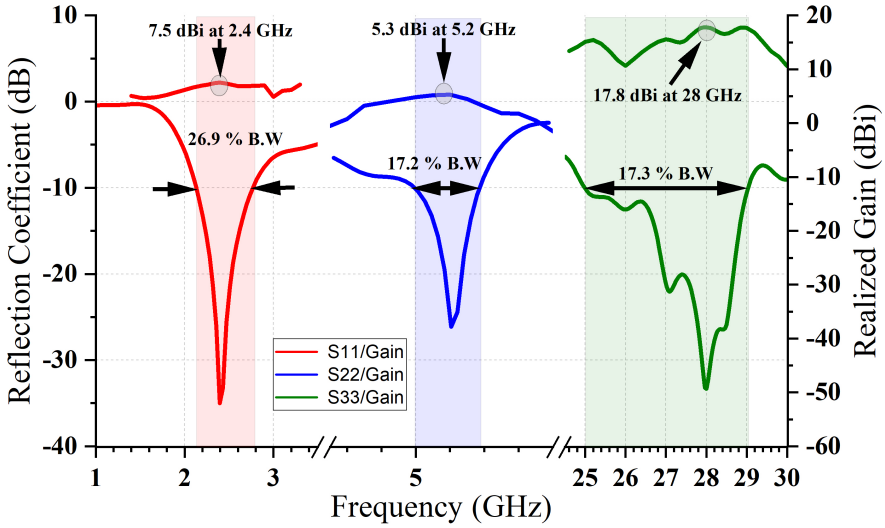

FIGURE 6.8 : The reflection coefficient and the gain for the three resonating frequencies.

the H-plane. Precisely, Fig. 6.9 c depicts that the antenna exhibits a low side-lobe level of -20 dB and cross-polarization levels of -30 dB.

6.2.4 Conclusion

In this paper, a triple-band dielectric resonator-based antenna for sub-6 and mm-wave has been designed and simulated. The proposed antenna contains three main parts : a CDR that resonates at 28 GHz for the mm-wave band and two RDRs operating at 2.4 and 5.2 GHz for the sub-6 band. The microstrips that feed these RDRs have two identical LPFs to mitigate any harmonicas above 6 GHz. The simulated results show that the antenna operates at 2.4 GHz, 5.2 GHz, and 28 GHz and

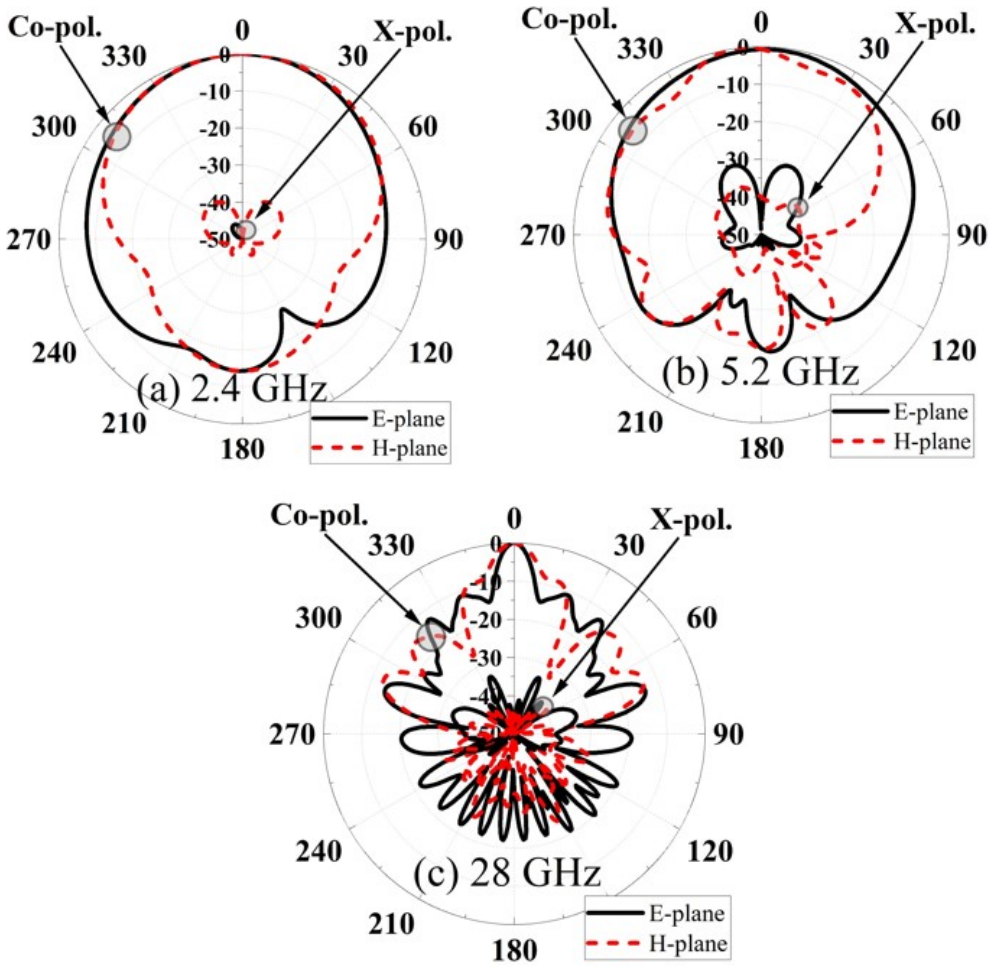

FIGURE 6.9 : Simulated 2-D radiation patterns, E-plane and H-plane at (a) 2.4 GHz, (b) 5.2 GHz, and (c) 28 GHz.

achieves a realized gain of 7.5 dBi, 5.3 dBi and 17.8 dBi with an impedance bandwidth of 26.9%, 17.2% and 17.3, respectively. The antenna demonstrates an isolation level better than 32 dB for both frequency bands, establishing its potential as a promising candidate for 5G applications.

7 CONCLUSION AND FUTURE WORK

7.1 Conclusion

This thesis has presented a comprehensive investigation into the design and implementation of novel dual-band antennas based on dielectric resonator technology for microwave and millimeter-wave applications. Motivated by the demands of next-generation wireless systems such as 5G and beyond, the research focused on developing compact antenna solutions that can operate efficiently across widely separated frequency bands, while meeting strict performance requirements in terms of gain, isolation, harmonic suppression, and tunability.

Three distinct dual-band antenna architectures were proposed, each addressing specific challenges associated with dual-band operation. The first design utilized two nested cylindrical dielectric resonators to support operation at 2.4 GHz and 28 GHz, and featured integrated low-pass filtering for harmonic suppression. The second design introduced a hybrid configuration that combined a cylindrical dielectric resonator with a series-fed patch array, supplemented by both low-pass and band-pass filters and shorting pins to achieve excellent isolation and independent control of the operating bands. The third and most advanced configuration integrated a sub-6 GHz elliptical filtenna with a 4×4 millimeter-wave dielectric resonator antenna array, significantly enhancing gain while maintaining spectral purity and compactness.

Across these three designs, the thesis successfully demonstrated several key achievements : high realized gain in both bands (up to 19 dBi at mm-wave frequencies), superior isolation (exceeding 70 dB in some cases), and truly independent frequency tunability. Furthermore, the proposed antennas were implemented using commercially available materials and verified through full-wave electromagnetic simulations and experimental measurements. The results validated the practicality and effectiveness of the designs and highlighted their potential for real-world deployment in wireless communication systems.

In summary, this thesis contributes a new class of dual-band dielectric resonator antennas that overcome key limitations in existing designs. The proposed solutions advance the state of the art in compact, high-performance antenna engineering, and offer practical, manufacturable platforms for integration into future wireless communication infrastructures.

7.2 Future Work

The proposed dual-band high-gain hybrid patch–dielectric resonator antenna has demonstrated promising performance for microwave and millimeter-wave applications. However, there are several directions in which this work can be extended to further enhance its applicability in modern and future wireless communication systems.

One potential extension is the development of beam-steering capabilities. By integrating phased-array techniques or employing reconfigurable metasurfaces, the antenna can dynamically steer its main beam toward desired directions. Such functionality is highly beneficial for 5G and upcoming 6G networks, where line-of-sight and adaptive coverage are critical, particularly in dense urban and vehicular environments. Future designs could explore low-cost and compact beam-steering mechanisms that maintain the high gain and isolation characteristics achieved in this work.

Another avenue for future research is the implementation of the antenna within a multi-input multi-output (MIMO) system. Expanding the single-element configuration into a multi-element array would significantly increase channel capacity, improve spectral efficiency, and enhance reliability through diversity gain. At the same time, careful design considerations are required to mitigate mutual coupling and ensure high isolation between adjacent elements, especially at millimeter-wave frequencies where compact integration becomes challenging. Incorporating MIMO functionality would make the antenna suitable for next-generation base stations and user terminals.

Additionally, the introduction of circular polarization (CP) represents an important future direction. Achieving CP operation in one or both bands would provide robustness against polarization mismatch and multi-path fading, which are common in mobile and satellite communication scenarios. This can be realized through hybrid feeding mechanisms, structural perturbations, or sequential rotation techniques, while preserving the antenna's dual-band operation and high gain performance. Circularly polarized designs would extend the antenna's applicability to satellite communication, vehicular networks, and emerging IoT devices.

In summary, future research can focus on integrating beam steering, MIMO operation, and circular polarization into the current dual-band antenna framework. These enhancements would significantly broaden the range of applications, making the antenna design more versatile and aligned with the evolving demands of 5G, 6G, and beyond.

BIBLIOGRAPHIE

[1] Y.-X. Wang, Z. Chen, and T. Yuan, "Design of a dual-band dielectric resonator antenna array for millimeter-wave communication," *IEEE Antennas and Wireless Propagation Letters*, vol. 22, no. 9, pp. 2190–2194, 2023.

[2] T. Upadhyaya, I. Park, R. Pandey, U. Patel, K. Pandya, A. Desai, J. Pabari, G. Byun, and Y. Kosta, "Aperture-fed quad-port dual-band dielectric resonator-mimo antenna for sub-6 ghz 5g and wlan application," *International Journal of Antennas and Propagation*, vol. 2022, no. 1, p. 4136347, 2022.

[3] H. Tang, C. Shao, J. Ge, Y. Yu, Q.-Y. Lu, and J.-X. Chen, "Use of the differential dielectric resonator antenna for an independently controllable dual-band filter," *IEEE Antennas and Wireless Propagation Letters*, vol. 20, no. 5, pp. 788–792, 2021.

[4] S. Varghese, P. Abdulla, A. M. Baby, and P. Jasmine, "High-gain dual-band waveguide-fed dielectric resonator antenna," *IEEE Antennas and Wireless Propagation Letters*, vol. 21, no. 2, pp. 232–236, 2021.

[5] S. Ballav, A. Chatterjee, and S. K. Parui, "Gain augmentation of a dual-band dielectric resonator antenna with frequency selective surface superstrate," *International Journal of RF and Microwave Computer-Aided Engineering*, vol. 31, no. 4, p. e22575, 2021.

[6] S. Lin, Y. Cao, F. Chen, Q. Xue, and W. Che, "Dual-band antenna with 2.4-ghz omnidirectional and 5.8-ghz pattern-reconfigurable radiation modes," *IEEE Antennas and Wireless Propagation Letters*, 2025.

[7] S. Mohanty and B. Mohapatra, "Dual band dielectric resonator antenna for high-speed applications," *J. Math. Comput. Sci.*, vol. 11, no. 4, pp. 4395–4410, 2021.

[8] P. Chakraborty, U. Banerjee, A. Saha, and A. Karmakar, "A compact ultra wideband dielectric resonator antenna with dual-band circular polarization characteristics," *International Journal of RF and Microwave Computer-Aided Engineering*, vol. 31, no. 4, p. e22577, 2021.

[9] H. C. Ye, C. Mao, L. L. Dai, and X. Y. Zhang, "Dual-band dual-polarized antenna and array with enhanced bandwidth for 5g millimeter-wave applications," *IEEE Antennas and Wireless Propagation Letters*, 2025.

[10] L. Yu, J. Wan, X. Yang, S. Shao, L. Bai, Y. Xi, K. Zhang, and Y. Li, "Compact dual-band, dual-circularly-polarized shared-aperture antenna based on the structure reuse of a dr," *IEEE Antennas and Wireless Propagation Letters*, 2024.

[11] K. Wei, J. Liu, R. Xu, W. Hu, C. Chen, W. Jiang, and S. Gao, "A dual-band rotational feed circularly polarized rfid reader antenna array with stable gain," *IEEE Antennas and Wireless Propagation Letters*, 2025.

[12] W. Liu, S. Li, L. Chen, C. Zhang, M. Qu, and L. Deng, "Dual-band low-profile hybrid antenna for bidirectional radiation," *IEEE Antennas and Wireless Propagation Letters*, 2025.

[13] K. W. Leung, S. A. Long, and K. Luk, "Overview of the dielectric resonator antenna," *Dielectric Resonator Antennas*, vol. 1, 2003.

[14] M. S. Bizan, *Ultra Wideband Stacked Rectangular Dielectric Resonator Antenna*. Institut National de la Recherche Scientifique (Canada), 2018.

[15] A. Petosa, *Dielectric resonator antenna handbook*. Artech, 2007.

[16] K. M. Luk, K. W. Leung *et al.*, "Dielectric resonator antennas," Research studies press, Tech. Rep., 2003.

[17] C. A. Balanis, *Antenna theory : analysis and design*. John wiley & sons, 2016.

[18] T. A. Denidni, Z. Weng, and M. Niroo-Jazi, "Z-shaped dielectric resonator antenna for ultra-wideband applications," *IEEE Transactions on Antennas and Propagation*, vol. 58, no. 12, pp. 4059–4062, 2010.

[19] S. Shum and K. Luk, "Stacked annular ring dielectric resonator antenna excited by axi-symmetric coaxial probe," *IEEE Transactions on Antennas and Propagation*, vol. 43, no. 8, pp. 889–892, 1995.

[20] R. K. Mongia and P. Bhartia, "Dielectric resonator antennas—a review and general design relations for resonant frequency and bandwidth," *International Journal of Microwave and Millimeter-Wave Computer-Aided Engineering*, vol. 4, no. 3, pp. 230–247, 1994.

[21] P. DM, "Microwave engineering," *Hoboken, NJ, USA : Wiley*, 2005.

[22] S. Long, M. McAllister, and L. Shen, "The resonant cylindrical dielectric cavity antenna," *IEEE Transactions on Antennas and Propagation*, vol. 31, no. 3, pp. 406–412, 1983.

[23] Y. M. Pan, P. F. Hu, K. W. Leung, and X. Y. Zhang, "Compact single-/dual-polarized filtering dielectric resonator antennas," *IEEE Transactions on Antennas and Propagation*, vol. 66, no. 9, pp. 4474–4484, 2018.

[24] M. S. Bizan, G. H. Elzwawi, M. M. Tahseen, and T. A. Denidni, "Bandwidth enhancement by position perturbations in stacked dielectric resonator antenna," in *2018 IEEE International Symposium on Antennas and Propagation & USNC/URSI National Radio Science Meeting*. IEEE, 2018, pp. 2091–2092.

[25] M. S. Bizan, M. M. M. Ali, and T. A. Denidni, "Design of sub-6 ghz and millimeter-wave 5g embedded dielectric resonator antenna," in *2022 IEEE International Symposium on Antennas and Propagation and USNC-URSI Radio Science Meeting (AP-S/URSI)*. IEEE, 2022, pp. 59–60.

[26] X.-C. Wang, L. Sun, X.-L. Lu, S. Liang, and W.-Z. Lu, "Single-feed dual-band circularly polarized dielectric resonator antenna for cnss applications," *IEEE Transactions on Antennas and Propagation*, vol. 65, no. 8, pp. 4283–4287, 2017.

[27] A. Gupta and R. K. Gangwar, "Dual-band circularly polarized aperture coupled rectangular dielectric resonator antenna for wireless applications," *IEEE Access*, vol. 6, pp. 11 388–11 396, 2018.

[28] A. Iqbal, A. J. Alazemi, and N. K. Mallat, "Slot-dra-based independent dual-band hybrid antenna for wearable biomedical devices," *IEEE access*, vol. 7, pp. 184 029–184 037, 2019.

[29] Z. Zhao, J. Ren, Y. Liu, Z. Zhou, and Y. Yin, "Wideband dual-feed, dual-sense circularly polarized dielectric resonator antenna," *IEEE Transactions on Antennas and Propagation*, vol. 68, no. 12, pp. 7785–7793, 2020.

[30] Z.-Y. Qian, L.-L. Yang, and J.-X. Chen, "Design of dual-/wide-band quasi-yagi antenna based on a dielectric resonator," *IEEE Access*, vol. 8, pp. 16 934–16 940, 2020.

[31] M. Niayesh and A. Kouki, "Ltcc-integrated dielectric resonant antenna array for 5g applications," *Sensors*, vol. 21, no. 11, p. 3801, 2021.

[32] K. Xu, L. Jin, H. Tang, W.-W. Yang, and J. Shi, "A high-efficiency dual-band self-filtering antenna based on three dense dielectric strip resonators," *IEEE Antennas and Wireless Propagation Letters*, vol. 21, no. 8, pp. 1532–1536, 2022.

[33] L.-X. Cui, X. Li, W.-W. Yang, L. Guo, and J.-X. Chen, "A dual-band millimeter-wave hybrid dielectric resonator antenna for 5g application," in *2021 IEEE Conference on Antenna Measurements & Applications (CAMA)*. IEEE, 2021, pp. 28–29.

[34] C. Tong, B. Yang, X. Huang, N. Yang, X. Liu, and K. W. Leung, "Compact shared-aperture slot/dr antenna with large frequency ratio," *IEEE Antennas and Wireless Propagation Letters*, vol. 22, no. 5, pp. 1119–1123, 2023.

[35] V. R. Gudivada, Y. Huang, H. Wang, Y.-C. Yang, and E. L. Bennett, "Undesirable higher order modes suppression using compact hybrid liquid antenna for wi-fi applications," *IEEE Access*, vol. 11, pp. 34 210–34 216, 2023.

[36] Y. C. Li, D.-S. Wu, T.-Z. Zhang, and Q. Xue, "Dual-band dual-channel bandpass filters using high quality factor dielectric resonators," *IEEE Transactions on Circuits and Systems II : Express Briefs*, vol. 70, no. 6, pp. 1931–1935, 2023.

[37] X.-H. Ding, Q.-H. Zhang, W.-W. Yang, W. Qin, L. Guo, and J.-X. Chen, "A dual-band antenna for lte/mmwave mobile terminal applications," *IEEE Transactions on Antennas and Propagation*, vol. 71, no. 3, pp. 2826–2831, 2023.

[38] L.-X. Cui, X.-H. Ding, W.-W. Yang, L. Guo, L.-H. Zhou, and J.-X. Chen, "Communication compact dual-band hybrid dielectric resonator antenna for 5g millimeter-wave applications," *IEEE Transactions on Antennas and Propagation*, vol. 71, no. 1, pp. 1005–1010, 2022.

[39] A. Yadav, M. Tiwari, and A. Sharma, "Dual-band quasi-isotropic dielectric resonator-based filtering antenna for iot applications," *Journal of Electronic Materials*, vol. 52, no. 2, pp. 1590–1598, 2023.

[40] L. Y. Feng and K. W. Leung, "Dual-frequency folded-parallel-plate antenna with large frequency ratio," *IEEE Transactions on Antennas and Propagation*, vol. 64, no. 1, pp. 340–345, 2015.

[41] ——, "Dual-fed hollow dielectric antenna for dual-frequency operation with large frequency ratio," *IEEE Transactions on Antennas and Propagation*, vol. 65, no. 6, pp. 3308–3313, 2017.

[42] ——, "Wideband dual-frequency antenna with large frequency ratio," *IEEE Transactions on Antennas and Propagation*, vol. 67, no. 3, pp. 1981–1986, 2019.

[43] C. J. Ma, Y. M. Pan, X. Y. Meng, and S. Y. Zheng, "A microwave/millimeter-wave shared-aperture antenna based on slow-wave parallel-plate waveguide," *IEEE Transactions on Antennas and Propagation*, vol. 71, no. 4, pp. 3022–3032, 2023.

[44] T. Li and Z. N. Chen, "A dual-band metasurface antenna using characteristic mode analysis," *IEEE Transactions on Antennas and Propagation*, vol. 66, no. 10, pp. 5620–5624, 2018.

[45] Y. Liu, Y.-C. Jiao, Z. Weng, C. Zhang, and G. Chen, "A novel millimeter-wave dual-band circularly polarized dielectric resonator antenna," *International Journal of RF and Microwave Computer-Aided Engineering*, vol. 29, no. 10, p. e21871, 2019.

[46] M. Al-Hasan, I. Ben Mabrouk, E. R. F. Almajali, M. Nedil, and T. A. Denidni, "Hybrid isolator for mutual-coupling reduction in millimeter-wave mimo antenna systems," *IEEE Access*, vol. 7, pp. 58 466–58 474, 2019.

[47] I. Ben Mabrouk, M. Al-Hasan, M. Nedil, T. A. Denidni, and A.-R. Sebak, "A novel design of radiation pattern-reconfigurable antenna system for millimeter-wave 5g applications," *IEEE Transactions on Antennas and Propagation*, vol. 68, no. 4, pp. 2585–2592, 2020.

[48] P. PourMohammadi, H. Naseri, N. Melouki, F. Ahmed, M. S. Bizan, A. Iqbal, and T. A. Denidni, "A fabry–perot antenna using a frequency selective surface layer with wideband and low rcs for mm-wave applications," *AEU-International Journal of Electronics and Communications*, vol. 169, p. 154736, 2023.

[49] U. Ullah, I. Ben Mabrouk, M. Al-Hasan, M. Nedil, and M. F. Ain, "A nested square-shape dielectric resonator for microwave band antenna applications," *International Journal of Electrical and Computer Engineering*, vol. 11, no. 1, pp. 481–488, 2021.

[50] Y. Su, X. Q. Lin, and Y. Fan, "Dual-band coaperture antenna based on a single-layer mode composite transmission line," *IEEE Transactions on Antennas and Propagation*, vol. 67, no. 7, pp. 4825–4829, 2019.

[51] T. Li and Z. N. Chen, "Shared-surface dual-band antenna for 5g applications," *IEEE Transactions on Antennas and Propagation*, vol. 68, no. 2, pp. 1128–1133, 2019.

[52] B. J. Xiang, S. Y. Zheng, H. Wong, Y. M. Pan, K. X. Wang, and M. H. Xia, "A flexible dual-band antenna with large frequency ratio and different radiation properties over the two bands," *IEEE Transactions on Antennas and Propagation*, vol. 66, no. 2, pp. 657–667, 2017.

[53] W.-W. Yang, X.-H. Ding, T.-W. Chen, L. Guo, W. Qin, and J.-X. Chen, "A shared-aperture antenna for (3.5, 28) ghz terminals with end-fire and broadside steerable beams in millimeter wave band," *IEEE Transactions on Antennas and Propagation*, vol. 70, no. 10, pp. 9101–9111, 2022.

[54] S. Ni, X. Li, X. Qiao, Q. Wang, and J. Zhang, "A compact dual-wideband magnetoelectric dipole antenna for 5g millimeter-wave applications," *IEEE Transactions on Antennas and Propagation*, vol. 70, no. 10, pp. 9112–9119, 2022.

[55] A. Petosa and A. Ittipiboon, "Dielectric resonator antennas : A historical review and the current state of the art," *IEEE Antennas and Propagation Magazine*, vol. 52, no. 5, pp. 91–116, 2010.

[56] H. Naseri, P. Pourmohammadi, M. S. Bizan, N. Melouki, F. Ahmed, A. Iqbal, and T. A. Denidni, "Reconfigurable dielectric resonator oam antenna with augmented modes," in *2023 IEEE International Symposium on Antennas and Propagation and USNC-URSI Radio Science Meeting (USNC-URSI)*. IEEE, 2023, pp. 703–704.

[57] J. Tao, Z. Yang, L. Ren, J. Liu, and H. Deng, "Dual-band structurally embedded high-temperature resistant antenna with high isolation and wide beam," in *2023 IEEE MTT-S International Wireless Symposium (IWS)*. IEEE, 2023, pp. 1–3.

[58] Y. Q. Guo, Y. M. Pan, S. Y. Zheng, and K. Lu, "A singly-fed dual-band microstrip antenna for microwave and millimeter-wave applications in 5g wireless communication," *IEEE Transactions on Vehicular Technology*, vol. 70, no. 6, pp. 5419–5430, 2021.

[59] N. Kalva and B. M. Kumar, "Feedline design for a series-fed binomial microstrip antenna array with no sidelobes," *IEEE Antennas and Wireless Propagation Letters*, vol. 22, no. 3, pp. 650–654, 2022.

[60] N. Nguyen-Trong, S. J. Chen, and C. Fumeaux, "High-gain dual-band dual-sense circularly polarized spiral series-fed patch antenna," *IEEE Open Journal of Antennas and Propagation*, vol. 3, pp. 343–352, 2022.

[61] W. Alshrafi, A. Al-Bassam, and D. Heberling, "Grating lobe mitigation in series-fed patch periodic leaky-wave antenna using parasitic monopoles," *IEEE Antennas and Wireless Propagation Letters*, vol. 19, no. 12, pp. 2472–2476, 2020.

[62] B. Wang, Z. Zhao, K. Sun, C. Du, X. Yang, and D. Yang, "Wideband series-fed microstrip patch antenna array with flat gain based on magnetic current feeding technology," *IEEE Antennas and Wireless Propagation Letters*, vol. 22, no. 4, pp. 834–838, 2022.

[63] T. H. Jang, H. Y. Kim, I. S. Song, C. J. Lee, J. H. Lee, and C. S. Park, "A wideband aperture efficient 60-ghz series-fed e-shaped patch antenna array with copolarized parasitic patches," *IEEE Transactions on Antennas and Propagation*, vol. 64, no. 12, pp. 5518–5521, 2016.

[64] M. S. Bizan, H. Naseri, P. PourMohammadi, and T. A. Denidni, "Integrate fabry–perot resonator into dielectric resonator antenna for microwave and mm-wave operations," in *2023 IEEE International Symposium on Antennas and Propagation and USNC-URSI Radio Science Meeting (USNC-URSI)*. IEEE, 2023, pp. 1161–1162.

[65] P. R. Girjashankar and T. Upadhyaya, "Substrate integrated waveguide fed dual band quad-elements rectangular dielectric resonator mimo antenna for millimeter wave 5g wireless communication systems," *AEU-international Journal of Electronics and Communications*, vol. 137, p. 153821, 2021.

[66] H. Xu, Z. Chen, H. Liu, L. Chang, T. Huang, S. Ye, L. Zhang, and C. Du, "Single-fed dual-circularly polarized stacked dielectric resonator antenna for k/ka-band uav satellite communications," *IEEE Transactions on Vehicular Technology*, vol. 71, no. 4, pp. 4449–4453, 2022.

[67] R. S. Malfajani, H. Niknam, S. Bodkhe, D. Therriault, J.-J. Laurin, and M. S. Sharawi, "A 3d-printed encapsulated dual wide-band dielectric resonator antenna with beam switching capability," *IEEE Open Journal of Antennas and Propagation*, vol. 4, pp. 492–505, 2023.

[68] X.-H. Ding, W.-W. Yang, W. Qin, and J.-X. Chen, "A broadside shared aperture antenna for (3.5, 26) ghz mobile terminals with steerable beam in millimeter-waveband," *IEEE Transactions on Antennas and Propagation*, vol. 70, no. 3, pp. 1806–1815, 2021.

[69] Y.-X. Sun and K. W. Leung, "Substrate-integrated two-port dual-frequency antenna," *IEEE Transactions on Antennas and Propagation*, vol. 64, no. 8, pp. 3692–3697, 2016.

[70] J. Lan, Z. Yu, J. Zhou, and W. Hong, "An aperture-sharing array for (3.5, 28) ghz terminals with steerable beam in millimeter-wave band," *IEEE Transactions on Antennas and Propagation*, vol. 68, no. 5, pp. 4114–4119, 2019.

[71] Y. Cheng and Y. Dong, "Dual-broadband dual-polarized shared-aperture magnetoelectric dipole antenna for 5g applications," *IEEE Transactions on Antennas and Propagation*, vol. 69, no. 11, pp. 7918–7923, 2021.

[72] M. S. Bizan, H. Naseri, P. Pourmohammadi, N. Melouki, A. Iqbal, and T. A. Denidni, "Dual-band dielectric resonator antenna with filtering features for microwave and mm-wave applications," *Micromachines*, vol. 14, no. 6, p. 1236, 2023.

[73] B. K. Shukla, N. Kashyap, and R. K. Baghel, "Circular slotted elliptical patch antenna with elliptical notch in ground," *Progress In Electromagnetics Research C*, vol. 74, pp. 181–189, 2017.

[74] S. K. Josan, J. Sohal, and B. S. Dhaliwal, "Design of elliptical microstrip patch antenna using genetic algorithms," in *2012 IEEE International Conference on Communication Systems (ICCS)*. IEEE, 2012, pp. 140–143.

[75] Y.-D. Zhou, Y.-C. Jiao, Z.-B. Weng, and T. Ni, "A novel single-fed wide dual-band circularly polarized dielectric resonator antenna," *IEEE antennas and wireless propagation letters*, vol. 15, pp. 930–933, 2015.

[76] X. Fang, K. W. Leung, and E. H. Lim, "Singly-fed dual-band circularly polarized dielectric resonator antenna," *IEEE antennas and wireless propagation letters*, vol. 13, pp. 995–998, 2014.

[77] M. S. Bizan and T. A. Denidni, "Dual-band hybrid dielectric resonator-patch antenna for microwave and mm-wave applications," in *2024 International Conference on Computing, Internet of Things and Microwave Systems (ICCIMS)*. IEEE, 2024, pp. 1–2.

[78] M. S. Bizan, H. Naseri, P. PourMohammadi, and T. Denidni, "Ultra-wideband dielectric resonator antenna fed by printed ridge gap waveguide technology," in *2024 IEEE International Symposium on Antennas and Propagation and INC/USNC-URSI Radio Science Meeting (AP-S/INC-USNC-URSI)*. IEEE, 2024, pp. 1933–1934.

[79] C. X. Mao, S. Gao, Y. Wang, B. Sanz-Izquierdo, Z. Wang, F. Qin, Q. X. Chu, J. Li, G. Wei, and J. Xu, "Dual-band patch antenna with filtering performance and harmonic suppression," *IEEE Transactions on Antennas and Propagation*, vol. 64, no. 9, pp. 4074–4077, 2016.

[80] S. Küçükcan and A. Kaya, "Dual-band microstrip patch antenna design for wi-fi applications," *Avrupa Bilim ve Teknoloji Dergisi*, vol. 70, no. 34, pp. 661–664, 2022.

[81] D. Fazal and Q. U. Khan, "Dual-band dual-polarized patch antenna using characteristic mode analysis," *IEEE Transactions on Antennas and Propagation*, vol. 70, no. 3, pp. 2271–2276, 2022.

[82] X. Yin, P. F. Hu, K. W. Leung, Y. M. Pan, N. Yang, and K. Lu, "Millimeter-wave dual-band filtering patch antenna and mimo array using multinull resonator," *IEEE Transactions on Antennas and Propagation*, vol. 72, no. 9, pp. 6897–6907, 2024.

[83] S. X. Ta, T. H. Bui, K. K. Nguyen, and N. Nguyen-Trong, "A compact dual-band tripolarized patch antenna with simple structure and very high isolation," *IEEE Open Journal of Antennas and Propagation*, vol. 5, no. 3, pp. 664–672, 2024.

[84] S. Mishra, S. Das, S. S. Pattnaik, S. Kumar, and B. K. Kanaujia, "Three-dimensional dual-band dielectric resonator antenna for wireless communication," *IEEE Access*, vol. 8, pp. 71 593–71 604, 2020.

[85] G. Das, A. Sharma, and R. K. Gangwar, "Dielectric resonator-based two-element mimo antenna system with dual band characteristics," *IET Microwaves, Antennas & Propagation*, vol. 12, no. 5, pp. 734–741, 2018.

[86] L. Guo, X. Li, W. Sun, W. Yang, Y. Zhao, and K. Wu, "Designing and modeling of a dual-band rectenna with compact dielectric resonator antenna," *IEEE Antennas and Wireless Propagation Letters*, vol. 21, no. 5, pp. 1046–1050, 2022.

[87] A. Altaf, J.-W. Jung, Y. Yang, K.-Y. Lee, and K. C. Hwang, "Reconfigurable dual-/triple-band circularly polarized dielectric resonator antenna," *IEEE Antennas and Wireless Propagation Letters*, vol. 19, no. 3, pp. 443–447, 2020.

[88] U. Patel and T. Upadhyaya, "Four-port dual-band multiple-input multiple-output dielectric resonator antenna for sub-6 ghz 5g communication applications," *Micromachines*, vol. 13, no. 11, p. 2022, 2022.

[89] R. S. Malfajani, H. Niknam, S. Bodkhe, D. Therriault, J.-J. Laurin, and M. S. Sharawi, "A dual wide-band mushroom-shaped dielectric antenna for 5g sub-6-ghz and mm-wave bands," *IEEE Open Journal of Antennas and Propagation*, vol. 4, pp. 614–625, 2023.

[90] B.-T. Chai, X. Geng, W.-W. Yang, and J.-X. Chen, "Compact aperture-shared tri-frequency antenna based on partial structure reutilization for millimeter-wave and sub-6 ghz applications," *IEEE Transactions on Antennas and Propagation*, 2024.

[91] J. Zhang, S. Zhang, and G. F. Pedersen, "Dual-band structure reused antenna based on quasi-elliptic bandpass frequency selective surface for 5g application," *IEEE Transactions on Antennas and Propagation*, vol. 68, no. 11, pp. 7612–7617, 2020.

[92] M. U. Khan, A. Muhammad, M. S. Sharawi, M. Alathbah *et al.*, "Singly-fed large frequency ratio composite dielectric resonator antenna for sub-6 ghz and mm-wave 5g applications," *IEEE Access*, 2024.

[93] M. S. Bizan, P. PourMohammadi, A. Iqbal, and T. A. Denidni, "High-gain dual-band antenna with independent frequency operation for sub-6 ghz and millimeter-wave applications," *AEU-International Journal of Electronics and Communications*, vol. 193, p. 155743, 2025.

[94] Z. Ren, S. Wu, and A. Zhao, "Coexist design of sub-6ghz and millimeter-wave antennas for 5g mobile terminals," in *2018 International Symposium on Antennas and Propagation (ISAP)*. IEEE, 2018, pp. 1–2.

[95] T. S. Rappaport, S. Sun, R. Mayzus, H. Zhao, Y. Azar, K. Wang, G. N. Wong, J. K. Schulz, M. Samimi, and F. Gutierrez, "Millimeter wave mobile communications for 5g cellular : It will work!" *IEEE access*, vol. 1, pp. 335–349, 2013.

[96] M. Ikram, N. Nguyen-Trong, and A. M. Abbosh, “Common-aperture sub-6 ghz and millimeter-wave 5g antenna system,” *IEEE Access*, vol. 8, pp. 199 415–199 423, 2020.

[97] K. S. Ryu and A. A. Kishk, “Ultrawideband dielectric resonator antenna with broadside patterns mounted on a vertical ground plane edge,” *IEEE Transactions on Antennas and Propagation*, vol. 58, no. 4, pp. 1047–1053, 2010.

[98] Y. Ding and K. Leung, “L-probe-fed fabry-perot resonator antenna for millimeter-wave applications,” in *2009 IEEE Antennas and Propagation Society International Symposium*. IEEE, 2009, pp. 1–4.

[99] K. Lu and K. W. Leung, “Differential fabry–perot resonator antennas,” *IEEE transactions on antennas and propagation*, vol. 61, no. 9, pp. 4438–4446, 2013.

[100] A. Muhammad, M. U. Khan, R. S. Malfajani, M. S. Sharawi, and M. Alathbah, “An integrated dra-based large frequency ratio antenna system consisting of a mm-wave array and a mimo antenna for 5g applications,” *IEEE Open Journal of Antennas and Propagation*, vol. 5, no. 2, pp. 368–378, 2024.

[101] P. F. Hu, K. W. Leung, Y. M. Pan, and S. Y. Zheng, “A tri-band dual-polarized omnidirectional dielectric resonator antenna with a planar feed for indoor applications,” *IEEE Transactions on Antennas and Propagation*, vol. 72, no. 1, pp. 401–411, 2023.

[102] I. K. C. Lin, M. H. Jamaluddin, A. Awang, R. Selvaraju, M. H. Dahri, L. C. Yen, and H. A. Rahim, “A triple band hybrid mimo rectangular dielectric resonator antenna for lte applications,” *IEEE Access*, vol. 7, pp. 122 900–122 913, 2019.

[103] H. Sarfraz, S. Khan, N. Khan, N. Gohar, S. A. A. Shah, J. Nasir, and M. Dalarsson, “Next-generation multiband wireless systems : A compact cssr-based mimo dielectric resonator antenna approach,” *IEEE Access*, vol. 12, pp. 4910–4924, 2023.